

Damping of wind waves in the IJmuiden breakwaters

H.G. Lavies

Delft University of Technology



Cover photo: *Northern IJmuiden breakwater, van der Veer (2014).*

Damping of wind waves in the IJmuiden breakwaters.

by

H.G. Lavies

in partial fulfilment of the requirements for the degree of

Master of Science
in Civil Engineering

at the Delft University of Technology,
to be defended publicly on Wednesday September 17, 2014 at 15:30.

Thesis committee:	Prof. dr. ir. W.S.J. Uijtewaal	TU Delft
	Ir. H.J. Verhagen	TU Delft
	Ir. J. van den Bos	TU Delft
	Ir. B. Reedijk	BAM Infraconsult bv

An electronic version of this thesis is available at <http://repository.tudelft.nl/>.



Preface

This thesis was written as the last part of the Hydraulic Engineering master curriculum at the Delft University of Technology. The research was carried out in cooperation with BAM Infraconsult. The topic of this thesis is wave damping in the IJmuiden breakwaters, in order to determine the stability of the asphalt slab.

First of all I would like express my gratitude to the members of my graduation committee; prof. dr. ir. W.S.J. Uijtewaal, ir. H.J. Verhagen, ir. J.P. van den Bos and ir. B. Reedijk. During meetings you provided useful information, appreciated feedback and guidance. With special thanks to Bas Reedijk, my daily supervisor at BAM Infraconsult, discussions often resulted in useful new insights.

Furthermore I would like to thanks BAM Infraconsult for providing me with the resources to work on my thesis. I also want to thank all my colleagues, I always felt very welcome, and I appreciated the nice working environment.

On a personal note, I would like to thank my parents, family, friends, roommates and girlfriend for their support and motivation.

Hugo Lavies,
Delft, September 2014

Abstract

The breakwaters of IJmuiden are of a unique design; a riprap core is covered with a thick impermeable asphalt slab. During construction and after completion, slope instability of the asphalt caused extensive damage. To prevent this weight was added by placing an armour layer consisting of concrete cubes. The added armour layer prevented further damage to the asphalt, but proved to be unstable and required a significant amount of maintenance. Rijkswaterstaat (RWS), the executive body of the Dutch Ministry of Infrastructure and Environment which is responsible for the maintenance of the breakwaters, contracted a number of companies to investigate the strength and loading of the breakwaters. Lifting of the asphalt slab as a result of overpressure in the breakwater core was found to be the decisive failure mechanism. In order to determine the amount of overpressure, measurements were performed in both breakwater heads. A bigger favourable damping of wind waves was measured in the southern breakwater.

Based on these measurements and other research outcomes RWS decided to change the maintenance strategy; damaged and removed armour units above the NAP-2 *m* line will not be repositioned or replaced in the future. The new strategy is based on the reasoning that the damping of wind waves reduces lifting forces and makes the weight of the armour layer redundant to prevent lifting. The mechanism(s) causing the larger damping in the southern breakwater are however unknown, this makes it hard to predict the amount of damping and therefore the magnitude of the loading of the asphalt during design storm conditions. Another uncertainty associated with the unknown damping mechanism is its development in time.

Aim of this thesis is to get insight in the stability of the asphalt slab during design storm conditions, and the necessity of an armour layer. Loading of the asphalt slab depends on the amount of wave damping. Therefore the mechanism causing the larger damping in the southern breakwater needs to be determined in order to be able to determine the amount of damping during storm events. Numerical modelling is performed to describe wave transmission through the breakwater and to evaluate the influence of different damping mechanisms.

Two mechanisms are found to cause the difference in damping between the southern and northern breakwater. The first mechanism is air trapped underneath the crown element and asphalt slab. During damping measurements trapped air was only present in the northern breakwater. The effect of trapped air on the magnitude of the damping depends on the height of the water level relative to the crown element. In case of relatively low water levels damping is reduced. In case of relatively high water levels trapped air will increase damping. For design storm conditions it is hard to predict the presence of trapped air due to an unknown airtightness of the breakwater, therefore the favourable higher damping due to trapped air is uncertain during design storms.

The second mechanism causing additional damping is siltation of the toe structure of the southern breakwater. Along the Dutch coast the net longshore sediment transport is directed northwards. Therefore sediment passes the southern breakwater, part of the sand might settle in the toe and core of the breakwater. This sand layer limits the flow of water through the toe into the core, resulting in an additional damping of wave energy. A sand layer with a height in the order of 3.3 *m* deposited in the toe is sufficient to cause the measured damping. The stability of the damping mechanism is checked during design storm conditions using open filter sediment transport formula. Erosion of the sand layer is expected, however the magnitude of the erosion is likely to be in the order of centimetres. This minor erosion will not have a significant influence on the damping mechanism. Therefore the damping mechanism in the southern breakwater is believed to be stable during design storm conditions.

The damping mechanism causing the measured damping in the southern breakwater is determined, hence loading of the asphalt slab during design storm conditions can be determined. The thickness and quality of the asphalt slab is uncertain and might vary significantly over the length of the breakwaters. In order to get insight in the quality of the asphalt two cores were drilled in 2004. One showed high quality cohesive asphalt, the other showed low quality with low cohesion. The amount and quality of asphalt required to prevent lifting is determined for four governing cross sections, representing the heads and trunks of both breakwaters. Three different situations were modelled, a complete armour layer, a partial armour layer below NAP-2 *m* in line with the new maintenance programme of RWS and a completely removed armour layer.

To prevent lifting of the entire asphalt slab over a certain cross section the dead weight of an asphalt slab with the designed thickness combined with a partial armour layer proved to be sufficient to prevent lifting. An additional shear and bending strength is not required. Local lifting of the asphalt can not be ruled out. The dead weight of the designed asphalt slab in combination with a partial armour layer is not sufficient to resist the upward pressures during a design storm. The additional resistance needed against lifting can be provided by the weight of a complete armour layer or bending strength of the asphalt slab. The bending strength of the asphalt slab depends on the quantity and quality of the asphalt present. In order for the asphalt slab to have sufficient bending strength a top layer of high quality cohesive asphalt is required.

Concluding, without additional information concerning the asphalt quality and thickness lifting of the asphalt slab and thereby failure of the breakwaters can not be ruled out in case the armour layer erodes above a level of NAP-2 *m*.

Contents

Preface	i
Abstract	ii
Acronyms	vii
Nomenclature	viii
1 Introduction	1
1.1 Background	1
1.2 Previous studies	3
1.3 Main research question	5
1.4 Plan of approach	5
1.5 Report structure	6
2 Failure mechanism	8
2.1 Structural parameters	9
2.2 Hydraulic parameters	10
2.3 Wave-structure interaction	11
2.4 Lifting of the asphalt layer	13
3 IJmuiden breakwaters	14
3.1 Breakwater layout	14
3.2 Cross sections	15
3.2.1 Breakwater heads	15
3.2.2 Breakwater trunks	16
3.3 Materials	17
3.3.1 Stone asphalt	17
3.4 Construction method	18
3.5 Hydraulic boundary conditions	19
4 Measured damping	20
4.1 Measurement setup	20
4.2 Damping of tide	21
4.3 Damping of wind waves during a mild storm	22
4.4 Damping of wind waves during a severe storm	24
4.5 Conclusions	25
5 Trapped air	26
5.1 Storage inertia resistance system	26
5.2 Influence of porous material	27
5.3 Influence of trapped air	28
5.4 Natural frequency	29

5.4.1	Natural frequency IJmuiden breakwaters	30
5.5	Trapped air decreasing damping	31
5.6	Trapped air increasing damping	32
5.7	Conclusions	32
6	Mechanisms causing damping	33
6.1	Wave damping mechanisms	33
6.2	Siltation of toe structure	34
6.3	Deeper asphalt slab	35
6.4	Approach comparing damping mechanisms	37
7	Used numerical model	39
7.1	Volume of fluid	39
7.2	Physics behind IH-2VOF	40
7.3	Input	41
7.4	Output	42
7.5	Limitations	43
8	Model calibration	44
8.1	Flow velocity profile	44
8.2	Pore pressure damping	46
8.3	Scale model tests breakwaters IJmuiden	51
8.3.1	Numerical model	54
8.4	Conclusions	58
9	Evaluation damping mechanisms	59
9.1	Baseline calculation	59
9.1.1	Results baseline calculations	60
9.2	Siltation of toe structure	63
9.3	Deeper asphalt layer	65
9.4	Selection damping mechanism	66
9.5	Damping during design storm	66
9.6	Stability of the sand layer	67
9.6.1	Transport rates	68
9.7	Conclusions	69
10	Stability of the asphalt slab	70
10.1	Nett upward pressure	71
10.1.1	Influence of the water level	72
10.1.2	Influence of a gap	72
10.1.3	Influence of the armour layer	74
10.2	Lifting of entire asphalt slab	75
10.2.1	Forcing	75
10.2.2	Resistance	75
10.3	Local lifting	77
10.3.1	Forcing	77
10.3.2	Resistance	78
10.4	Conclusions	80
11	Final conclusions and recommendations	81
11.1	Conclusions	81
11.2	Recommendations	83
	References	85

List of Figures	87
List of Tables	90
Appendices	91
A Flow through porous media	92
A.1 Flow regimes	92
A.2 Darcy flow	94
A.3 Forchheimer model	94
A.4 Fully turbulent flow	96
A.5 Shape factors	97
B Sediment transport	99
B.1 Sediment transport of a sand bed	99
B.2 Sediment transport in filters	101
B.3 Sediment transport under wave loading	104
B.4 Stability parameters silted sand IJmuiden breakwater	105
C Hydraulic boundary conditions	106
C.1 Field measurements	106
C.2 Normative hydraulic boundary conditions	107

Acronyms

KC	Keulegan-Carpenter number
NA	Neutral Axis
NAP	Normaal Amsterdams Peil, Dutch reference datum
RANS	Reynolds Averaged Navier-Stokes
Re	Reynolds number
RWS	Rijkswaterstaat
VARANS	Volume Averaged Reynolds Averaged Navier-Stokes
VOF	Volume Of Fluids
WL	Waterloopkundig Laboratorium, current Deltares

Nomenclature

Roman symbols

a	Laminar Forchheimer term	$[s/m]$
A	Amplitude	$[m]$
A	Area	$[m^2]$
a''	Hydraulic conductivity	$[s/m]$
b	Turbulent Forchheimer term	$[s^2/m^2]$
c	Time dependant Forchheimer term	$[s^2/m]$
d	Grain diameter	$[m]$
d_{50}	Median grain diameter	$[m]$
d_{n50}	Mass median grain diameter	$[m]$
Fr	Friction	$[s/m^2]$
F	Force	$[N]$
g	Gravitational acceleration	$[m/s^2]$
h	Water depth	$[m]$
H	Wave height	$[m]$
H_s	Significant wave height	$[m]$
I	Inertia	$[s^2/m^2]$
k	Wave number	$[m^{-1}]$
k	Permeability	$[m/s]$
L	Wave length	$[m]$
M	Bending moment	$[kNm]$
P	Pressure	$[N/m^2]$
\bar{P}	Mean pressure	$[N/m^2]$
P'	Turbulent pressure	$[N/m^2]$
n	Porosity	$[-]$
s_0	Wave steepness	$[-]$
T	Wave period	$[s]$
T_m	Mean wave period	$[s]$
T_s	Significant wave period	$[s]$
T	Sediment transport rate	$[kg/m/s]$
u	Filter flow velocity	$[m/s]$
\bar{u}	Mean filter velocity	$[m/s]$
u'	Turbulent filter velocity	$[m/s]$
V	Volume	$[m^3]$
W	Section modulus	$[m^{-3}]$

Greek symbols

α	Laminar shape factor Forchheimer flow	[–]
β	Turbulent shape factor Forchheimer flow	[–]
γ	Added mass coefficient	[–]
δ	Damping coefficient	[–]
ζ	Damping	[–]
η	Surface elevation	[<i>m</i>]
λ	Leakage length	[<i>m</i>]
ν	Kinematic viscosity	[<i>m</i> ² / <i>s</i>]
ξ	Iribarren number	[–]
ρ	Density	[<i>kg/m</i> ³]
σ	Stress	[<i>kn/m</i> ²]
$\bar{\tau}$	Mean viscous stress tensor	[<i>Nm</i> ²]
ψ	Shields parameter	[–]
ω	Angular frequency	[<i>Rad/s</i>]

Chapter 1

Introduction

This chapter will provide a short introduction to the breakwaters of IJmuiden, focussing on the major expansion performed in the sixties of last century and the maintenance issues since. Subsequently findings of the most important researches into the stability of the IJmuiden breakwaters are presented, leading to the main research question of this thesis. Last part of this chapter will present the approach followed to answer this research question and provides the structure of the report.

1.1 Background

The breakwaters of IJmuiden are located in the Dutch province of North-Holland at the entrance of the North Sea Canal. The canal provides passage to the harbour of IJmuiden and Amsterdam, see figure 1.1.



FIG. 1.1: *Location of IJmuiden, Maps (2014).*

The original breakwaters were built in the 19th century and consisted of two 1,400 m long gravity based breakwaters, O'Prinsen (1993). In the early 1950's industry and international trade developed rapidly, resulting in growing ship dimensions. In order to make the ports of Amsterdam and IJmuiden accessible for these new larger ships an upgrade of the outer harbour of IJmuiden was necessary. Most important part of this upgrade was enlarging the breakwaters. The new breakwaters reach 2,800 m and 2,200 m into the sea, the southern breakwater reaching furthest into the sea, see figure 1.2.



FIG. 1.2: *Layout of the outer harbour of IJmuiden, Maps (2014).*

Different breakwater designs were investigated, a revolutionary new design was selected consisting of a riprap core covered with a 2 – 2.25 m thick stone asphalt layer, see figure 1.3. Stone asphalt was never used as a breakwater cover. The design was economically attractive and therefore selected, despite a total lack of experience constructing stone asphalt breakwater covers.

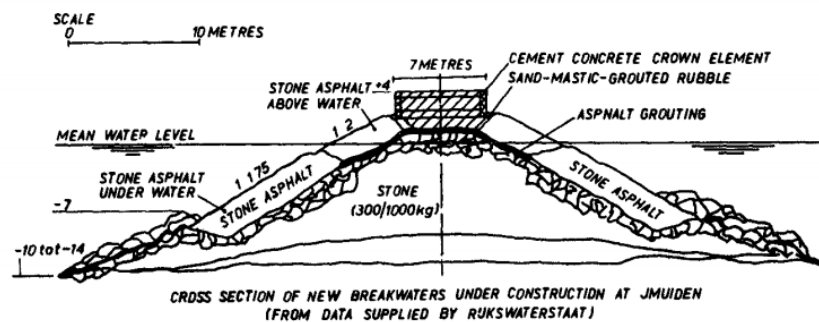


FIG. 1.3: *Designed cross section of the breakwater.*

Construction of the breakwater began in 1964, the lack of design and construction experience with stone asphalt covered breakwaters resulted in a trial on error kind of approach. The mixture of the stone asphalt was frequently adjusted in order to get a stable covering layer. During construction an unexpected failure mechanism occurred, large settlements of the asphalt slab during and directly after summers was observed. Damaged areas were repaired by casting more asphalt. In order to prevent these damages the design was slightly altered, slopes became more gentle, different asphalt mixtures were applied above and below water and concrete blocks were placed on the lower parts of the slopes with the highest wave loading to stabilise the asphalt slab, Koene et al. (2013). Construction finished in 1968.

Big storms hit the Dutch coast during the summers of 1968 and 1970 resulting in damage due to slope instability, see figure 1.4. The breakwaters were not breached, but extensive repairs were necessary. Designers estimated yearly maintenance would require 1,000 tonne of stone asphalt, during the first four years after completion the yearly maintenance budget was 20,000 tonne on average, Davidse (2012). Less damage was observed at the locations where concrete blocks were placed to stabilize the asphalt slab. This resulted in placement of concrete blocks along the whole breakwater. Depending on the magnitude of the wave loading concrete blocks weighing 22, 30 or 45 tonne were placed from 1970 till 1993.



FIG. 1.4: *Damaged asphalt slab after summer storm of 1970, Davidse (2012).*

Placement of the blocks did not result in a maintenance free breakwater; blocks started to crack, break into pieces and wash away. Biggest damage to the armour layer occurred in 1999, it required 38 blocks of 45 tonne to repair the armour layer, Koene et al. (2013). Until 2013 the damaged armour layer was repaired by repositioning old and placing new armour units.

Debate is rising whether the armour layer is necessary for the stability of the breakwater. In June 2013 Rijkswaterstaat (RWS) decided to stop repairing the armour layer above a level of NAP-2 m and only monitor the breakwater, de Baar and Schravendeel (2013). This approach is based on new insights into the hydraulic loading and strength of the breakwater as a result of multiple researches. The next section treats the most important researches.

1.2 Previous studies

The breakwaters of IJmuiden have been topic of numerous researches. This overview will focus on the research concerning the stability of the breakwater after the elongation of 1964. Research can be divided into two main groups: research into the stability of the armour layer and research into the stability of the breakwater without an armour layer.

First research on the stability of the armour units was performed by the Waterloopkundig Laboratorium (WL), currently Deltares, in 1971. Model tests showed the concrete blocks were unstable during storm events, especially the rows close to the crown element; despite this outcome placement of blocks continued. Kuiper and van Gent (2006) continued research into the stability of the current breakwaters. Scale model test were performed to formulate the decisive failure mechanisms and to design a new stable armour layer. Washing out of sand from underneath the breakwater, toe instability and lifting of the asphalt slab due to pressure buildup in the core were determined to be normative. The proposed new stable armour layer was never constructed due to the high cost.

From 2012 onward research focused on the strength and loading of the current breakwaters, in order to investigations whether the breakwater would be stable without an armour layer. First step was redetermining the hydraulic boundary conditions, all research before was executed using the hydraulic boundary conditions determined during design and construction of the breakwater. Smale and Groeneweg (2012) performed research into the hydraulic boundary conditions, they concluded the significant wave heights are lower than previously assumed.

Research by Davidse (2012) focused on the strength of the asphalt slab, due to the changing asphalt mixtures and the occurred damages there was a high degree of uncertainty about the strength of the asphalt slab. A literature study on the construction and maintenance of the breakwater was performed and two boreholes were taken from the asphalt. Researchers concluded it is likely a stone skeleton is formed in the asphalt layer, failure due to slope instability like seen in 1970 are unlikely to occur. The local quality of the asphalt is however highly uncertain, one borehole showed good quality asphalt the other showed a lack of mastic and thereby little cohesion. Most important recommendation is to drill more cores to get a better insight in the quality of the stone asphalt.

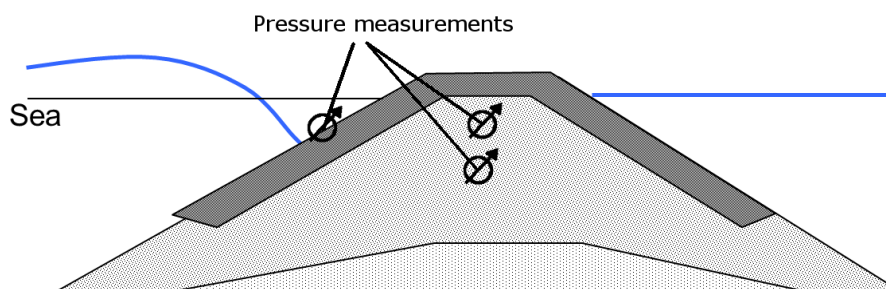


FIG. 1.5: Configuration of pressure sensors, van Hoven (2012).

Concluding from the previous two researches the decisive failure mechanism is determined to be lifting of the asphalt due to pressure buildup underneath the asphalt slab. Pressure measurements were performed by van Hoven (2012) to get insight in the amount of over pressure in the core of the breakwater. In order to be able to determine the magnitude of the forcing of the asphalt slab. A set of four pressure sensors was installed near the heads of each breakwater, figure 1.5 shows the configuration of the sensors. Observations showed a bigger favourable damping in the southern breakwater. The measured damping is assumed to be the result of siltation of the toe structure increasing the flow resistance of water. The siltation is however never proven, and a recommendation was made to further investigate the origin of the measured damping and the stability of the damping mechanism during storm events.

Final research by van Hoven (2013) used the outcome of the previously stated researches as input. Goal of this research was establishing the failure probability of the breakwaters in case all armour units above a level of NAP -2 m are washed away. Failure was defined as the moment the port is inaccessible due to siltation of the channel, the acceptable failure probability was set to be 1 % per year. The highly uncertain asphalt quality was dealt with using two different models to represent the asphalt slab, a clamped continuous beam representing a strong area, and a beam with a hinge at NAP -0.5 m representing a weak spot. The measured wave damping in the southern breakwater was concluded to be sufficient and necessary for an acceptable failure probability.

1.3 Main research question

From the researches described in the section above one can conclude lifting of the impermeable asphalt slab is the normative failure mechanism for the breakwaters of IJmuiden. Lifting is caused by an upward pressure difference over the asphalt slab, magnitude depends on the amount of wave energy transmitted through the breakwater. Field measurements showed a favourable larger damping of wind waves in the southern breakwater compared to the northern breakwater. The mechanism(s) causing this difference are unknown, hence it is hard to predict the magnitude of the loading of the asphalt slab during design storm conditions. Another unknown aspect is the development of the damping mechanism in time, the amount of damping could be influenced by storm events.

This leads to the following research question for this thesis:

”What causes the larger damping of wind waves in the southern breakwater of IJmuiden, and is the asphalt slab stable during storm conditions?”

In order to get a conclusive answer to the main research question a couple of sub question need to be answered:

- What mechanisms can cause the measured difference in damping of wind waves?
- Which mechanism is most likely to cause the measured difference in damping of wind waves?
- Is the damping mechanism influenced by storm events?
- Can lifting of the asphalt slab during storm events be ruled out?

1.4 Plan of approach

Main input for this research are the results of the researches by, Smale and Groeneweg (2012), van Hoven (2012) and van Hoven (2013). Correctly describing the flow of water through the porous parts of the breakwater will be essential in order to get insight in the damping of waves. Therefore a literature study into flow of water through porous media is performed. Knowledge from this study will be used to draw the possible damping mechanisms able to cause the measured damping.

Scaling effects will limit the correct description of flow through the porous media, therefore a numerical model will be used. The numerical model will first be calibrated, to ensure the data produced is useful.

Next step is the evaluation of the damping mechanisms, aim is to reproduce the measured damping applying similar hydraulic conditions. The most promising damping mechanism will be selected and its behaviour during design storm conditions is tested. Not only the magnitude of the damping but also the stability of the damping during storm conditions will be of great importance for the loading of the asphalt slab. Last part of the thesis will present a brief calculation of the effect of the modelled damping on the stability of the asphalt slab.

1.5 Report structure

This section describes the subjects that are being addressed in the respective chapters of this report.

Chapter 2: Failure mechanism

Previous research into the breakwaters of IJmuiden concluded lifting of the asphalt is the decisive failure mechanism. This chapter will treat the most important structural and hydraulic parameters influencing both loading and resistance of breakwaters with respect to lifting.

Chapter 3: IJmuiden breakwaters

A more elaborate introduction into the breakwaters of IJmuiden is provided, keeping in mind the decisive failure mechanism; lifting of the asphalt slab. Layout of the breakwaters, used materials, hydraulic boundary conditions and construction method are discussed. Four governing cross sections are selected which will be used to determine the stability of the asphalt slab in the final chapter of this thesis.

Chapter 4: Measured damping

Field measurements were performed in both the southern and northern breakwater, main purpose was to get insight in the amount of wave damping and thereby the magnitude of the loading of the asphalt slab. Damping of both wind and tidal waves was investigated. Results of these measurements are presented in chapter four.

Chapter 5: Trapped air

From the measurements described in chapter four the presence of trapped air in only the northern breakwater was concluded. The influence of this trapped air on the amount of damping is investigated in order to determine whether trapped air can cause the difference in wave damping between the southern and northern breakwater.

Chapter 6: Mechanisms causing damping

The measured damping can not solely be addressed to the trapped air discussed in chapter five. Two mechanisms likely to be able to cause the difference in damping between the southern and northern breakwater are introduced. Both damping mechanisms focus on an increased flow resistance of the breakwater toe. The first is a lower asphalt slab, the second is siltation of the toe structure.

Chapter 7: Used numerical model

A numerical volume of fluid model, IH-2VOF, is selected to assess the influence of the damping mechanisms and to determine the forcing of the asphalt slab. Chapter seven describes the physics behind the model, the main simplifications, advantages and limitations.

Chapter 8: Model calibration

The model described in chapter seven is calibrated for the modelling of flow through porous media. Correct modelling of this flow is essential to determine wave damping and forcing of the asphalt slab. Results of the model are compared to both analytical formula and measurement data from other researches.

Chapter 9: Evaluation damping mechanisms

Aim of this chapter is to determine which of the damping mechanism described in chapter six is most likely to cause the measured difference in damping between the northern and southern breakwater described in chapter four. Insight in the damping mechanism present is required to be able to predict the amount of damping and thereby the loading of the asphalt slab during design conditions. Besides the amount of damping the stability of the damping mechanism is considered.

Chapter 10: Stability of the asphalt slab

The new understanding of the damping mechanism provided in chapter nine make it possible to determine the loading of the asphalt slab during design conditions. The required quality and quantity of asphalt to prevent lifting is determined for all four decisive cross sections.

Chapter 11: Final conclusions and recommendations

The main research question and the sub questions of this thesis are answered. Besides a couple of recommendations are presented regarding topics for additional research.

Appendices

The first two appendices present a literature study on flow of water through porous media and sediment transport. Knowledge of the flow through porous media is essential to get an understanding of the movement of water inside the breakwater and therefore to understand wave damping and forcing of the asphalt slab. Information about the sediment transport is essential to determine the stability of the damping mechanism as a result of a silted toe structure. The last appendix provides an overview of all hydraulic boundary conditions used in this thesis.

Chapter 2

Failure mechanism

Like stated in the previous chapter lifting of the asphalt is considered to be the decisive failure mechanism for the breakwaters of IJmuiden. This chapter provides an overview of parameters influencing strength and loading of a breakwater. Followed by different wave-structure interaction mechanisms, leading to the forces contributing to lifting of the asphalt slab.

In order to determine the stability of the asphalt slab it is necessary to be able to formulate both strength and loading. Parameters influencing stability can be divided into two groups; hydraulic and structural parameters. The relation between those parameters is shown in figure 2.1.

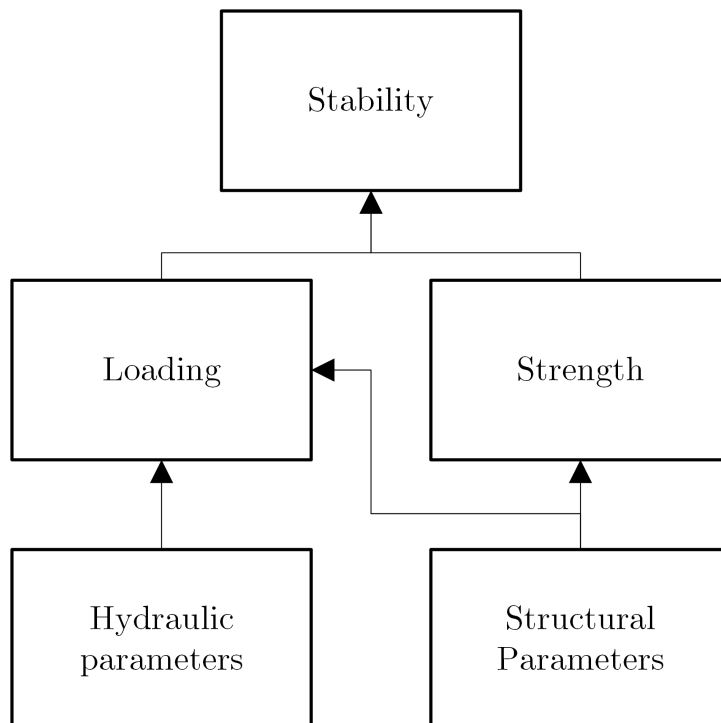


FIG. 2.1: *Scheme of the influence of hydraulic and structural parameters on stability.*

Like every structure, loading and strength determine the stability of a hydraulic structure under wave attack. Structural parameters influence both strength and loading and will be discussed in section 2.1. Hydraulic parameters describe the water motion in front of the breakwater they will be described in section 2.2. These parameters combined will result in wave-structure interaction which is described in section 2.3. Selection of the described parameters is performed keeping the primary failure mechanism, lifting of the asphalt in mind.

2.1 Structural parameters

Structural parameters can be divided into two groups: parameters describing the asphalt slab itself and parameters describing the other parts of the breakwater. A typical cross section of a breakwater is presented in figure 2.2, in the IJmuiden case the under layer is replaced by the impermeable asphalt slab that runs from the toe upward.

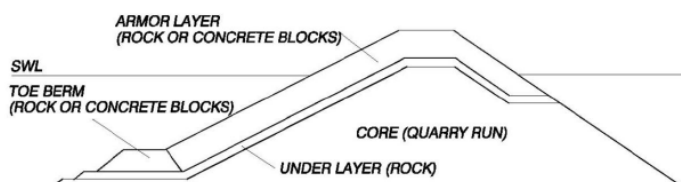


FIG. 2.2: Clarification breakwater elements, coastal engineering manual (2006).

The asphalt slab is described by its density, permeability, length, thickness and bending strength. Bending strength is a function of thickness, tensile strength, cohesiveness and amount, size and location of any weak spots. The asphalt slab will also influence loading, local permeability of the asphalt slab will prevent or lower pressure buildup, smoothness of the outside slope will influence run-up and run-down described in section 2.3.

Parameters of interest describing other parts of the breakwater are mainly related to the motion of water inside the breakwater. Most important parameters are: geometry of the different layers, porosity, grain diameter, shape and grading. Porosity is defined as the volume of pores divided by the total volume. The average stone diameter can be characterised in two different ways, the mass median grain diameter d_{n50} is defined as the diameter of the stone weight exceeded by half of the stones $d_{n50} = W_{50}^{1/3}$ and the median grain diameter d_{50} which is defined as the diameter exceeded by half of the stones. Grading describes the distribution in block weight or size of a sample, table 2.1 describes the different ranges of grading.

TAB. 2.1: Ranges of grading, CIRIA (2007).

	d_{85}/d_{15}	W_{85}/W_{15}
Narrow or <i>single-sized gradation</i>	Less than 1.5	1.7-2.7
Wide gradation	1.5-2.5	2.7-16.0
Very wide or <i>quarry run gradation</i>	2.5-5	16.0-125+

Where W_{85} is the weight for which 85 % of the block is lighter than this block weight, W_{15} , d_{85} and d_{15} are defined in a similar way.

2.2 Hydraulic parameters

Hydraulic parameters describe water level and motion of water. A great deal of parameters describe the different properties of waves. A single wave is defined as the profile of the surface elevation between two successive downward zero-crossings, Holthuijsen (2007). The definition is clarified in figure 2.3, where η is the water surface elevation and the hatched part represents one wave.

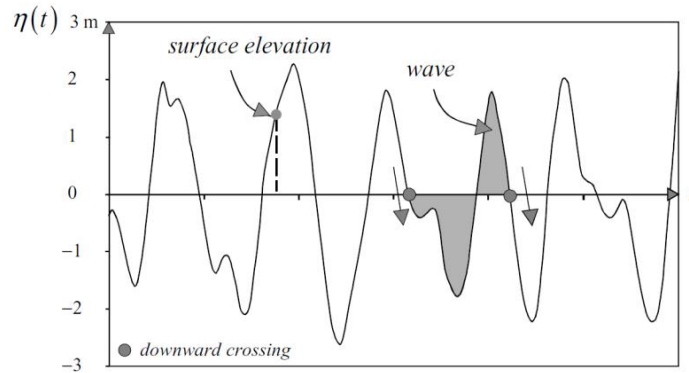


FIG. 2.3: Definition of a wave, Holthuijsen (2007).

Wave height H is defined as the vertical distance between the highest and lowest surface elevation occurring in one wave. In the field the surface elevation profile will be fairly irregular like illustrated in figure 2.3 each wave will have a different wave height. For designing purposes it is necessary to be able to describe wave fields instead of individual wave heights, for this purpose the the significant wave height H_s is commonly used to describe wave fields. The significant wave height is the mean value of the 1/3 highest waves.

The wave period T is the time elapsed between two downward zero-crossings. Like the wave height the wave period is commonly described using a significant value T_s as well. Also the mean wave period T_m is used in literature.

The wave length L is the horizontal distance between two wave troughs, the wave length can be determined using the wave period and water depth. In case of regular linear waves (small amplitude compared to wave length) linear wave theory can be used to determine the wave length.

$$L = \frac{g \cdot T^2}{2\pi} \tanh\left(\frac{2\pi h}{L}\right) \quad (2.1)$$

Where h is the water depth and g is the gravitational acceleration. In case the wave height and the wave length are known the wave steepness s_0 can be determined using the following formula:

$$s_0 = \frac{H}{L} \quad (2.2)$$

2.3 Wave-structure interaction

The presence of a structure will influence wave and flow patterns. This section will describe different wave-structure interaction, both outside and inside the breakwater. Only 2-dimensional effects perpendicular to the axis of the breakwater are treated. 3-dimensional effects like diffraction and refraction are outside the scope of this report.

Breaker type

First wave-structure interaction takes place on the foreshore. A mechanism called shoaling sets in. The wave period of a wave is constant, a lower water depth will therefore result in a shorter wave length, see equation 2.1. The amount of water is constant so wave height increase if wave lengths decrease, resulting in steeper waves. If a wave becomes too steep breaking will occur. Depending on waves and geometry of the structure different breaker types can occur, often described by the Iribarren number ξ :

$$\xi = \frac{\tan(\alpha)}{\sqrt{H/L}} \quad (2.3)$$

Where α is the slope angle and H/L is the deep water wave steepness. The different breaker types and the corresponding Iribarren number are shown in figure 2.4.

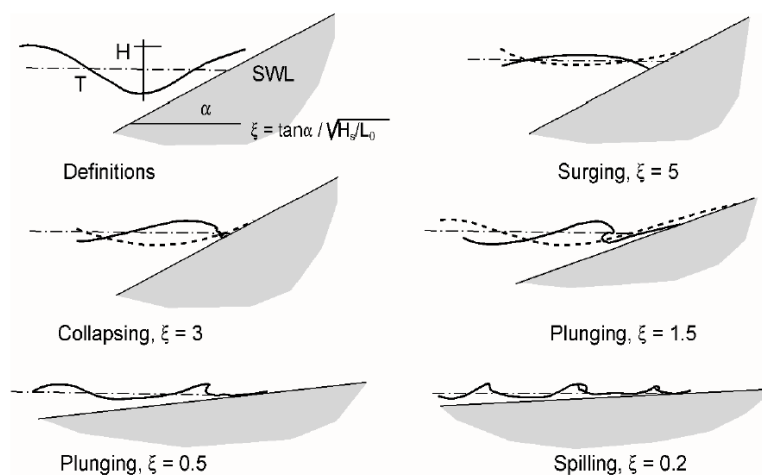


FIG. 2.4: Breaker types, Schiereck (2001).

Wave motion on a structure can be divided into two main groups, breaking waves ($\xi < 2.5 - 3$) and non-breaking or surging waves ($\xi > 2.5 - 3$). Both type of waves will result in a different loading. Breaking waves dissipate energy by turbulence, surface rollers or a jet-like impact on the surface. A jet results in relatively high local force, especially in case of an impermeable outer layer.

Strongly related to the breaker type is the wave run-up and run-down. Run-up is defined as the highest water level on a slope during a wave, run-down the lowest level both are measured vertically with respect to still water level, see figure 2.5. Due to the dissipation of energy in

turbulence breaking waves will have a reduced run-up and run-down compared to surging waves. Besides the breaker type the magnitude of run-up depends on surface roughness, permeability and shape. An impermeable smooth surface will result in the largest run-up and run-down.

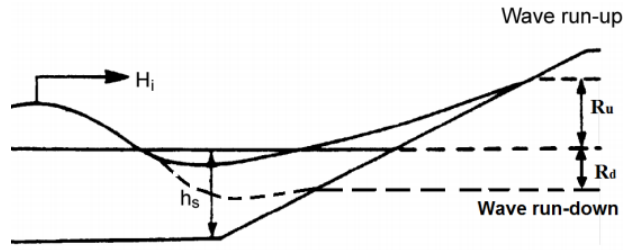


FIG. 2.5: Schematic representation of wave run-up and run-down, Prashanth et al. (2012).

Internal water motion

In case of a (partly) permeable breakwater there is a water table present inside the core. The height of this internal water table will be influenced by the water level outside the breakwater, the internal water table will follow outside water level changes. However a gradient is necessary to force the water in and out of the breakwater core due to flow resistance of the structure. As a result of this resistance the internal water table follows the external water level with a certain delay and the amplitude of the movement is less. The decrease of the amplitude is called damping, from now on damping is defined by $\zeta = 1 - H_c/H_i$, H_c is the wave height in the core and H_i the incoming wave height. The amount of phase shift and damping is related to the flow resistance of the breakwater, appendix A discusses flow of water through porous media.

Wave induced pressures

Besides changing water levels waves can cause movement of water inside a breakwater. Through the permeable parts of a breakwater wave energy will penetrate into the breakwater resulting in fluctuating pore pressures. As waves are transmitting through the breakwater energy dissipates due to turbulence and friction. Oumeraci and Partenscky (1991) proposed a model for wave induced pore pressure damping inside rubble mound breakwaters. An exponential damping was found empirically described by the following formula:

$$P_x = P_0 e^{-\delta(2\pi/L')x} \quad L' \approx L/\sqrt{D} \quad (2.4)$$

Where P_x is the pore pressure at a distance x from the interface, P_0 is the pressure at the interface. L' is the wave length inside the breakwater, which is related to L the wave length outside the breakwater, and D a coefficient describing the increase of seepage length as a result of flow around grains, the empirical found value $D \approx 1.4$, δ is the damping coefficient. A sketch of the pore pressure damping according to this model is presented in figure 2.6.

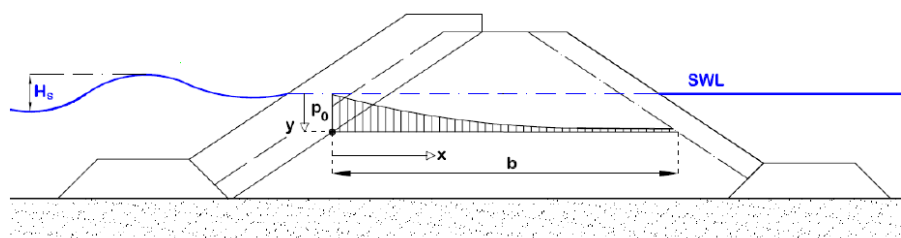


FIG. 2.6: Sketch of pore pressure damping in a core, Vanneste and Troch (2010).

2.4 Lifting of the asphalt layer

Movement of water both inside and outside the breakwater result in forces acting on the asphalt slab. There are two main cases resulting in a lifting force.

First case is the phase shift of tidal waves inside the breakwater like explained in the previous section. In case of a dropping tide the phase shift results in a higher internal water level compared to the water level outside. Due to the fact the asphalt slab is impermeable this results in an upward forcing, see figure 2.7. The magnitude of the acting force is linear related to the water level difference, the water level difference is related to the flow resistance of the permeable parts of the breakwater.

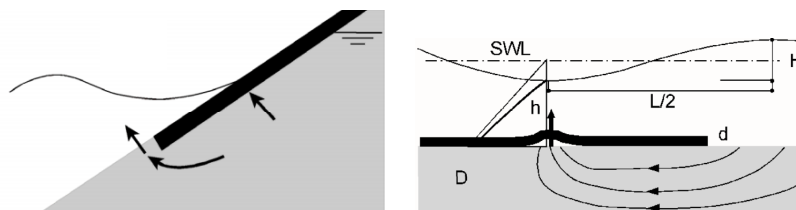


FIG. 2.7: Lifting forces due to water level difference (left) and passing wave (right), Schiereck (2001).

Second case is an incoming wave, at the moment the head of the wave is over a relatively permeable part of the breakwater and the trough is over an impermeable part. In this case a lifting pressure will occur due to pressure differences. The right part of figure 2.7 illustrates this mechanism for a horizontal impermeable layer.

An important parameter to determine the magnitude of the upward pressure is the leakage length λ which is defined as the length of revetment in which the flow resistance in the top layer and filter layer are the same. The leakage length is defined by:

$$\lambda = \sqrt{\frac{k_f D_f D_t}{k_t}} \quad (2.5)$$

Where k are the permeability of the filter and top layer, and D is the layer thickness. In case of an impermeable slab the leakage length would be infinitely large, or the length of the slab in practice. Due to this large λ exchange of water is limited. Like in the previous case flow resistance of the permeable parts influences the magnitude of the upward force, but also wave length and in case of a sloped impermeable layer the run down are of importance.

Chapter 3

IJmuiden breakwaters

Like described in the introduction of this thesis the breakwaters of IJmuiden are of a unique design. The application of stone asphalt as a cover was revolutionary at the time, and not often applied afterwards. This chapter treats the design, construction method and used materials for the IJmuiden breakwaters.

3.1 Breakwater layout

The layout of the breakwater was optimized in order to minimize wave penetration and currents due to tides and wind across the approach channel. This resulted in an asymmetric design, the southern breakwater extending furthest into sea. Figure 3.1 shows the layout of the breakwaters including distance indicators.



FIG. 3.1: *Breakwater layout, GeoWeb (2014).*

3.2 Cross sections

As a result of bathymetry and orientation of the breakwaters wave loading of the southern and northern breakwater will not be the same. The southern breakwater is extending further into the sea and therefore wave loadings are expected to be bigger, last section of this chapter will treat the hydraulic conditions more elaborately. The cross section of the breakwaters are adopted to the hydraulic conditions. Resulting in differences between the northern and southern breakwater, as well as differences along each breakwater.

Both breakwaters can roughly be divided into two parts, a part near the head and the trunk. Biggest difference between the heads and trunks is the slope of the asphalt slab, during construction it became clear more gentle slopes, at both the sea and harbour side, were needed near the heads of the breakwater in order to withstand the wave loading.

Cross sections presented below are the constructed cross sections, changes to these cross sections as a result of damages or siltation are treated in chapter 6. The design of the cross section is based on information of GeoWeb (2014) and Kuiper and van Gent (2006). GeoWeb (2014) performed measurements on behalf of RWS with boat and air based equipment, aim of these measurements was to get insight in the current shape of the breakwater compared to the original design and the magnitude of sedimentation near the toe structure of the breakwater. Kuiper and van Gent (2006) performed scale model test into the stability of the armour layer and toe structure.

Note, for a easy comparison between the different breakwater cross sections the seaward side of all cross sections is located at the left.

3.2.1 Breakwater heads

Shape of both the northern and southern breakwaters near the head is nearly identical. Biggest differences are the crown height and the bed level in front of the breakwater. Figures 3.2 and 3.3 show both cross sections.

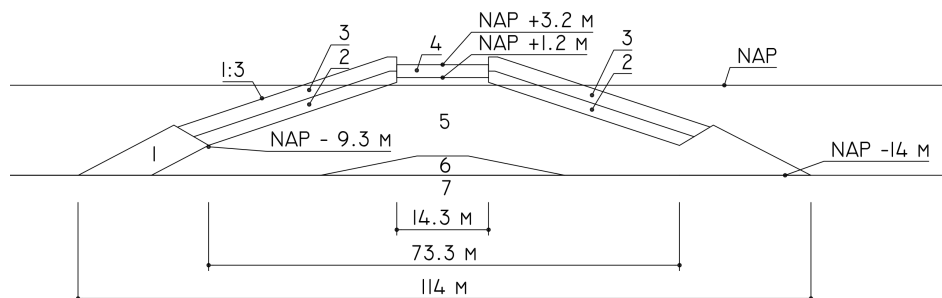


FIG. 3.2: Cross section northern breakwater head.

Numbers in the drawing indicate the different parts of the breakwater; 1 indicates the toe structure, 2 the 2 – 2.25 m thick stone asphalt slab, 3 the armour layer, 4 the concrete crown element, 5 the core, 6 the pebbles and 7 is the sand bed supporting the breakwater. Due to the similar location of all elements in the cross sections presented below the indicating numbers are left out in order to make the sketches more clear.

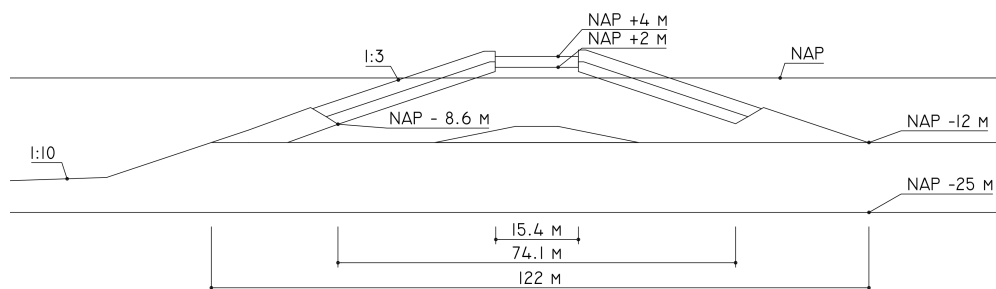


FIG. 3.3: *Cross section southern breakwater head.*

At the southern breakwater head the slope of the foreshore is 1:10 until the NAP -25 m depth contour is reached.

Mattresses were placed between the supporting sand layer and the toe structure to prevent washing out of the sand bed. These mattresses are believed to have no significant influence on the wave damping and are therefore not treated in this report.

3.2.2 Breakwater trunks

Cross sections of the trunks of both breakwaters are not constant over the entire length. Selecting the normative cross section is a combination of hydraulic loading and strength of the cross section. Near the head the asphalt slab has a constant slope, nearer to the shore a berm is installed. This berm is believed to improve stability of the asphalt slab. Near to the head hydraulic load conditions are expected to be largest, therefore the cross sections closest to the head with a steeper 1 : 1.75 slope are selected to be the normative cross sections representing the trunk sections of the breakwaters. For the northern breakwater this cross section is located at 1,900 m, for the southern at 3,000 m, see figure 3.1 for the location of these cross sections. The cross sections are shown in the figures below.

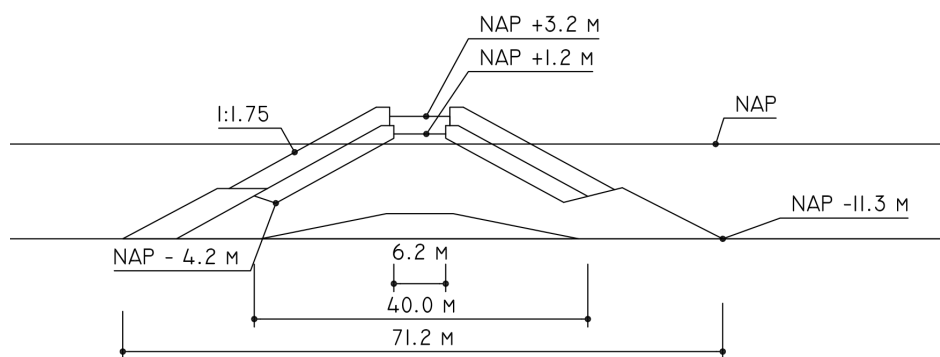


FIG. 3.4: *Cross section northern breakwater trunk.*

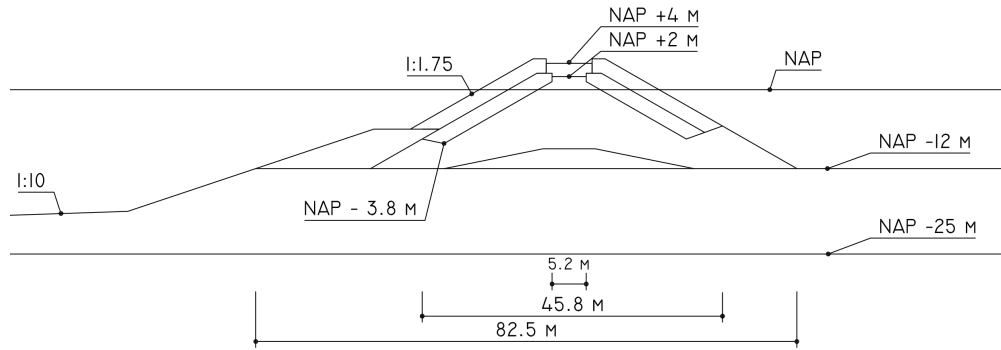


FIG. 3.5: Cross section southern breakwater trunk.

3.3 Materials

Like indicated in the previous section each cross section can be divided into seven parts; a stone asphalt slab, concrete crown element, pebble core, core, toe, armour layer and a supporting sand bed. These materials can be divided into two groups, permeable impermeable materials.

Due to the large dimensions of both stone asphalt slabs and concrete crown element these elements are assumed impermeable. All other parts are permeable media, the grading, median grain diameter d_{50} and porosity n are presented in the table below. The diameter of the sand bed is based on information provided by Northsea-atlas (2014) all other diameters are based on the report by Kuiper and van Gent (2006).

TAB. 3.1: Grading, stone diameter and porosity of construction materials.

	Grading	d_{50} [m]	n
Armour	-	2.20	0.30
Toe	1-6 tonne	1.31	0.38
Core	300-1,000 kg	0.75	0.38
Pebble core	40-110 mm	0.095	0.38
Sand	125-250 μm	$0.22 \cdot 10^{-3}$	0.38

3.3.1 Stone asphalt

Stone asphalt has two main ingredients, mastic and aggregates. Mastic bounds together the aggregates and provides cohesiveness and tensile strength, the aggregates form a stone skeleton, providing resistance against pressures and prevent the mixture from settling into the core.

The asphalt slab is composed of three different asphalt layers. First a mixture was cast directly on the core to stabilise it, second the main stone asphalt layer was cast, this layer was covered with a third layer of asphalt. Mixtures of the first and last asphalt layer are believed to be relatively constant over both breakwater. Aggregates in the first layer consist of relatively small stones 1 – 10 kg, the aggregate in the top layer was sand to provide a smooth surface. For the main stone asphalt layer there is not one single mixture. Due to damages during construction the mixture was altered numerous times in order to create a stable structure. Biggest change was

selecting a different mixture for the area above and below the still water level. In the underwater part of the breakwater a stone weight of 10 – 60 *kg* was used, for the part above water 1 – 10 *kg* were selected, Davidse (2012).

Current state of the asphalt

The current state of the asphalt is hard to predict, both thickness and quality might vary substantial along the breakwaters. Density and thickness of the asphalt layer make it impossible to perform measurements with sonar equipment. Therefore drilling cores is the only option to get insight in the amount and quality of the stone asphalt present on the breakwaters. Length of the breakwater, presence of armour units and the asphalt partly being submerged make a complete measurement of the asphalt slab expensive and time consuming.

In order to get insight in the quality of the asphalt slab two cores were drilled in 2004. One core showed high quality asphalt with enough mastic providing a cohesive bound. One core showed low quality asphalt, there was not enough mastic to provide cohesiveness between the aggregate. Still the quality of the asphalt layer is hard to predict, the low quality core could be the exception in a mainly high quality asphalt slab, or the other way around. Also the research did not provide any information about the amount of asphalt present. These uncertainties will have a great influence on determining the strength of the asphalt slab.

3.4 Construction method

The breakwaters were constructed using both land and water based equipment, the underwater part of the breakwater is mainly construction using stone dumping vessels. The above water part is constructed using cranes on jack up rigs. Material is supplied by trucks driving over the already constructed breakwater, see figure 3.6. Two cranes on the jack up rigs performed profiling of the core. Since the core consists of riprap of 300 – 1000 *kg*, it is sensitive to wave attack, mild waves might already change its profile. Therefore it was important the core was covered as fast as possible after profiling to minimize the effects of wave attack. First the core was cover with a special stone asphalt mixture, consisting of small stones. This mixture penetrated into the top layer of the core in order to provide some wave resistance.

The first stabilizing asphalt layer is not strong enough to resist waves close to design waves. Therefore this layer is again covered as fast as possible. The next stone asphalt layer is about 2 *m* thick and cast in the same manner as the first layer. Afterwards the stabilizing toe structure, consisting of 1 – 6 tonne stones, is placed using a side dumping vessel.

Last part to be installed were the crown elements consist of large prefabricated H shaped concrete profiles. The profiles were placed on top of the breakwater and concrete was cast in the volume between the profiles resulting in a 2 *m* thick concrete cover. Last step in construction was casting the final covering asphalt layer providing a smooth asphalt surface and an impermeable connection between the asphalt slab and crown element.

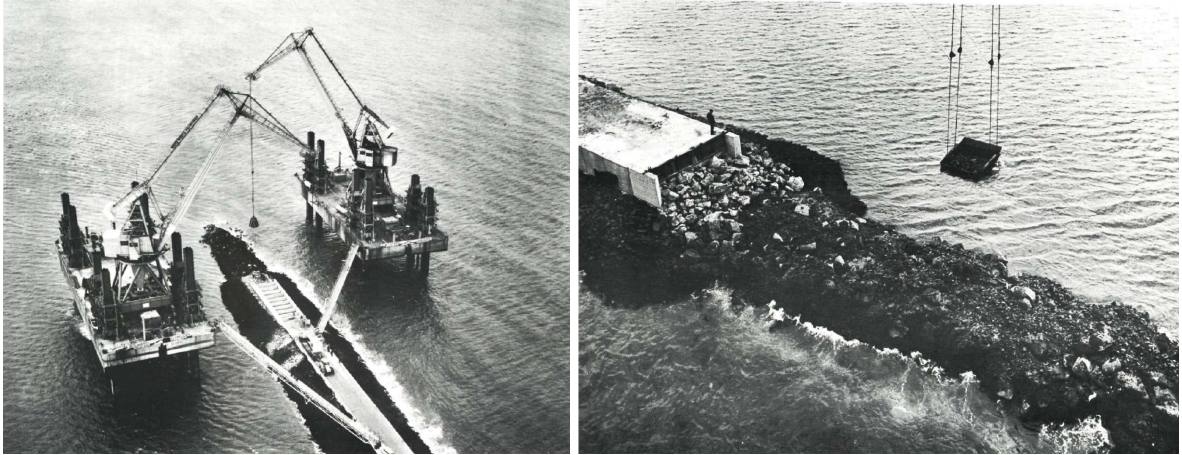


FIG. 3.6: *Picture of the construction of the IJmuiden breakwaters, Davidse (2012).*

3.5 Hydraulic boundary conditions

The hydraulic boundary conditions will vary along the breakwater due to the surrounding bathymetry and orientation of the breakwater. Smale and Groeneweg (2012) performed research into the normative hydraulic boundary conditions at different locations along the breakwater. Wave heights were expected to be the decisive parameter for the failure probability of the breakwater, this parameter was leading for drafting of the decisive hydraulic conditions. The table below shows the hydraulic boundary conditions with a exceedance frequency of once every 50 years. A more elaborate description of this research and the hydraulic boundary conditions used in this report can be found in appendix C.

TAB. 3.2: *Hydraulic boundary conditions for the normative cross sections.*

	H_s [m]	T_p [s]	h [m]
North head	5.46	9.1	+3.37
North trunk	4.75	8.98	+3.37
South head	5.55	8.61	+3.17
South trunk	5.83	8.76	+3.17

Where H_s is the significant wave height, T_p is the peak wave period and h is the water level relative to NAP.

Note to these wave conditions is the large difference with the wave conditions based on Kieftenburg (2006). A significant wave height around 7.5 m was found for the breakwaters of IJmuiden. Difference can be partly explained by the method used to determine the wave conditions.

Chapter 4

Measured damping

Like described in chapter 2, upward pressures underneath the asphalt slab are the driving force for lifting of the asphalt and therefore the driving force for failure of the breakwater. Upward pressures are a result of wave energy transmitting into the breakwater core, due to friction and turbulence a certain amount of wave energy dissipates resulting in wave damping. This chapter treats wave damping measured in the field by van Hoven (2012) and van Hoven (2014).

4.1 Measurement setup

In order to get a better insight into the failure probability of the breakwaters RWS asked Deltares to perform measurements into wave induced pressures in the core of both breakwaters. Near the heads of both breakwaters pressure buildup was measured, figure 4.1 shows the configuration of the pressure sensors.

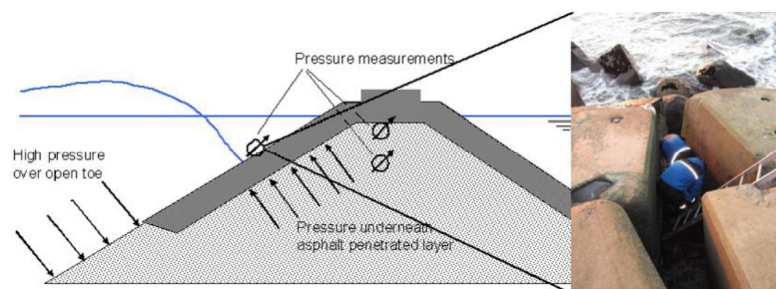


FIG. 4.1: Configuration of the pressure sensors installed near both breakwater heads, van Hoven (2012).

Each set of sensors consists of 4 sensors, two in the core and two on the seaward slope between the armour layer. Sensors in the core material were installed on different heights relative to still water, one directly beneath the crown element, to be referred to as the shallow pressure sensor and one 3.8 m below the crown element referred to as the deep pressure sensor. To install the pressure sensors a hole was drilled through the crown element and core material in which a perforated tube containing two pressure sensors was installed.

In an ideal situation wave pressure in front of the breakwater would be measured right above the toe element. However the toe is submerged and hard to reach because of the armour units, therefore the pressure sensors were installed on the seaward slope as low as working conditions allowed.

Like described in section 2.4 two situations will result in a pressure difference over the asphalt slab. Dropping tide and a wave at maximal run down. Movement of water was measured in both time scales. Damping is defined as $1 - H_c/H_i$, where H_c is the wave height inside the core and H_i is the incoming wave height.

4.2 Damping of tide

During the research by van Hoven (2012) the pressure inside both breakwater was measured during a tide cycle. The hydraulic heads were averaged over 5 minute intervals to eliminate the influence of wind waves. The results for both the deep and shallow pressure sensor in the core of the breakwater and the sea water level on one tide cycle on 9 December 2012 are plotted in figures 4.2 and 4.3.

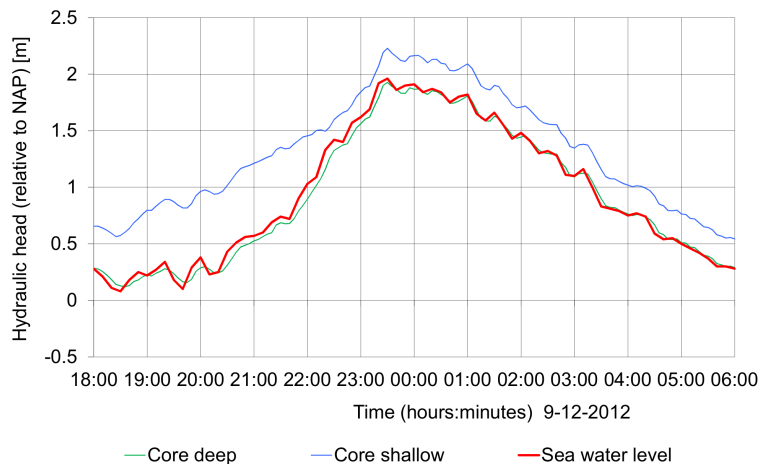


FIG. 4.2: Measured tidal wave in and on the northern breakwater, data by van Hoven (2012).

The hydraulic head measured by the deep pressure sensor in the northern breakwater is nearly identical to the hydraulic head outside the breakwater, the tidal wave is nearly undamped and there is only a minor phase shift. The shallow pressure sensor located right underneath the crown element at NAP+1.2 m measured pressure fluctuations before the outside water level reached NAP+1.2 m. This indicates the sensor measured air pressure fluctuations. This is only possible if air is trapped underneath the asphalt slab and crown element. Chapter 5 will evaluate the influence of this trapped air on the movement of water inside the breakwater.

The hydraulic head in the southern breakwater as a result of tidal movement is in contrast to the northern breakwater damped and a phase shift is present. On average a damping of the tide of $\pm 20\%$ in the southern breakwater was found by van Hoven (2012). The shallow pressure sensor located right beneath the crown element at NAP+2.0 m also measured a small fluctuation of the air pressure, however this fluctuation is significantly smaller than the air pressures measured

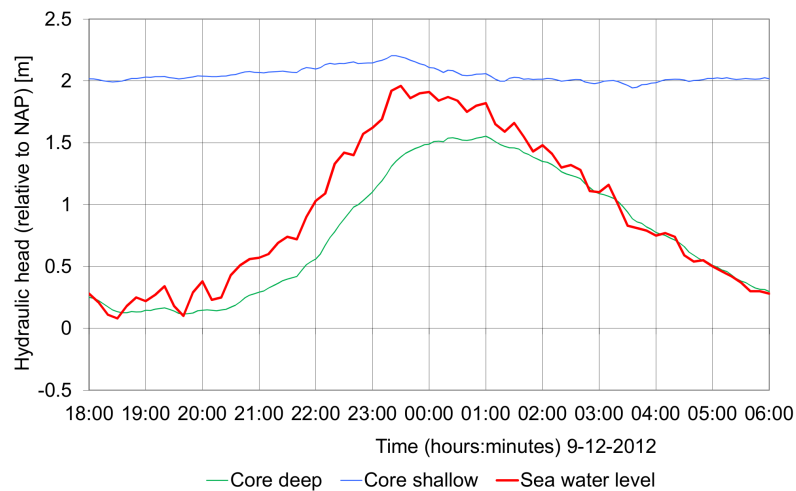


FIG. 4.3: Measured tidal wave in and on the southern breakwater, data by van Hoven (2012).

in the northern breakwater, indicating the air in the southern breakwater is flowing out of the core more easily.

4.3 Damping of wind waves during a mild storm

The report of van Hoven (2012) is based on measurements from February 2012 till December 2012, during this period only one major storm event occurred, however the equipment was damaged by the waves therefore the measured data lack major storm events. One mild storm was measured on the 15th of February 2012. During the peak of the storm the still water level was NAP+1.45 m waves had a significant wave height of $H_s = 2.9$ m and a mean wave period $T_m = 9$ s. Fluctuations of the hydraulic heads as a result of these waves are shown in figure 4.4 and 4.5.

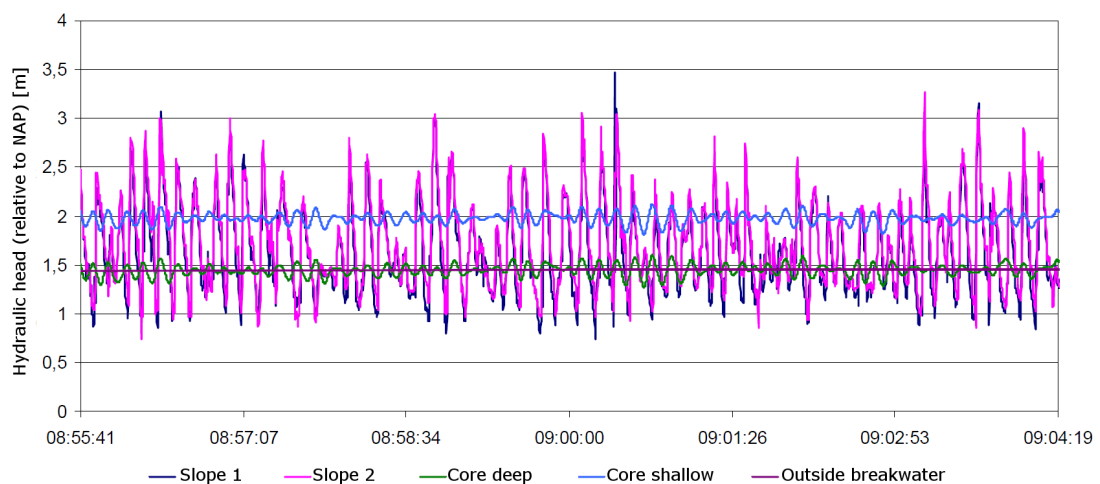


FIG. 4.4: Measured wind waves in and on the northern breakwater during a mild storm, van Hoven (2012).

In the northern breakwater there is clearly a response to wave loading. A fluctuation in the hydraulic head in the order of 0.25 m was measured in the core. Damping of wind waves is determined to be about $70 - 90\%$ for these mild storm conditions.

The wave response of the internal water level measured by both the shallow and deep sensor is nearly identical, however the equilibrium value around which the measurements are fluctuating is different. Both pressure sensors are located underneath the still water level outside of the breakwater, respectively $\text{NAP} - 2.6\text{ m}$ and $\text{NAP} + 1.2\text{ m}$. The hydraulic head measured by the deep pressure sensor fluctuates like expected round the still water level outside the breakwater, $\text{NAP} + 1.45\text{ m}$, the measurements of the shallow sensor fluctuate round $\text{NAP} + 1.95\text{ m}$. The extra 0.50 m of pressure height could be explained by trapped air.

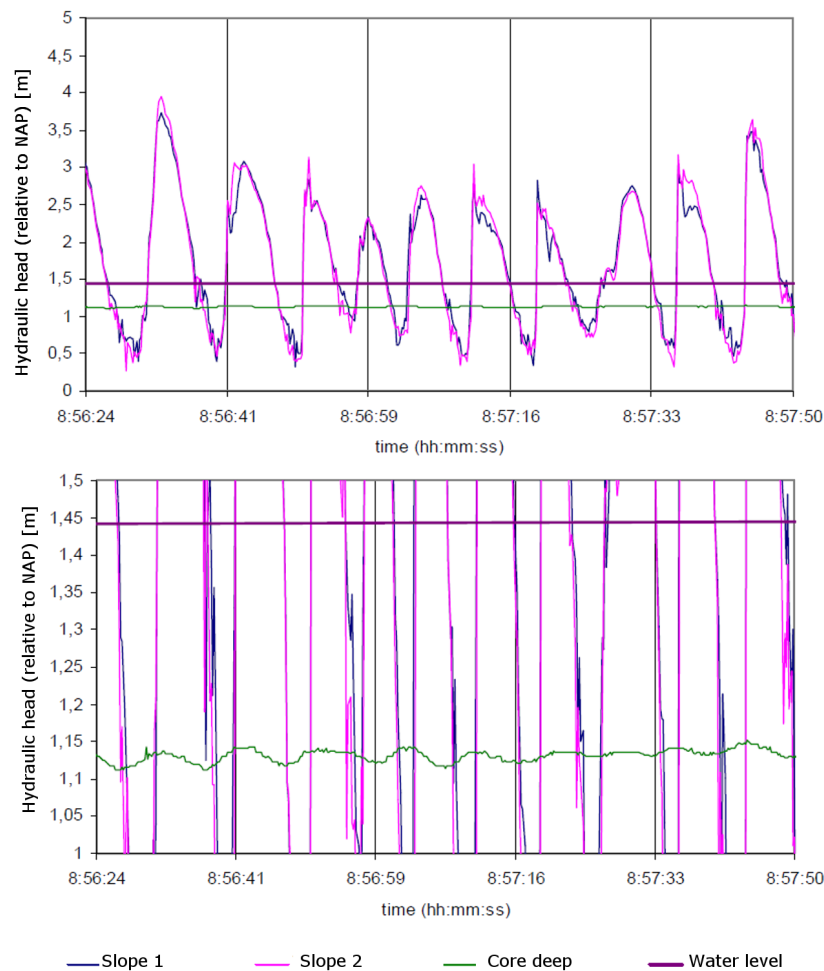


FIG. 4.5: Measured wind waves in and on the southern breakwater during a mild storm, van Hoven (2012).

In the southern breakwater the measured waves are significantly lower compared to the northern breakwater. The response inside the southern breakwater is divided in two plots with different vertically scaled axes to make it more clear. The upper plot shows the whole fluctuation of the water surface outside the breakwater, the lower plot zooms in on the fluctuation of the hydraulic head inside the breakwater. A fluctuation of the hydraulic head in the order of $1 - 2\text{ cm}$ was measured. The determined damping of wind waves in the southern breakwater is about 99% for $H_s = 2.9\text{ m}$, $T_m = 9\text{ s}$. Based on the tidal damping measured a total damping was expected.

4.4 Damping of wind waves during a severe storm

Measurements continued in both breakwaters after the report of van Hoven (2012), using the same equipment described in section 4.1. On the 5th of December 2013 a severe storm hit the Dutch coast. A water level of NAP+2.93 m, a significant wave height of $H_s \approx 5$ m and a mean wave period of $T_m = 7.9$ s were measured. Again wave directions were not included in the measurements, the wind was measured and shifted from West-southwest to West-northwest. The internal wave action in both breakwaters during the peak of the storm is plotted in figures 4.6 and 4.7.

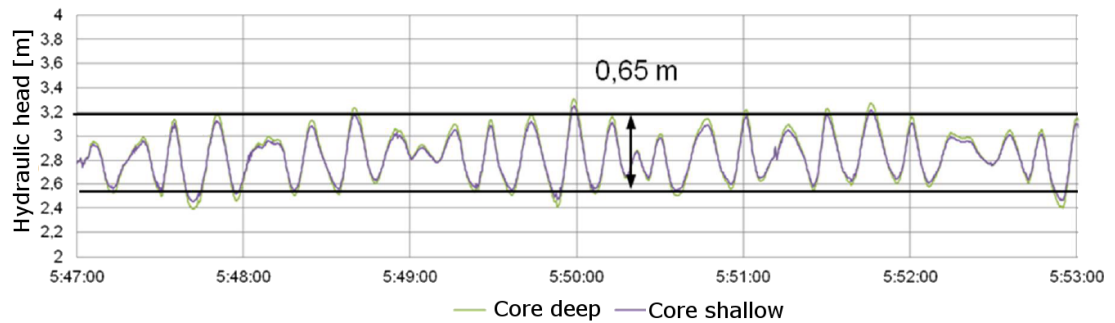


FIG. 4.6: Measured wind waves in the northern breakwater during a severe storm, van Hoven (2014).

Wave action in both breakwaters is significantly larger than during the measurements described in the previous section. Wave damping in the northern breakwater is concluded to be 62 – 87% which is in the same order of magnitude as previously determined. A difference of 3 – 5 cm of hydraulic head was measured between the shallow and deep pressure sensor. No phase shift between both sensors was measured ruling out the presence of additional damping between both sensors. Trapped air is believed to cause this difference.

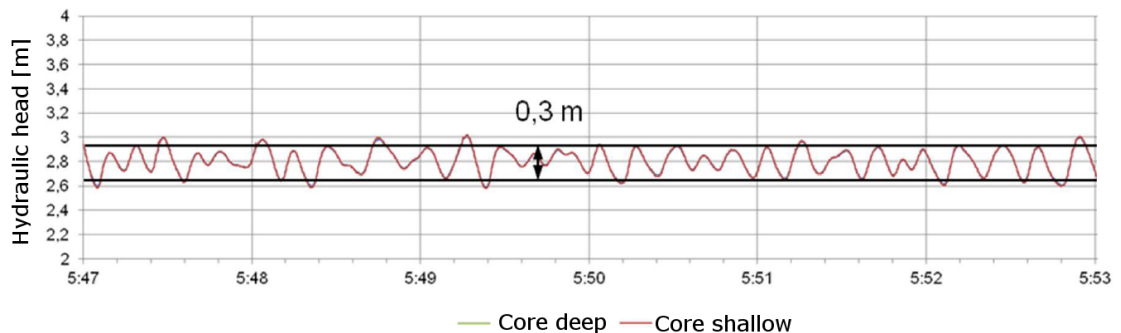


FIG. 4.7: Measured wind waves in the southern breakwater during a severe storm, van Hoven (2014).

Damping in the southern breakwater is 82 – 94%, which is significantly lower than the previous 99%. Main reason for this difference is believed to be caused by the water level. During the measurements in 2012 the water level was lower than the bottom of the crown element. During the measurements in 2013 the water level was higher than the bottom of the crown element. The height of the water level relative to the bottom of the crown element highly influences the manner wave energy transmits through the breakwater, this will be treated in section 9.1

4.5 Conclusions

Field measurements performed by Deltares show a bigger damping of both tide and wind waves in the southern breakwater. Furthermore the amount of damping in the northern breakwater is relatively constant for different hydraulic conditions, during a mild storm a damping of 70 – 90 % was measured, a severe storm resulted in a damping of 62 – 87 %. Influence of the hydraulic conditions on the amount of damping in the southern breakwater is stronger; measurements during the same storm events resulted in a damping of 99 % and 82 – 94 % for respectively the mild en severe storm.

The difference in damping indicates the presence of a damping mechanism in the southern breakwater. Determining the mechanism present and the amount of damping during design storm events is essential to be able to determine the stability of the asphalt slab.

The pressure sensor placed directly underneath the northern crown element measured fluctuations of air pressures, indicating air is trapped underneath the asphalt slab and crown element. The amount of trapped air is significantly larger during mild storm conditions compared to the severe storm conditions. The influence of this trapped air on the damping and whether this can cause the difference in damping is discussed in the next chapter.

Chapter 5

Trapped air

The presence of trapped air underneath the asphalt slab and crown element at the measurement location at the northern breakwater is concluded in chapter 4. The trapped air will influence the movement of water in the core of the breakwater, and therefore influence the amount of damping. This chapter outlines the effect of the trapped air in a quantitative manner, a reasoning will be presented whether this trapped air has a positive or negative influence on the internal water movement.

5.1 Storage inertia resistance system

A model representing the breakwater is used to get insight in the influence of the different parameters on the movement of water inside the breakwater due to wave loading. The breakwater is split into two parts, a pipe and a storage basin. Figure 5.1 shows a cross section of the breakwater and the representing model.

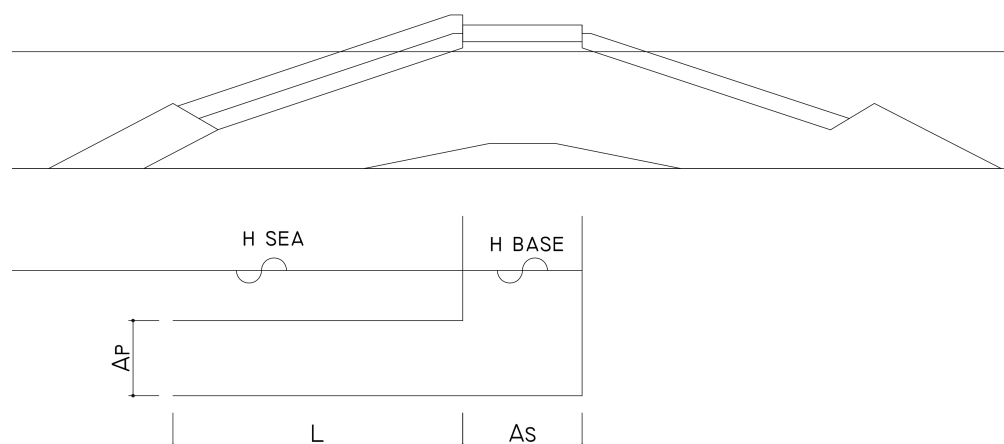


FIG. 5.1: *Storage inertia resistance model representing the northern breakwater head.*

There are a couple of important assumptions leading to this model. First there is no water exchange at the harbour side of the breakwater, in other words no wave transmission through

the breakwater. Second water is incompressible and the density is constant over the entire model. At last the water level inside the storage basin is flat, this simplification is justified since the wave length will be considerably longer than the width of the crown element. These simplifications lead to the following equation of motion:

$$A_s I \frac{d^2 h_b}{dt^2} + A_s Fr \frac{dh_b}{dt} + h_b = h_{sea} \quad (5.1)$$

$$I = \int_0^L (1/gA_p) dx \quad (5.2)$$

Where A_s is the storage area and A_p the area of the pipe, I is the inertia term, h_b is the water level in the basin, Fr is a friction coefficient, L is the length of the pipe and h_{sea} is the water level at sea.

The model will not be used to calculate the exact movement of water inside the breakwater in order to determine the forcing of the asphalt slab. The simplifications are of too great influence to be able to do this. Instead the model will be used to quantitatively reason the influence of the different parameters, especially the presence of trapped air. Main focus will be on the natural frequency of the system. The ratio between the natural frequency of the system and the frequency of the loading is of great importance for the magnitude of the response.

5.2 Influence of porous material

The breakwaters of IJmuiden consist of porous media. Therefore the pipeline and basin can not be described by hollow elements, porous media should be implemented. Due to the presence of porous media all three terms will be influenced, the storage area, inertia and friction term.

The presence of impermeable parts in the basin, stones in this case, will reduce the storage capacity. The same amount of water flowing in or out will result in a bigger fluctuation of the water level, since water can only occupy the pores. The nett storage area is the gross storage area times the porosity n .

Inside porous parts the breakwater turbulent flow or Forchheimer flow is expected, see appendix A. Therefore the flow resistance coefficient Fr depends on the flow velocity. Resulting in a non-linear differential equation. Later on in section 5.4 one can see the friction term does not influence the natural frequency, since the natural frequency of the system is the main focus of this chapter the friction term will not be further discussed in this section.

The inertia term is influenced by the presence of porous media in a way similar to the storage area, the amount of water present in the pipe is reduced. Second effect of the porous media on the inertia term is a mechanism called added mass. Due to the porous media it takes more effort to accelerate the same amount of water through a porous media. This mechanism is described in more detail in appendix A.3.

5.3 Influence of trapped air

The model presented in figure 5.1 assumes an open top of the basin. Trapped air between the water and crown element will exert a resisting force to both dropping and rising water levels. To take this resistance against motion into account the h_b term in equation 5.1 should be multiplied with a coefficient. To determine this coefficient air is modelled as an ideal gas, which makes Boyle's law applicable:

$$PV = nRT \quad (5.3)$$

Where P is the pressure, V is the volume of the gas, n is the amount of substance, R is the gas constant and T is the temperature. Assuming the amount of substance and temperature are constant the following relation can be derived:

$$P_1V_1 = P_2V_2 \quad (5.4)$$

The storage basin in the representing model has straight vertical walls therefore the volume of air is inversely proportional to the internal water level. The air pressure is proportional to the internal water level and is expressed by:

$$P_{air} = \frac{d_{air}}{d_{air} - h_b} P_{atmos} \quad (5.5)$$

Where P_{air} is the pressure of the air, d_{air} is the height of the air bubble before compression and P_{atmos} is the atmospheric pressure. Combining the resisting pressure as a result of trapped air and the normal resistance of the water against elevation, due to gravity, results in the following equation, where c_a is the coefficient should be added to the equation of motion, equation 5.1.

$$\rho_w g h_b + \Delta P_{air} = c_a \rho_w g h_b \quad (5.6)$$

$$\rho_w g h_b + \left(\frac{d_{air}}{d_{air} - h_b} - 1 \right) P_{atmos} = c_a \rho_w g h_b \quad (5.7)$$

$$c_a = (\rho_w g h_b + \left(\frac{d_{air}}{d_{air} - h_b} - 1 \right) P_{atmos}) / (\rho_w g h_b) \quad (5.8)$$

The added resistance coefficient depends on the ratio between the amount of trapped air and the amplitude of the water movement inside the basin. This results in a non-linear equation of motion which is given by:

$$A_s I \frac{d^2 h_b}{dt^2} + A_s F r \frac{dh_b}{dt} + c_a h_b = h_{sea} \quad (5.9)$$

5.4 Natural frequency

The natural frequency of the system is important due to the possibility of resonance to occur. Resonance occurs in case the natural frequency of the system and the frequency of the loading are the same or close, and the level of damping is lower than a critical value. Resonance causes extreme load cases see figure 5.2, therefore it should be avoided. This section will focus on the natural frequency of the system.

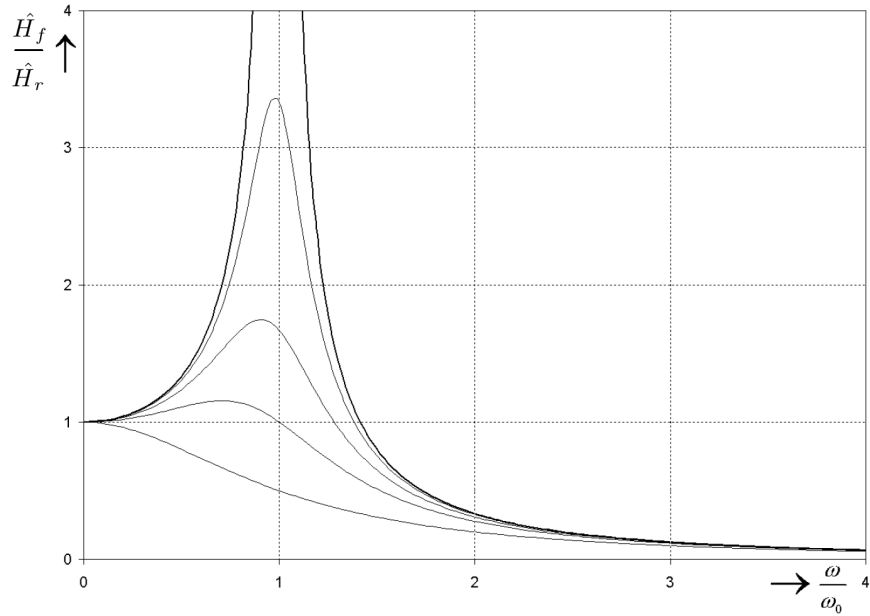


FIG. 5.2: Reaction to a harmonic excitation in case of resonance, Blauwendraad (2008).

Where \hat{h}_f and \hat{h}_r are the amplitudes of the forcing and the response, ω is the frequency of the loading and ω_0 is the natural frequency of the system. The different lines in the plot are for different levels of damping and are given by:

$$\frac{\hat{h}_f}{\hat{h}_r} = \frac{1}{\sqrt{\left(1 - \frac{\omega^2}{\omega_0^2}\right)^2 + (\omega A_s F r)^2}} \quad (5.10)$$

The natural frequency of the system is, like a spring-mass system, not influenced by the friction coefficient and can be determined using the undamped equation of motion:

$$A_s I \frac{d^2 h_b}{dt^2} + c_a h_b = 0 \quad (5.11)$$

The general homogeneous solution is given by:

$$h_b = A \cos(\omega t + \phi) \quad (5.12)$$

In this case A represents the amplitude of the water level and ω the angular frequency. Substituting this equation into equation 5.11 results in:

$$-A_s I A \omega^2 \cos(\omega t + \phi) + A c_a \cos(\omega t + \phi) = 0 \quad (5.13)$$

From this equation the natural frequency can be determined and is given by:

$$\omega_0 = \sqrt{\frac{c_a}{A_s \cdot I}} \quad \omega_o = 2\pi/T_0 \quad (5.14)$$

Where T_0 is the natural period of the system. One can conclude the natural frequency is influenced by the added coefficient representing the trapped air. The ratio between the amount of trapped air and amplitude of the movement of the water inside the breakwater is therefore influencing the natural frequency of the system. If this ratio becomes smaller, c_a becomes bigger and ω_0 becomes bigger.

5.4.1 Natural frequency IJmuiden breakwaters

Using the measured wave damping in the northern breakwater shown in figure 4.4 the response period of the system can be estimated by dividing the total measured time by the amount of waves. In this case the measured time was 578 seconds with a total of 57 waves, resulting in a period of just over 10 seconds, well in the range of expectable wave periods. Therefore resonance can not be ruled out.

From equation 5.14 one can conclude trapped air enlarges the natural frequency of the system. Therefore removing the trapped air will result in a smaller natural frequency and a bigger natural period. In order to get an idea of the magnitude of the influence of trapped air, the coefficient c_a is determined using the conditions present during measurements in the northern breakwater, see section 4.3. During measurements the thickness of the trapped air was 0.5 m and the wave height in the core of the breakwater was in the order of 0.2 m. Filling in those numbers in equation 5.8 results in a coefficient c_a of around 40. Due to the square root the natural frequency of the system will be about 6.3 times smaller if there is no air in the system, resulting in a natural period of the system big enough to rule out resonance due to wind waves.

Level of airtightness

Two important comments should be placed concerning the numbers mentioned above about the influence of trapped air. First is the assumption of an airtight stone asphalt slab and crown element at the measured location in the northern breakwater. In case these elements or the connections between these elements are not airtight air will be able to flow out of the core reducing the affect of trapped air on the natural frequency. There are indications the breakwater is not perfectly airtight, measurements showed the air is able to escape on a tidal time scale.

The escape of air on a tidal time scale was implemented in the equations mentioned above by using the atmospheric pressure as the air pressure at an equilibrium water level inside the breakwater. This leads to the second comment, the influence of the trapped air could also be bigger in case the breakwater is airtight on a tidal time scale due to the fact the air is pressurized and the air pressure in an equilibrium situation will be larger than the atmospheric pressure.

Other cross sections

The level of airtightness might vary a lot over the length of the breakwaters. Due to the fact there are only two field measurements performed, one at each breakwater head, it is not possible to give an indication of the level of air entrapment at other parts of the breakwater.

The natural frequency, in case of a similar level of airtightness, of the different cross sections can be estimated by comparing the cross sections with the cross section of the northern head. Each breakwater is divided into a head and base section, cross sections and dimensions are presented in section 3.2.

Shape and dimensions of the southern breakwater head design are similar to that of the northern head, therefore a natural frequency close to that of the northern breakwater is expected. However the measured damping could have two origins which will be described in section 6.1, a lower asphalt slab which increases the inertia term due to a smaller flow area, or the presence of a sand layer increasing the friction term. First will lead to a unfavourable higher natural frequency second will have no influence on the natural frequency.

For both bases of the southern and northern breakwater the crown element is narrower resulting in a storage area of about half the size of that of the northern head. Due to the steeper stone asphalt slab the length of the pipe is reduced by about 1.7. Both effects will lead to a bigger natural frequency of about 1.5 – 2 times that of the northern breakwater, in case of a similar level of air entrapment.

5.5 Trapped air decreasing damping

Like indicated in figure 5.2 resonance increases the response of the internal water level and therefore decreases damping. Resonance is influence by the amount of friction present in the system and the ratio between the natural frequency of the system and the harmonic loading. Like described in the previous section the natural frequency of the breakwater system can be close or equal to the period of wind waves.

Due to the flow of water through porous media the friction coefficient Fr depends on the flow velocity. Combining this with the complex geometry of the breakwater make it hard to determine the total amount of friction, and thereby impossible to easily calculate whether the friction is large enough to prevent resonance to occur. Therefore a numerical calculation is performed on the cross section of the head of the northern breakwater, recreating the conditions present during field measurements, see section 9.1. From this calculation it was concluded trapped air reduced the amount of wave damping, therefore resonance can not be ruled out.

Besides the possibility of resonance the trapped air might have another negative effect on the forcing of the asphalt slab. Forcing of the asphalt slab is dictated by the pressure difference over the asphalt slab. In case of a high pressure in the breakwater core and a low pressure on the asphalt slab this forcing is biggest. Due to friction there will be a certain phase shift between high upward pressures inside and downward pressures on the asphalt slab. If the magnitude of the phase shift is half a wave period high internal pressure and low external pressure will coincide resulting in the highest forcing, if the phase shift is higher or lower forcing of the asphalt slab

will be lower. In case of trapped air the breakwater has an own frequency and the internal water level will oscillate with a different frequency than the loading. There is not a fixed phase shift between upward and downward pressures therefore high internal and low external pressures might coincide, resulting in a high load case. This changing phase shift is clearly visible in the measurements taken in the northern breakwater, figure 4.4.

5.6 Trapped air increasing damping

Trapped air might have a favourable influence on the amount of damping under certain hydraulic conditions. In case the water level is higher than the height of the bottom of the crown element the core of the breakwater is filled with water in case there is no trapped air. Water entering the core will not be able to flow into the core, therefore wave energy will transmit by a pressure wave through the breakwater. This pressure wave results in a nearly instant high pressure in the entire breakwater core, and little damping occurs, see section 9.1. In case of trapped air water is able to flow into the core resulting in a bigger damping.

During design storm conditions water levels are higher than the bottom of the crown element. The presence of trapped air during these events is uncertain due to the unknown airtightness of the breakwater.

5.7 Conclusions

The influence of trapped air on the magnitude of the damping is hard to predict and is highly influenced by the water level relative to the height of the bottom of the crown element. From the reasoning above one can conclude the presence of trapped air is unfavourable during relatively low water levels due to the possibility of resonance to occur, reducing the amount of damping.

On the other hand trapped air is believed to increase damping during relative high water levels. However during design storm conditions the presence of trapped air is uncertain, since the airtightness of the breakwater is unknown and might deviate over the length of the breakwater. Due to the uncertainty of trapped air being present during design storm conditions trapped air is not taken into account while determining the loading of the asphalt slab.

Despite the influence of trapped air on the movement of water inside the northern breakwater. The difference in damping measured between both breakwaters can not be addressed to only trapped air. An additional damping mechanism is therefore present in the southern breakwater. The next chapter introduces two possible damping mechanisms.

Chapter 6

Mechanisms causing damping

The trapped air in the northern breakwater described in the previous chapter will influence the movement of water. Whether damping increases or decreases depends on structural and hydraulic parameters. However not all differences in damping between both breakwaters could be caused by trapped air in the northern breakwater. Damping of tidal waves in the southern breakwater, see section 4.2, indicate the presence of an additional damping mechanism in the southern breakwater. This chapter will discuss two damping mechanisms that might cause the additional damping measured in the southern breakwater.

6.1 Wave damping mechanisms

Measurements indicating the presence of wave damping are only performed at two locations, one in each breakwater near the head. The large length of the breakwater make it very well possible the magnitude of damping is not the same over the entire breakwater. Therefore selection of damping mechanisms should include mechanisms causing only local damping instead of global.

The presence of an over two meters thick stone asphalt slab limits the flow of water into the core of the breakwater. Locally the slab might be damaged and might be slightly permeable, this local permeability is however assumed to be insignificant for the damping of waves. Due to the impermeable asphalt slab water can only flow through the toe structure and the sand bed underneath the toe structure. The toe structure will therefore be the prime area of interest for drafting damping mechanisms. Two different approaches are investigated, changes in the flow resistance of the toe, handled in section 6.2, and changes in the geometry handled in section 6.3. Influence of (parts) of armour units deposited near the toe of the breakwater is not taken into account, effect of these armour units is believed to be small and independent of the investigated damping mechanism.

6.2 Siltation of toe structure

Placement of a breakwater will influence the coastal dynamics in the surrounding area, especially in an area with a longshore sediment transport. At the Dutch coast the net sediment transport is directed northwards, resulting in a stream of sediment passing the southern breakwater. Development of the bathymetry as a result of the breakwaters is shown in figure 6.1, clearly there is interaction between sediment transport and the breakwaters, especially at the southern breakwater.

Sand rich water might enter the breakwater, due to friction flow velocities lower. Sediment transport rates are related to the flow velocity, lower flow velocities will result in lower sediment transport rates. A lower sediment transport rate will result in sand settling in the toe or core of the breakwater.

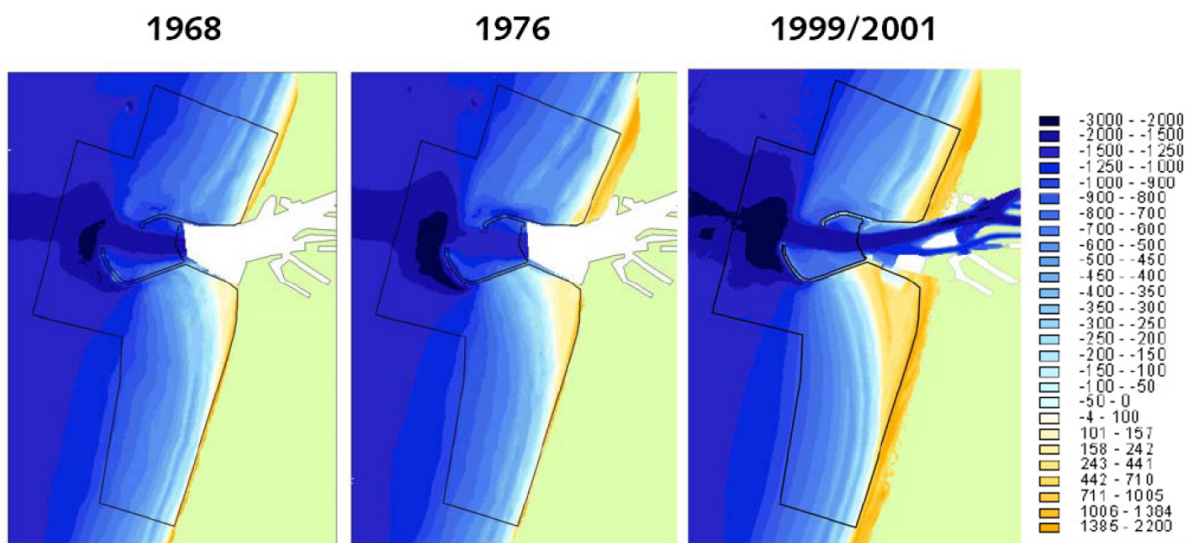


FIG. 6.1: Development of the bathymetry in the vicinity of the IJmuiden breakwaters, Luijendijk et al. (2011).

Different materials have different flow resistances. Generally water flows easier through materials with bigger diameters. Like presented in table A.2 for riprap of 1 – 6 tonne, the material the toe is constructed from, flow velocities are in the order of 1 m/s for sand in the order of 10^{-3} m/s. These numbers are only a rough indication but clearly flow velocities are lower in sand. Lower flow velocities through the toe result in less water exchange and a damping of the wave motion inside the breakwater.

These damping mechanisms will be evaluated by modelling layers of sand at the bottom of the toe structure. The thickness of the layer will be increased until the measured damping is reached. When a satisfying sand layer is found the stability of the sand layer during storm events is tested. It could be possible the sand is deposited during calm wave conditions and washed out of the toe structure during storm events, similar to the summer and winter profile of a beach. The stability of the sand inside the toe will be determined using open filter layer rules and pressure gradients and flow velocities occurring during storm events.

6.3 Deeper asphalt slab

The height of the toe structure and core underneath the stone asphalt slab is relatively small, the vertical distance between the sand bed and the asphalt slab is about 4 metres. A (local) reduction in height, will result in a reduction of water exchange and thereby wave damping. The next sections will describe three possible causes for a (local) reduction of this height compared to the original design i.e. deviations during construction, creep of the asphalt and repaired damages.

Deviations during construction

Deviations during construction highly depend on the construction method and the material used, both are described in chapter 3. This section will treat a couple of aspects of construction that might have resulted in a different shaped asphalt slab than originally designed.

Biggest uncertainty is the quality and composition of the stone asphalt. During construction the mixture was changed frequently due to occurring damages. Viscosity of the stone asphalt mixture during casting is of great importance, in case the mixture had a too low viscosity it could have penetrated further into the toe and core than intended.



FIG. 6.2: *Asphalt cast to stabilize core during construction, Davidse (2012).*

A fast stabilization of the core material is essential in order to create the designed cross section. The core material when exposed is sensitive to wave loading. If the first covering asphalt mixture is not cast fast enough after profiling the core the asphalt slab will not have the same profile as intended. Stabilization of the core however also has a downside. The completed part of the breakwater was used for trucks to deliver building material in order to extend the breakwater further into the sea. This implies like shown in figure figure 6.2 the front of the breakwater needs to be fixated to ensure the core is not washed out. This asphalt will highly influence the local cross section of the breakwater.

Settlements of stone asphalt

Mechanical properties of asphalt are related to temperature. Viscosity of asphalt lowers when temperatures rises. This characteristic resulted in unexpected damage during the summers after completion. Settlements of the asphalt slab resulted in cracks and local slope instability, called the summer effect, figure 6.4 gives an impression of damages due to this summer effect.

Damages like these have not occurred since the placement of concrete blocks on the breakwater, the fluid properties of the stone asphalt layer is however still noticeable, figure 6.3 shows armour units settling into the asphalt layer. The Xblocs, right picture, are placed in 2008, over 40 years after completion of the breakwaters. The armour units were placed directly on the asphalt layer, the mud in the picture is only a layer of a couple of millimetres, deposited during the dropping tide the day the picture was taken. Clearly the nose of the Xbloc settled into the asphalt layer.

Settling of the armour units indicates the asphalt layer is still liquid, even 40 years after the structure was completed. One can assume these properties will be present over the entire asphalt slab. Asphalt can settle in two directions, the mastic can flow vertically into the toe and core, or the entire slab might be sliding downward along the slope pushing away toe material. If these processes are present at the bottom of the asphalt slab velocities might be lower due to the lower temperatures because of the lack of exposure to sunlight. Bigger downward pressures from the material above might partly compensate this.



FIG. 6.3: *Armour units settling into the asphalt slab, pictures taken by author in January 2014.*

Previously damaged cross section

Like described in the introduction of this thesis, the breakwaters of IJmuiden have been damaged numerous times during construction and in the years after completion. Repairs were performed by dumping rock and casting more asphalt. From 1968 till 1972 a total of 80,000 tonne of asphalt was cast for repair and maintenance purposes, Davidse (2012). The same report provided the density of the stone asphalt being $2,300 \text{ kg/m}^3$, taking a combined length of the breakwaters of $3,200 \text{ m}$ measured from the shoreline, this adds up to nearly 11 m^3 asphalt per running meter on average, in the first four years after completion. This indicates the cross sections of the breakwater might be different than designed for.

The majority of the asphalt was cast to repair damages. Most of the damages started with the formation of cracks due to settlements of the asphalt. These cracks if not repaired resulted in slope instability, figure 6.4 shows a couple of damages. These slope instabilities resulted in big gaps in the asphalt layer. If the core material was partly eroded or repositioned this would result in a different shaped asphalt layer if repaired. Also the new cast asphalt might penetrate into the core material.

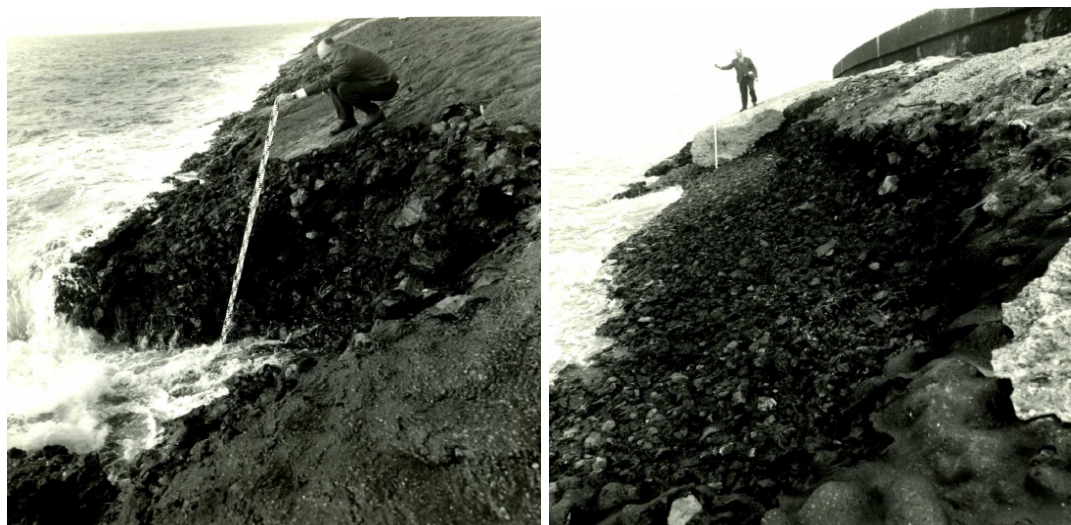


FIG. 6.4: *Slope instability of the asphalt slab, Davidse (2012).*

The three cases introduced in this section might all lead to a (local) lower asphalt slab compared to the original design. The magnitude of this lowering is hard to predict and might vary substantially between different locations along the breakwater. Evaluation of this damping mechanisms will be performed modelling the cross section with a decreasing height between the asphalt slab and the sand bed underneath the structure. This height is lowered until the measured damping is found. The magnitude of the lowering needed will determine whether this damping mechanism is plausible to cause the measured damping.

6.4 Approach comparing damping mechanisms

There are different approaches possible to evaluate the likeliness of the different damping mechanisms. An option would be to measure the profile of the asphalt slab and determine the presence and amount of sand in the toe structure. Measuring the whole breakwater without any prior knowledge about decisive locations is however expensive. Determining the presence of sand in the toe is difficult, the thick asphalt slab makes acoustic imaging impossible, drilling will be necessary. Another drawback is the lack of insight in future developments of the damping mechanism, longer observations are required to get insight in the time dependency of the damping.

In case of a rubble mound breakwater another option would be an analytical approach like the pore pressure damping model introduced by Oumeraci and Partenscky (1991), see section 2.3. However in the IJmuiden case exchange of water is only possible through the toe structure and the sand bed underneath the toe structure. The layout of the breakwater is too complex to describe the pore pressure damping with this simple model.

Scale model tests and a numerical model should be able to cope with the complex design of the breakwater of IJmuiden. Drawback of scale model testing is the difficulty related to correctly scaling materials in order to get the correct flow of water. Due to the fact correct modelling of flow of water inside the breakwater is essential for determining wave damping a numerical model is preferred. Other advantages of numerical modelling is the possibility to run a large amount of tests in a relatively short amount of time and the amount of data generated. The numerical model will calculate pressures and flow velocities at every time step at every grid point, this amount of sensors would never be possible in a scale model test. The numerical model used is described in chapter 7. In chapter 9 the evaluation of the damping mechanisms is performed.

Additional downside of scale model testing and the specific numerical model used during this thesis is limitations concerning trapped air. During scale model tests the compressibility of air needs to be scaled in order to include the effect of trapped air, this proved to be difficult in past. The selected numerical model is not able to cope with any trapped air, the importance of this phenomena was discovered at a stage of the thesis were changing to another numerical programme was not desirable.

Chapter 7

Used numerical model

Research into the wave damping in the IJmuiden breakwaters is performed using a numerical model. This chapter will describe the model, its abilities, limitations, required input and possible output. The numerical model IH-2VOF is used, a volume of fluid model (VOF), developed by the university of Cantabria Spain. IH-2VOF is a two dimensional model, in other words only cross sections can be modelled. Unlike physical scale modelling this numerical model does not show any damage, changing cross sections due to a high forcing is not possible.

7.1 Volume of fluid

The VOF method was first introduced by Hirt and Nichols (1975). It is a method using a static layout of grid cells. In contrast to other numerical models where grid cells follow the free water surface, in this model the free surface will be drawn through the grid cells. The VOF approach makes it possible to model breaking waves.

Modelling of the free surface is performed using the following method. For each cell of the grid only one value for each dependent variable of the fluid state is used. Suppose F represents the amount of fluid in a cell, one for a full cell zero for an empty cell. A value between zero and one implies the presence of a free water surface. Using the direction the value of F is changing most rapidly the surface normal can be determined, and a line through the cell can be constructed approximating the free surface. This method makes the modelling of breaking waves possible. F is described by:

$$\frac{\partial F}{\partial t} + u \frac{\partial F}{\partial x} + v \frac{\partial F}{\partial y} = 0 \quad (7.1)$$

Where u and v are the horizontal and vertical fluid velocities.

7.2 Physics behind IH-2VOF

In order to be able to calculate flow of water with acceptable computation time a couple of simplifications are necessary. Fluid is modelled as an isotropic, incompressible, homogeneous and Newtonian fluid. Breaking waves will result in air entrapment inside the water, this entrapment will result in non-homogeneous water density and a compressibility of the water, this effects will be ignored by the numerical model.

Like stated in appendix A motion of water through porous media is different from that in open water. The numerical model implements a different calculation method for these two domains.

Fluid domain

In the fluid domain the Reynolds averaged Navier-Stokes (RANS) equations are governing. A velocity field u can be divided in a mean flow part \bar{u} and a turbulent flow part u' , this also holds for pressures. Resulting in:

$$u_i = \bar{u}_i + u'_i \quad \text{and} \quad P = \bar{P} + P' \quad (7.2)$$

$i = 1, 2$ for the two dimensional flow. When applying these decompositions to the Navier-Stokes equations and assuming an incompressible fluid the RANS equations derived:

$$\begin{aligned} \frac{\partial \bar{u}_i}{\partial x_i} &= 0 \\ \frac{\partial \bar{u}_i}{\partial t} + \bar{u}_j \frac{\partial \bar{u}_i}{\partial x_j} &= -\frac{1}{\rho} \frac{\partial \bar{P}}{\partial x_i} + g_i + \frac{1}{\rho} \frac{\partial \bar{\tau}_{ij}}{\partial x_j} - \frac{\partial \overline{(u'_i u'_j)}}{\partial x_j} \end{aligned} \quad (7.3)$$

Porous media

Due to the presence of impermeable soil particles in porous media flow will not be uniform, water will only flow through the porous around the particles. It is impossible to model shape, location and flow velocities in all the pores, averaging over a certain area is necessary to describe the motion of water. The size of the averaging area should be sufficiently larger than the pore size and smaller than the characteristic length scale of the flow. Averaging over a certain volume, the brown square in figure 7.1 results in the volume averaged Reynolds averaged Navier-Stokes (VARANS) equations.

This approach of averaging results in volume averaged material parameters like porosity and nominal grain diameter. Flow resistance is calculated using the extended Forchheimer equation (equation A.5).

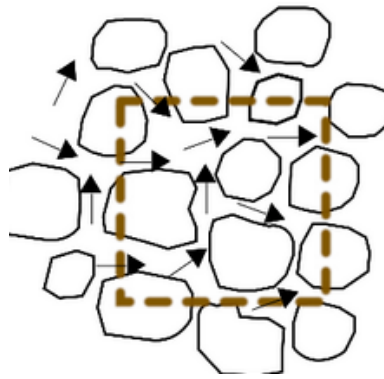


FIG. 7.1: *Averaging area for porous flow, IH-Cantabria (2012).*

7.3 Input

The numerical model has different input parameters which can be divided into geometrical, wave and computational parameters.

Geometrical parameters

First of all the size of the two dimensional numerical wave flume should be provided. The size depends on the size of the cross section of interest, and the length of waves modelled, IH-Cantabria (2012) recommends at least 1.2 times the wave length in front of the object of interest, in order for the waves to be generated correctly. The cross section of interest is divided into obstacles and porous media. Obstacles are impermeable, the only parameter necessary to define them is coordinates describing the geometry. To define porous media the following additional material characteristics need to be provided: Forchheimer shape factors α , β and γ , see section A.3, porosity and nominal grain diameter. All obstacles and porous media are defined using straight lines, modelling of curved lines is not possible.

Hydraulic parameters

First of all the water volume and density should be provided. Three types of waves can be generated, a single wave, regular waves and irregular waves. Also different wave theories can be applied, for single waves Boussinesq and Grimshaw. Regular waves can be described by linear wave theory, Cnoidal, stokes II and V. For each type wave height and period and the length of the wave series can be selected.

Waves are generated using a static or dynamic paddle. Some distance is required for the waves to form properly, IH-Cantabria (2012) recommends a distance of 1.2 times the wave length before any object are placed. At each boundary there is the option to activate wave absorption.

Computational parameters

In order to be able to run the model a computational grid, a mesh, is required. IH2-VOF uses a rectangular static mesh, which means the coordinates of the grid points are stationary in time. At each grid the model calculates the amount of water present at the grid, pressure and flow velocities at every time interval. A finer mesh results in more accurate results, but will require more calculation time. In case a mesh is too coarse nearly full cells might be adjacent to nearly empty cells, even when the wave steepness is relatively low, a non existing flow of water can be modelled. This mechanism is called false breaking, figure 7.2 shows this mechanism.

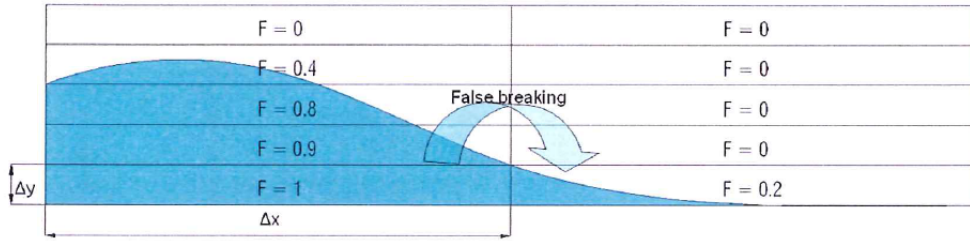


FIG. 7.2: False breaking phenomena, IH-Cantabria (2012).

In order to prevent false breaking IH-Cantabria (2012) recommends to cover a wave with at least ten grid cells in vertical direction. The acceptable ratio between the horizontal and vertical dimensions of grid cells is determined via the wave steepness just before breaking. Wave steepness just before breaking is:

$$\left(\frac{H}{L}\right)_{max} = \tan(23^\circ) \quad (7.4)$$

Where H is wave height and L is wave length. Putting in n_x and n_y for the number of grid cells in respectively the x and y direction results in:

$$\left(\frac{H/n_y}{L/n_x}\right) > \tan(23^\circ) \quad \frac{\Delta_y}{\Delta_x} < \tan(23^\circ) \quad \Delta_x < 2.36\Delta_y \quad (7.5)$$

Rounded this results in a $\Delta_x < 2.5 \cdot \Delta_y$.

In a lot of numerical models the time step is an important parameter balancing between numerical stability and calculation time. The IH-2VOF software automatically adjusts the magnitude of the time step, to ensure a stable calculation.

7.4 Output

Power of the numerical model lies in the ability to produce large quantities of information. The software can provide pressure and flow velocities at each time step at each grid. This would never be possible using a scale model or taking field measurements. The sampling frequency

can be selected, the frequency should be big enough to capture the extreme values, on the other hand a smaller sampling frequency results in less data, and therefore a faster processing.

Drawback of storing for instance pressure information per time step for all the grid points is the size of the stored data files. For a wave series of 100 seconds information will be in the order of a couple of gigabytes. Therefore some options are integrated in the software to extract more specific data. One can install wave gauges, providing free surface level and flow velocities for every grid in vertical direction per time step. Also wave run up and overtopping in a certain area can be determined.

7.5 Limitations

The model calculates a surface elevation without taking two kinds of air entrapment into account. The first kind is the entrapment of air in the water column. Breaking waves can be modelled, however the density of water is taken constant. In case waves brake air bubbles are mixed with water changing its density, this is not taken into account since the density of water is a constant. Another kind of air trapping is the air trapped underneath impermeable parts of for instance a breakwater. Due to wave action air enclosed by the impermeable part and the water body is compressed, see chapter 5. This compression of air is a resisting force against movement of water, air and therefore this force is not modelled with this model.

There is no possibilities to model a water flow through the model boundaries. Due to this limitation it is only possible to model wave induced processes without the influence of currents.

Chapter 8

Model calibration

Before a numerical model is useful it needs to be calibrated in order to determine whether results are correct. Calibration can be performed using scale model or prototype measurements or analytical formula. The model will be calibrated using different test cases with increasing complexity.

First elementary step in the process is the velocity profile. The profile computed by the model will be compared to the profile determined with linear wave theory. Second step is comparison of pore pressures inside a simplified porous breakwater, lab results by Troch (2000) will serve as reference. If results of both previous steps are satisfying the last step of calibration will be performed. This last step is based on research by Kuiper and van Gent (2006), a scale model research into the breakwaters of IJmuiden.

8.1 Flow velocity profile

A flow velocity profile shows the flow velocities at different depths under a passing wave. The numerical model should be able to model flow velocities correct in order to be of any value when calculating loading of hydraulic structures. This fundamental calibration step is performed using linear wave theory. Harmonic small amplitude waves will be modelled, resulting flow velocity profiles will be compared to the profiles determined analytically. The ranges of applicability of different wave theories is shown in figure 8.1, linear wave theory is only valid for deep water and relatively small amplitude waves.

The following formula, presented in Holthuijsen (2007), expresses the horizontal flow velocities using linear wave theory:

$$u_x = \omega A \frac{\cosh(k(h+z))}{\sinh(kh)} \sin(\omega t - kx) \quad (8.1)$$

Where ω is the angular velocity, k the wave number, h the water depth, z the depth coordinate and x the horizontal coordinate of the point of interest. A is the amplitude of the surface elevation, for a harmonic wave $A = H/2$.

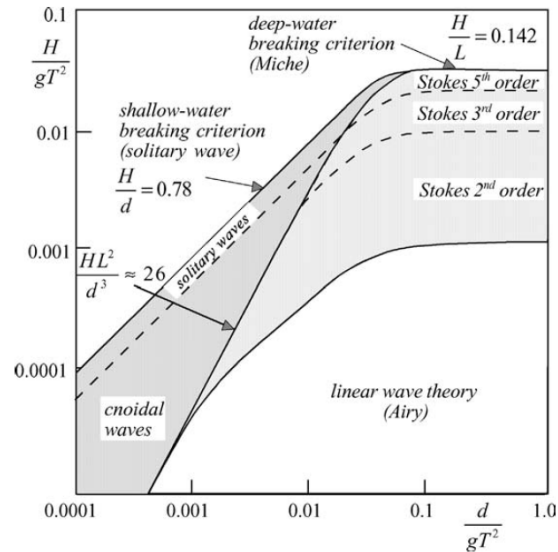


FIG. 8.1: Ranges of applicability of different wave theories, Holthuijsen (2007).

Results

A regular harmonic wave with $H = 0.01$ m, $T = 1.4$ s combined with a water depth of $h = 0.9$ m lies inside the range described by linear wave theory, see figure 8.1. Using equation 2.1 the wave length is determined to be $L = 2.93$ m. A wave flume of 10 m should therefore be sufficiently long to correctly model this wave.

The ratio between horizontal and vertical mesh size prescribed by IH-Cantabria (2012) is based on breaking waves. Waves described by linear wave theory are not steep enough for breaking, therefore a larger ratio between horizontal and vertical mesh is possible, decreasing calculation time. A mesh of 1000x500 cells is selected, describing each wave with 10 horizontal and 145 vertical cells. Both the velocity profile from the model and linear wave theory are plotted in figure 8.2.

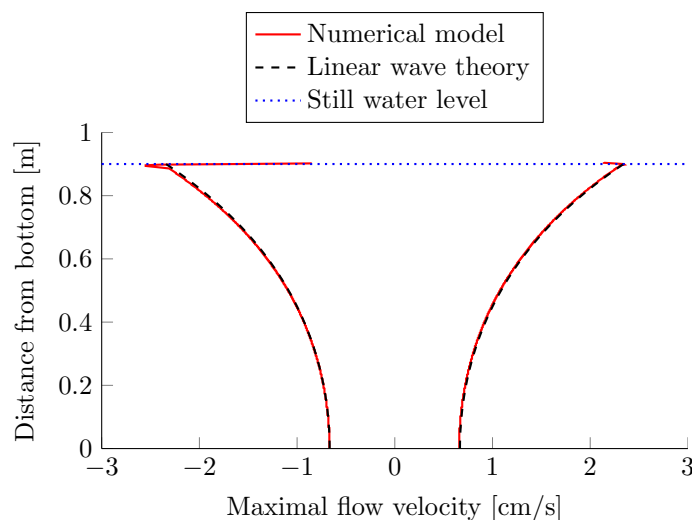


FIG. 8.2: Comparison between modelled flow velocity profile and linear wave theory.

Hydraulic parameters

A set of regular and irregular waves was tested, using the same water depth $h = 0.4 \text{ m}$. Two wave conditions are selected for calibration in this report. One regular wave series REG16 ($H = 0.06 \text{ m}$, $T = 1.6 \text{ s}$ test duration of 100 s) and an irregular series IRR04, (JONSWAP wave spectrum $H_s = 0.10 \text{ m}$, $T_p = 2.18 \text{ s}$ test duration of 300 s), names correspond with the names used by Troch. Both boundary conditions were absorbent, preventing wave reflection from the boundaries influence measurements.

Results scale model

Focus of this research was pore pressure damping inside a rubble mound breakwater. Pore pressure damping was described using the model introduced in section 2.3:

$$p_x = P_0 e^{-\delta(2\pi/L')x} \quad (8.2)$$

Where δ is the damping coefficient, P_0 the pressure at the breakwater interface between breakwater and fluid domain, L' the wave length inside the breakwater and x the distance from the interface. The magnitude of δ is calculated using pressure data at three different depths, $z = 0.1 \text{ m}$, $z = 0.2 \text{ m}$ and $z = 0.3 \text{ m}$. Pore pressure damping for regular and irregular wave series is presented in figure 8.4. These scale model measurements will be used to calibrate the abilities of the numerical model to describe the motion of water through porous media.

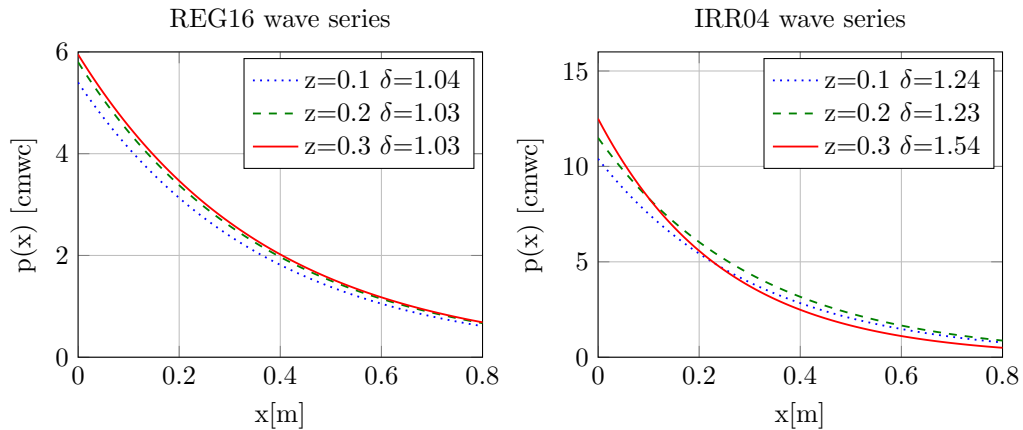


FIG. 8.4: Measured pore pressure damping for regular (left) and irregular (right) wave serie, data by Troch (2000).

Results numerical model

The numerical model has the same dimensions as the scale model presented in figure 8.3, material properties are also the same. Both boundaries are modelled absorbent. The smallest wave modelled is 0.06 m applying the mesh size ratios recommended by IH-Cantabria (2012), see section 7.3, results in a mesh of 1700 by 170 grid cells.

Regular waves

Damping of pore pressure is significantly larger in the numerical model when the same α and β values are used. Scale model test with the REG16 wave series resulted in δ values of 1.03-1.04, see figure 8.4 for the numerical model depending on the depth values of 1.43-2.34 are found. The difference between numerical and scale model results is too big. Adjustments to the input of to numerical model are necessary in order to get results fitting the scale model tests.

Like described in section A.3 the relative importance of the three resistance terms is related to the Keulegan-carpenter KC and Reynolds number Re. These numbers are determined inside the porous media, at the location of the pressure gauges. Magnitude of Re is between 12 and 200 depending on location of the wave gauge, Re/KC is a constant $6.5 \cdot 10^{-3}$. From figure A.2 one can conclude the laminar and turbulent resistance term are of greater importance than the inertia term. To check this first estimated relative importance the model is run with one of the resistance terms set to zero. The table below presents the determined δ values.

TAB. 8.1: *Determined δ values applying different Forchheimer shape factors.*

	δ z=0.1	δ z=0.2	δ z=0.3
Scale model	1.04	1.03	1.03
Standard numerical model	2.34	1.68	1.425
$\alpha=0$	1.99	1.58	1.4
$\beta=0$	1.46	1.24	1.1
c=0	2.31	1.66	1.41

The β value seems to have the biggest influence on the pore pressure damping. This can be explained by the fact that lowering the flow resistance terms results in higher flow velocities and thereby larger Re number. An increasing Re number increases the relative importance of the β Forchheimer term. Due to the fact the β is most important more runs are performed with both α and c set to zero and the β value is lower with steps of 0.5. The best fit was found with a β value of 1. For these settings the Re was calculated, values of over 350 were found, therefore the flow can be quantified as fully turbulent, making the linear resistance term insignificant. Pressure damping determined using the numerical model and the scale model are presented in figure 8.5.

The δ values determined using the numerical model are close to the values found by scale model research. The slightly higher wave induced pore pressure heights in the model can partly be explained by the slightly higher incoming waves.

Another approach to check the amount of damping is measuring the wave transmitted through the breakwater. During the scale model test there was a wave gauge installed for this purpose, WG5 in figure 8.3. The figure below shows the waves transmitted in the scale model and the numerical model, note the scale in both plots is different. Both the numerical determined δ values and the transmitted wave height match the scale model measurements close enough to have confidence in the ability of the model to calculate pressure damping for these conditions.

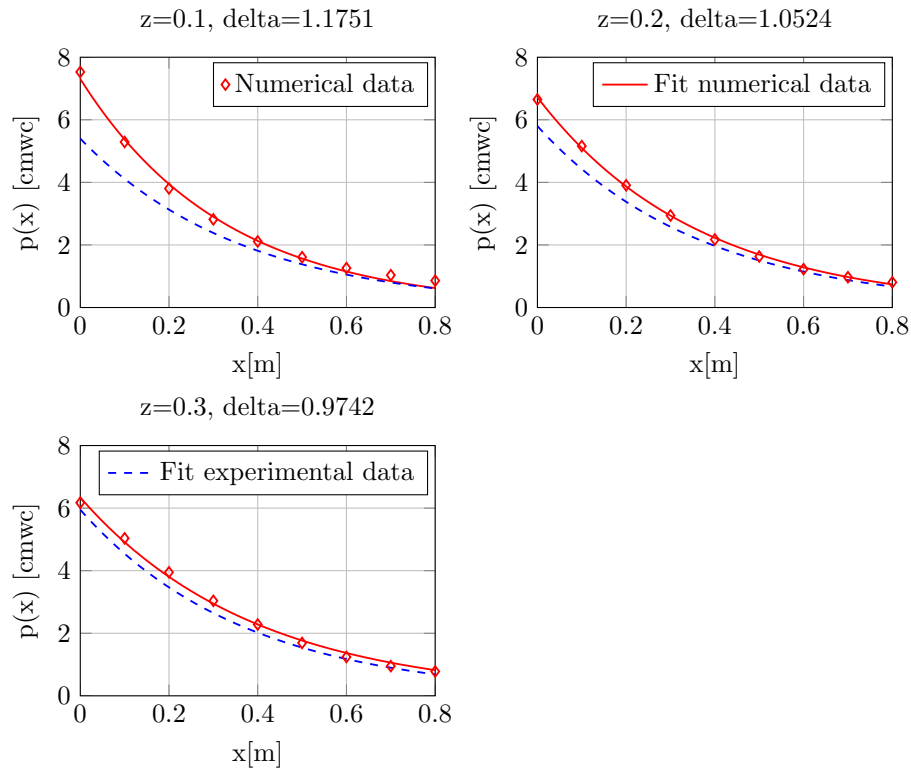


FIG. 8.5: Comparison between modelled and measured damping for regular wave series.

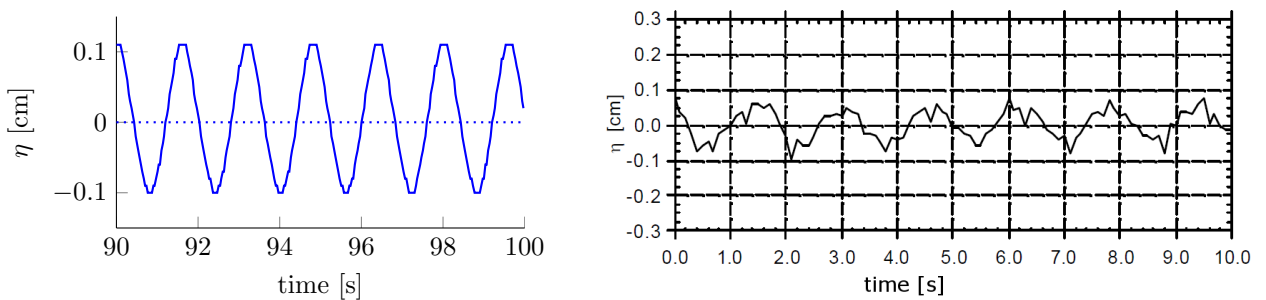


FIG. 8.6: Transmitted regular waves, numerical model (left) and scale model (right).

Irregular waves

The previous section showed an acceptable match in pore pressure damping in case β is 1, α and c set to zero. In order to make sure this is not a coincidence the model is compared with scale model results for irregular waves with higher waves and longer wave periods. The JONSWAP wave spectrum used in the numerical is shown in figure 8.7 by the blue line, the black line represents the wave spectrum used during scale model testing. The model is compared to the IRR04 wave series Troch used in his research. The difference between the spectra is small enough in order to compare damping.

The results from irregular waves are compared in a similar way results of regular waves were compared in the previous section. For irregular waves only the results are presented in figure 8.8 and 8.9.

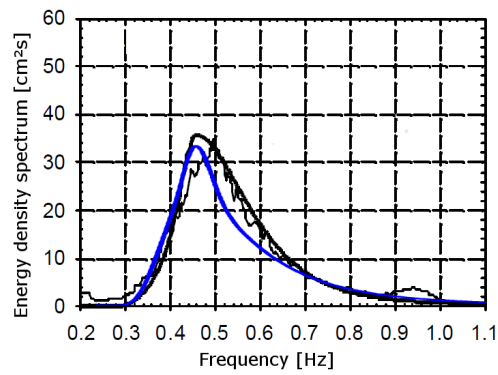


FIG. 8.7: Comparison between energy density spectra numerical model (blue) and scale model (black).

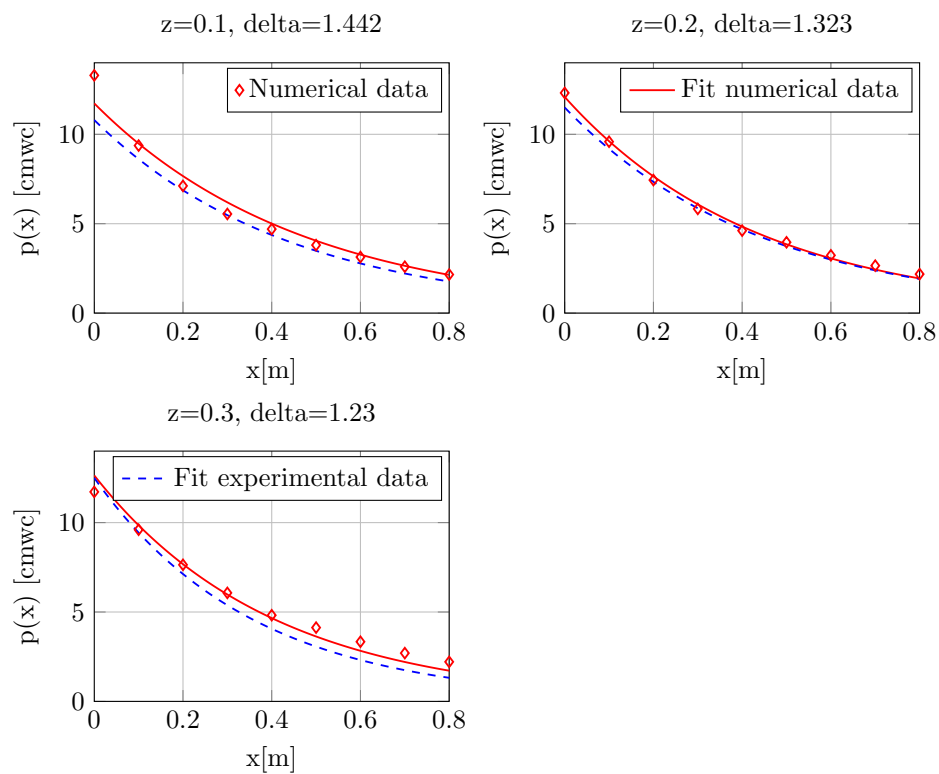


FIG. 8.8: Numerical determined δ values.

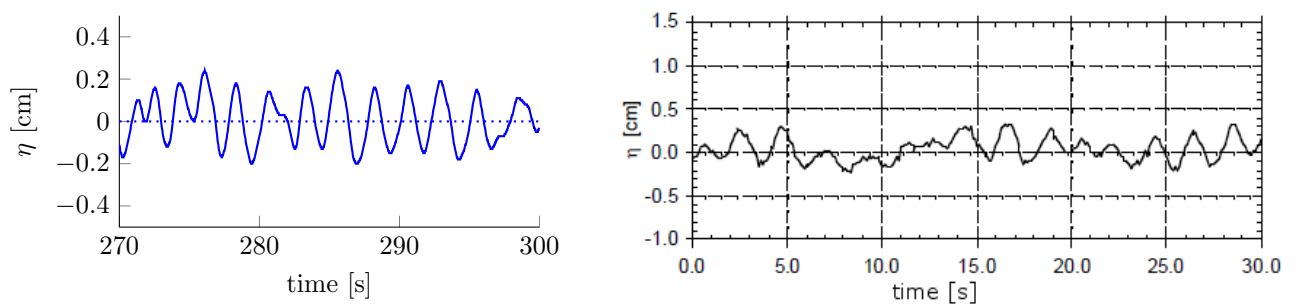


FIG. 8.9: Transmitted irregular waves, numerical model (left) and scale model (right).

Like the regular wave series the results from the irregular wave series approximate the scale model results. These two results combined give enough confidence to proceed to a more complex calibration test case.

8.3 Scale model tests breakwaters IJmuiden

In 2006 Deltares perform research into the stability of the IJmuiden breakwaters on behalf of RWS. Prime focus of this research was to determine the decisive failure mechanism and using this new insight to design a new stable armour layer.

Research was performed using scale models. Pressure build up under the asphalt slab and pressure gradients over the toe structure were prime areas of interest during this research. Making the measurements of this research suitable for calibrating the flow of water through different porous media.

Structural parameters

The geometry of the researched cross section is shown in figure 8.10. The sloped foreshore and the supporting layer underneath the breakwater were modelled as an impermeable layer, concrete was used. Strength and stability of the asphalt layer was not inside the scope of this research, therefore the asphalt slab was modelled using a wooden board with the same scaled dimensions. To prevent disturbance of the measurements due to movement of the wooden board it was secured to the walls of the flume. Although stability of the current armour layer was not of interest of this research an armour layer was installed, because this armour layer will influence the flow of water over the outside of the breakwater. To prevent movement of the armour layer the blocks were secured. The distance between the wave maker and the sloped foreshore was 31.3 m, this length is necessary for the generation of the correct wave spectrum.

In order to get realistic results different parts of the model need different types of scaling. Depending on whether the flow resistance stability or geometry should be the same in the model and prototype. Table 8.2 shows the parameters used in the research by Kuiper and van Gent (2006) and the type of scaling performed, subscript p indicating prototype and m indicating model. Stability of the toe structure was one of the focusses of this research, therefore the toe is scaled on stability instead of permeability, this will lead to a lower water exchange in the model than in prototype situation. This has no effect on the value of these measurements for calibration purposes, but should be taken into consideration when comparing the results with field measurements.

Hydraulic parameters

Relatively low water levels were assumed to be normative for the tested failure mechanisms, toe instability and lifting of the asphalt slab. Therefore relatively low water levels of NAP+0.5 m and NAP+2 m were selected for scale model testing. A total of ten combination of waves and water levels were tested, two are used for this calibration process, the highest wave with $h = \text{NAP}+2 \text{ m}$

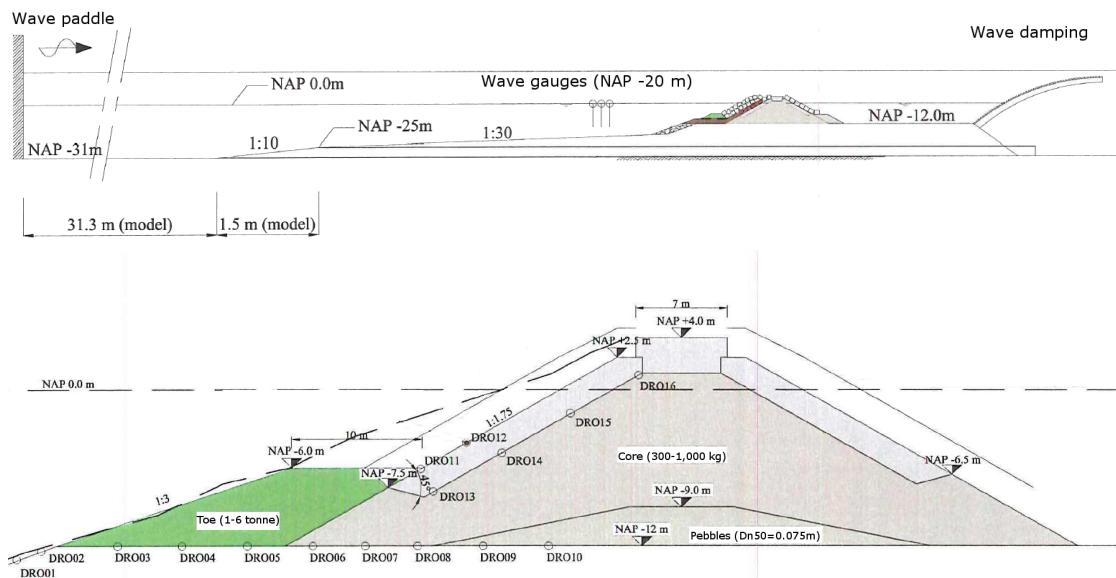


FIG. 8.10: Cross section scale model IJmuiden breakwater, used by Kuiper and van Gent (2006).

TAB. 8.2: Scaling breakwater materials, Kuiper and van Gent (2006).

	Grading	Scaling method	$d_{n50,p}$ [m]	$d_{n50,m}$ [m]	$d_{50,m}^*$ [m]
Armour layer	-	Geometrical	2.2	0.055	0.055
Toe	1 – 6 tonne	Stability	1.10	0.026	0.031
Core	300 – 1000 kg	Permeability	0.63	0.020	0.024
Gravel core	40 – 110 mm	Permeability	0.08	0.010	0.012

* Determined using $d_{n50} = 0.84d_{50}$, CIRIA (2007)

and the lowest wave series with $h = \text{NAP} + 0.5$ m, respectively called HP05 and HP06 during Kuipers his research. Wave properties are presented in table 8.3. Storms of 3 hours in prototype scale were modelled, resulting in 1,700 s in model scale. During this timespan over 1000 waves are modelled, enough to statistically analyse pressures and pressure gradients.

TAB. 8.3: Waves generated during scale model tests by Kuiper and van Gent (2006).

	Water level [m] NAP	$H_{s,p}$ [m]	$H_{s,m}$ [m]	$T_{p,p}$ [s]	$T_{p,m}$ [s]
1	+0.5	4.9	0.1225	9.4	1.49
2	+2	8.6	0.215	12.4	1.96

Results scale model

Both pressure gradients over the toe structure and upward pressure underneath the asphalt slab were measured. The pressure gradient were measured by pressure sensors DR001-DR010, upward pressures with sensors DR011-DR016, see figure 8.10. Pressure gradients were calculated between sensors in the same material using the following formula:

$$i = \frac{P_{i+1} - P_i}{\rho_w \cdot g \cdot \Delta x} \quad (8.3)$$

Where i is the pressure gradient, P_i is the pressure at a certain point, ρ_w is the density of the water and Δx is the distance between the two pressure gauges. A positive pressure gradient will result in a seaward directed flow using this definition. The 2 % highest seaward pressure gradients are presented in figure 8.11, these results will be used for the calibration of the numerical model.

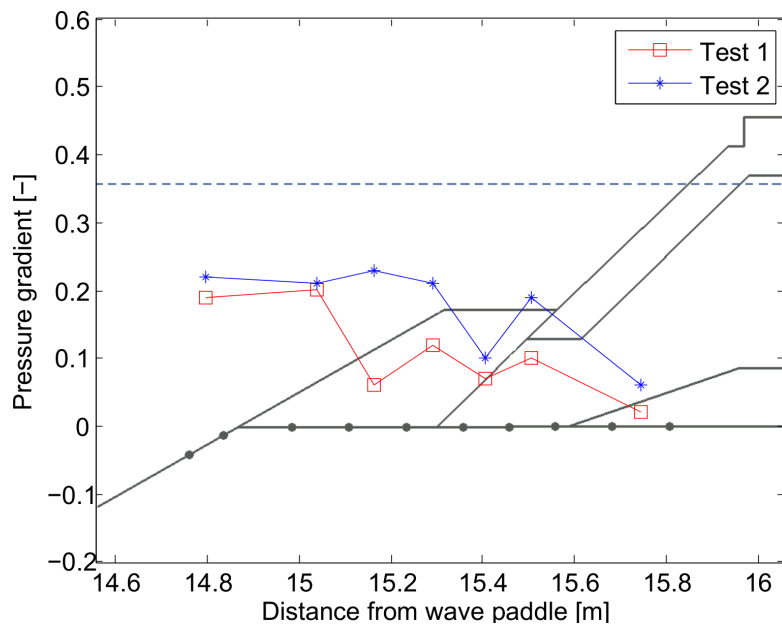


FIG. 8.11: Measured 2 % highest seaward pressure gradients, Kuiper and van Gent (2006)

Besides the pressure gradient over the toe structure the upward forcing of the asphalt slab will be compared. During scale model testing six pressure gauges were installed to determine this force. Four underneath the slab and two on top of the slab, see the figure below.

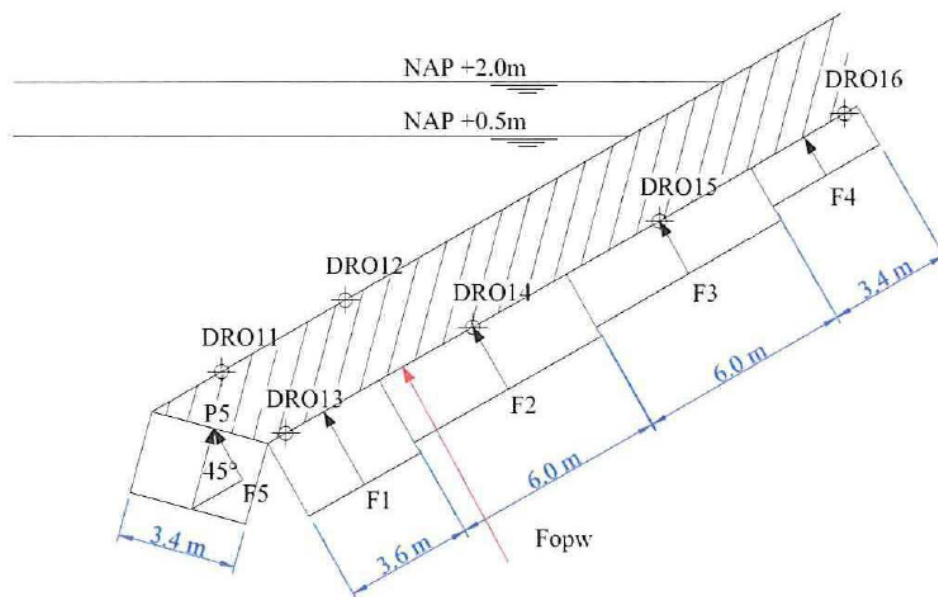


FIG. 8.12: Schematic representation of the calculation of upward forces, Kuiper and van Gent (2006).

The pressures measured by the gauges were translated to five representative pressures ($P_1 - P_5$), these pressures are integrated over the distance indicated in blue, assuming a constant pressure over this distance resulting in five forces acting on the asphalt slab represented by the arrows in the picture above. Translation from measured pressures to forces is performed in the following manner:

$$\begin{aligned}
 P_1 &= P_{DR013} & F_1 &= 3.6P_1 \\
 P_2 &= P_{DR014} & F_2 &= 6.0P_2 \\
 P_3 &= P_{DR015} & F_3 &= 6.0P_3 \\
 P_4 &= P_{DR016} & F_4 &= 3.4P_4 \\
 P_5 &= (P_{DR013} + P_{DR011})/2 & F_5 &= 3.4\cos(45^\circ)P_5
 \end{aligned} \tag{8.4}$$

$$\underbrace{F_{up} = F_1 + F_2 + F_3 + F_4 + F_5}$$

Values of the upward pressures with an exceedance probability of 2 % are presented in table 8.4, weight of the asphalt slab and water column on top of the asphalt are not taken into account.

TAB. 8.4: *Measured upward pressures with 2% exceedance probability, Kuiper and van Gent (2006).*

	P_1 [kN/m ²]	P_2 [kN/m ²]	P_3 [kN/m ²]	P_4 [kN/m ²]	P_5 [kN/m ²]	F_{up} [kN/m]
1	99	67	36	10	0,2	1,012
2	135	99	65	34	0,4	1,598

8.3.1 Numerical model

First steps in creating the model is the selection of the flume dimensions and the computational grid. The numerical wave flume has a height of 1.2 m, resulting in a free height above the crown of the breakwater of 13 m in prototype scale, high enough to model the expected overtopping. Taking into account the prescribed length in front and behind the breakwater a length of 20 m is chosen.

The computational grid highly depends on the height of the modelled waves. IH-Cantabria (2012) recommends at least ten grid cells per wave in vertical direction, and in case wave breaking is expected a ratio of 2.5 between vertical and horizontal grid size. The smallest waves modelled are $H = 0.1225$ m applying both requirements results in a mesh of 700 by 100 cells.

Structural parameters

The used cross section is shown in figure 8.13. One can see the distance between the wave generation and the breakwater is significantly smaller compared to the distance in the scale model. A shorter flume will result in a shorter computation time, computation time can be of great importance using computer models. The different way waves are generated in the computer

model make it possible to shorten the distance. A distance of at least 1.2 times the wavelength is advised, IH-Cantabria (2012).

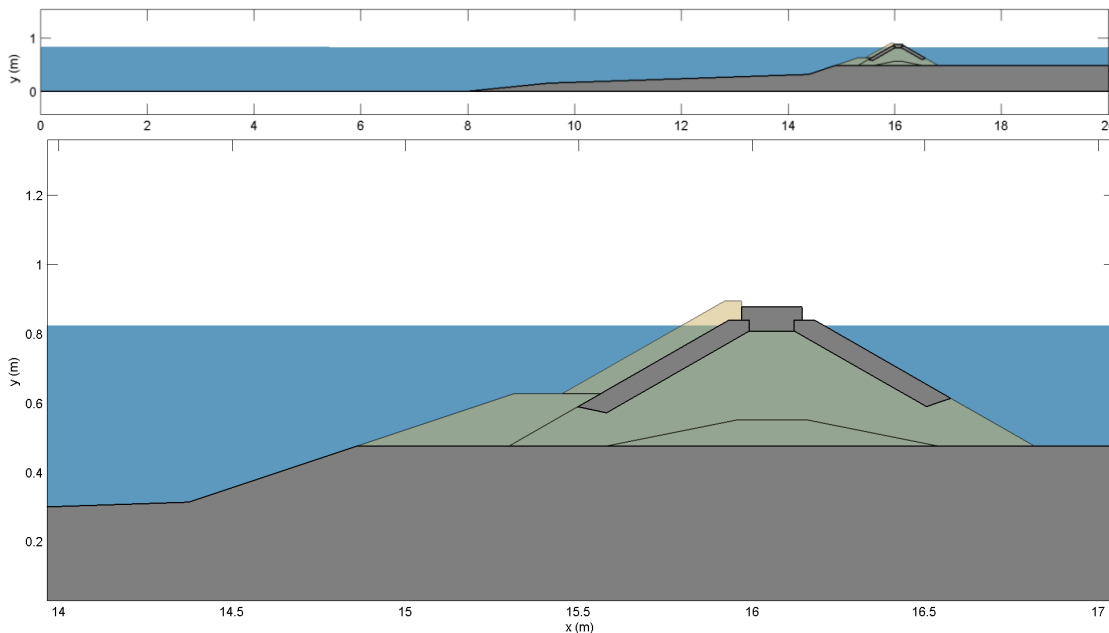


FIG. 8.13: *Cross section of the numerical model.*

The amount of water flowing through the sand at the foreshore and the supporting sand bed underneath the breakwater was believed to be insignificant for the pressure underneath the asphalt slab. Combined with the difficulties associated with scaling sand in a model it was determined to model these parts as impermeable layers, both were constructed using concrete. In the numerical model those layers are therefore modelled as impermeable obstacles, like the asphalt slabs and the crown element.

The armour layer, toe and core are modelled as permeable media. The d_{50} is chosen like stated in table 8.2. The n for the armour layer is set to 0.30 see Kuiper and van Gent (2006), the porosity of the other media is selected according to Bregman (1998) and results in n is 0.38, irregular not compressed stone.

Due to the relatively large stones in the armour layer, toe and core of the breakwater turbulent flow is expected. Therefore the findings of the previous calibration step are expected to be applicable to this case. The shape factor β is set to one and α is set to zero, assuming the linear resistance term is negligible.

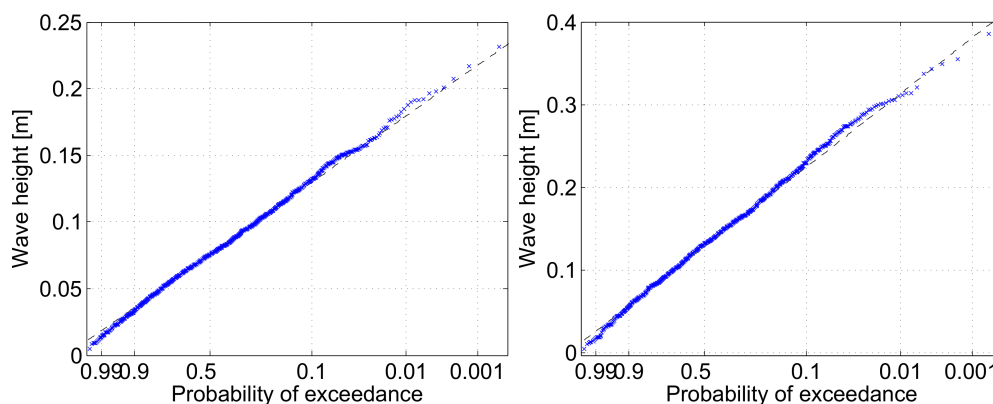
Hydraulic parameters

Kuiper and van Gent (2006) measured wave heights and periods at the NAP-20 m depth contour. The wave parameters in the numerical model are dictated at the wave paddle, therefore some effort needs to be put into adjusting wave conditions to fit the conditions at the NAP-20 m line. Two wave series matched the properties fairly close. The table below shows the significant wave properties modelled and the properties modelled during scale model test. Subscript n indicating the properties of the numerical model and s the scale model by Kuipers.

TAB. 8.5: *Modelled wave properties, at NAP-20 m.*

	$H_{s,s}$	$H_{s,n}$	$T_{p,s}$	$T_{p,n}$
	[m]	[m]	[s]	[s]
1	0.1225	0.1217	1.49	1.53
2	0.215	0.214	1.96	2.06

During scale model testing the wave height was Rayleigh distributed. The probability of exceedance of the numerically modelled wave heights is plotted on a Rayleigh scaled horizontal axis in figure 8.14. In case of a perfect Rayleigh distributed wave series all results would fit the straight dashed line. Due to wave breaking and other small deviations in generation and propagation of waves the line is not straight. During scale model tests similar results were found. The modelled wave represent the wave series used by Kuipers close enough to compare the calculated results with the scale model measurements.

FIG. 8.14: *Probability of exceedance of the modelled waves at NAP-20 m .*

Results numerical model

The results of the numerical model are compared using the pressure information provided by the software. The sampling frequency is set to 10 Hz, during each wave period at least 150 times the pressure information is stored for every grid point. This should provide sufficient amount of data point per wave to include extreme values. The pressure information at the points of interest is then extracted from these files.

To determine the upward force underneath the asphalt slab a slightly altered equation 8.4 was used. During wave flume experiments the armour layer was modelled using separate blocks the pressure sensors were installed between them. In the numerical model the armour layer is modelled as a porous medium, believed is that the gross movement of water on the outside of the breakwater is the same. However local pressures will be different. Therefore pressure sensor DR011 in figure 8.12 will give an global pressure instead of a local pressure between the armour blocks. Therefore P_5 and F_5 are removed from equation 8.4. The adopted upward pressures are presented in table 8.6, subscript s and n indicating values from the scale and numerical model.

TAB. 8.6: Numerical determined pressures with 2% exceedance probability.

	P_1 [kN/m ²]	P_2 [kN/m ²]	P_3 [kN/m ²]	P_4 [kN/m ²]	F_{up}^* [kN/m]
1_s	99	67	36	10	1,012
1_n	92	59	29	9.3	891
2_s	135	99	65	34	1,598
2_n	126	90	60	30	1,459

* Upward force without P_5 and F_5 , see equation 8.4.

The upward pressures underneath the asphalt slab are approximately the same in the numerical model. The forces are slightly underestimated, this would imply the flow resistance of the porous media in the breakwater is still slightly overestimated.

Pressure gradients over the toe are determined using equation 8.3. Pressure information is determined like described at the beginning of this section. The figure below shows the two percent exceeded pressure gradients determined by the numerical model and scale model plotted together.

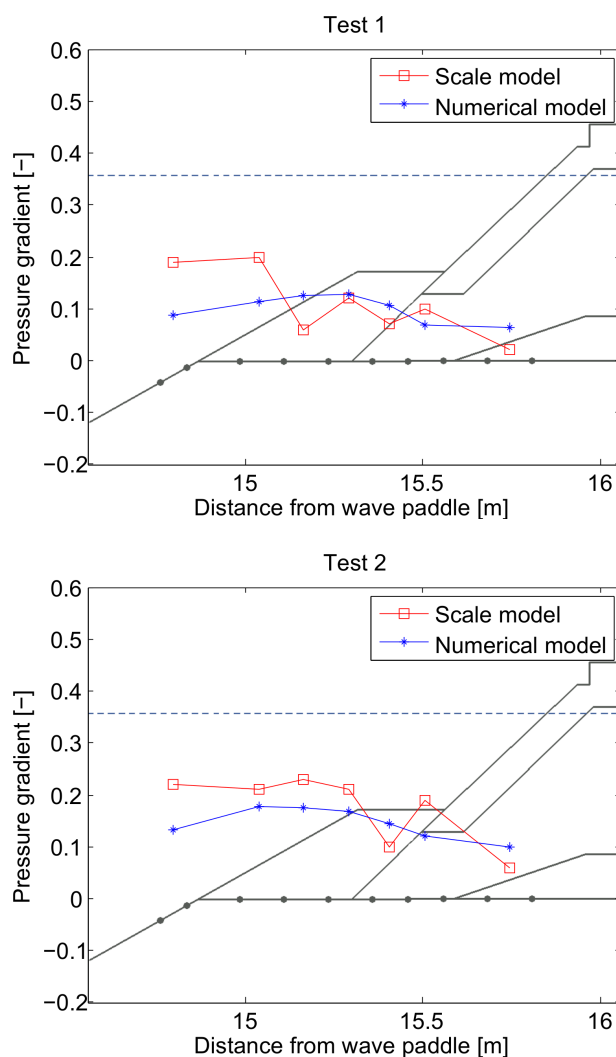


FIG. 8.15: Comparison numerical determined and measured pressure gradients.

Shape of the pressure gradient is not the same in both cases, the pressure gradients calculated by the numerical model are smoother. This difference might be the result of the way pressures are calculated. Due to area averaging, described in section 7.2, there is a lack of local extreme pressures and flow velocities. In scale model tests shape and size of pores directly surrounding the pressure gauges will influence measurements and might cause the rougher shape of the pressure gradient. Magnitude of the pressure gradient especially over the area of greatest interest, the toe, is similar.

8.4 Conclusions

From the sections above one can conclude the IH-2VOF model is able to correctly model flow through porous media, and is able to cope with the complex geometry of the IJmuiden breakwaters. Therefore the model is selected to determine wave damping and forcing of the asphalt slab. Magnitude of the Forchheimer shape factors proved to highly influence the outcome of the model. Due to the turbulent flow inside the breakwater the laminar shape factor α and added mass γ proved to be insignificant, both factors set to zero and a turbulent shape factor β set to a value of 1 led in the best results for both regular and irregular waves. In the remaining part unless otherwise stated these Forchheimer shape factors are applied for porous media during modelling.

Chapter 9

Evaluation damping mechanisms

This chapter will evaluate the damping mechanisms introduced in section 6.1. In order to be able to assess the influence of the damping mechanisms first a baseline calculation is performed. This baseline calculation will evaluate the amount of wave damping based on the original cross section design applying the hydraulic boundary conditions present during field measurements described in chapter 4.

To evaluate the impact of the different damping mechanisms the original cross section used for the baseline calculation is altered, either changes to the geometry of the asphalt slab or the flow resistance of the toe are applied depending on the damping mechanism tested. Aim of this chapter is to get insight which of the damping mechanisms is able to cause the measured damping in the southern breakwater and what changes should be present to the cross section.

Finally the damping mechanism most likely to cause the measured damping is selected and a more thorough evaluation is conducted. During this evaluation the amount of damping during storms and the vulnerability of the damping mechanism is investigated.

9.1 Baseline calculation

A baseline calculation will provide data to compare the influence of the two damping mechanisms. Like described in chapter 3 the breakwaters are not identical and the cross sections of the breakwaters are not constant over the entire length. Therefore two baseline calculations will be performed, one for each breakwater near the head where damping measurements were performed by van Hoven (2012). Dimensions and shape of the cross sections are presented in figures 3.2 and 3.3.

During research by van Hoven (2012) the incoming wave was determined using pressure sensors between the armour units. This approach was selected because placement of pressure sensors on the toe structure was too difficult. Due to the fact the armour layer is modelled as a permeable medium, it is impossible to measure pressures between the separate armour units. Therefore a wave gauge is installed halfway the toe structure to measure the incoming waves. The wave

height in the breakwater core is in both field measurements and numerical modelling determined using a pressure sensor. Damping is defined by the following equation:

$$\zeta = 1 - H_c/H_i \quad (9.1)$$

Where ζ is the amount of damping, H_c is the wave height in the core and H_i is the incoming wave height.

Input parameters

In order to be able to model the flow through the porous media of the breakwater a couple of parameters should be provided. Table 9.1 presents the structural parameters of the different porous media in the breakwater.

TAB. 9.1: *Structural parameters applied for baseline calculation.*

	d_{50} [m]	n	α	β	γ
Armour	2.20	0.30	0	1	0
Toe	1.31	0.38	0	1	0
Core	0.75	0.38	0	1	0
Gravel core	0.095	0.38	0	1	0
Sand	$0.22 \cdot 10^{-3}$ *	0.38	1000	0	0

* Smallest diameter accepted by the model is $1.0 \cdot 10^{-3} m$

Nominal diameters of the porous media, except for the sand, are based on research into the breakwater of IJmuiden by Kuiper and van Gent (2006). According to Northsea-atlas (2014) the grain diameter of the sand near IJmuiden is between $125 - 250 \mu m$, however it is not possible to implement values smaller than $1.0 \cdot 10^{-3} m$ in the model used, therefore the flow resistance of sand will be under estimated.

The Forchheimer shape factors for the coarse porous media are based on the model calibration process described in section 8.2. For sand a laminar flow is expected instead of turbulent, therefore different shape factors are applied, based on Jensen et al. (2014). For a more elaborate description of these terms and flow of water through porous media one can read appendix A.

In order to be able to compare the modelled damping with the damping measured by van Hoven (2012) it is necessary the same hydraulic conditions are applied. Therefore a storm covering a 1000 waves with $H_s = 2.9 m$ and $T_m = 9 s$ is modelled with a water level of $h = \text{NAP} + 1.45 m$. For a more elaborate description of the wave field one can read appendix C.

9.1.1 Results baseline calculations

Modelled wave heights at the toe structure deviate slightly from the measured incoming waves by van Hoven (2012), in both cases the modelled waves are slightly bigger. The differences are however small enough to be able to compare the magnitude of the damping. Table 9.2 shows the results of the baseline calculation.

TAB. 9.2: Comparison between results of the baseline calculation and field measurements.

	$H_{s,i}$ [m]	$H_{s,c}$ [m]	ζ modelled [-]	ζ measured[-]
Northern	3.08	1.00	0.65	0.7-0.90
Southern	3.29	0.18	0.94	0.99

Note to these results is the orientation of the incoming waves. The numerical model is two dimensional, therefore incoming waves are perpendicular to the breakwater. Wave directions were not measured during field measurements, however waves were estimated to be obliquely incoming with 40° at the northern and 60° at the southern breakwater relative to the perpendicular. Resulting in an estimated extra damping of 30 % for the northern breakwater, van Hoven (2012).

Results northern breakwater

Wave damping in the northern breakwater varies significantly from measurements, wave heights in the order of 0.25 m were measured in the core. The trapped air described in chapter 5 is believed to have a big influence on the measured damping. The trapped air is not taken into account by the numerical model, therefore the whole breakwater is filled with water since the bottom of the crown element is located at NAP+1.2 m and the water level is NAP+1.45 m. The fact the breakwater is filled with water has a great influence on the way wave energy is transmitted inside the breakwater. Due to the fact the internal water level is not able to rise the incoming wave will generate a pressure wave in the breakwater. This pressure wave transmits nearly instantly through the entire breakwater, resulting in high pressures without any phase shift. The figure below shows the wave pressure half way the toe and in the middle of the core clearly showing the pressure wave.

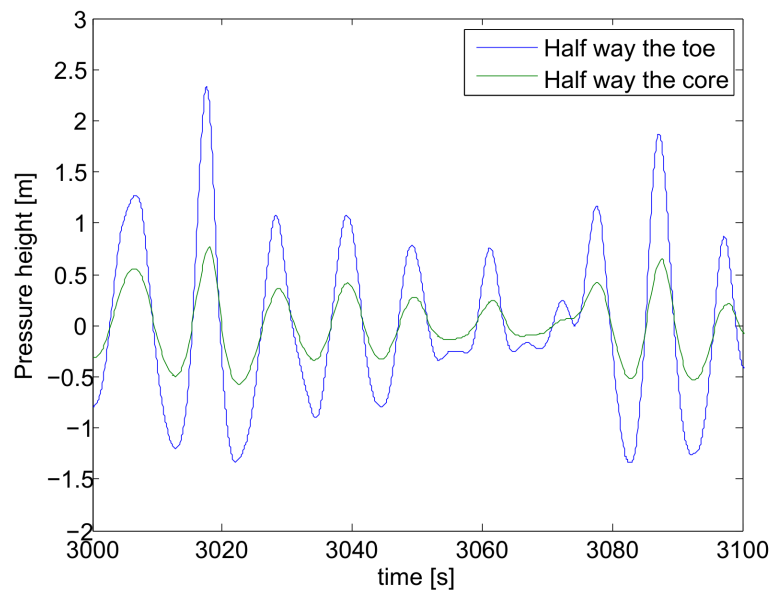


FIG. 9.1: Wave transmission in the northern head with a relative high water level.

To investigate the influence of the breakwater being filled with water the same model is run with a crown high enough to prevent any interaction between the crown element and the internal water level, the crown is located at NAP+4.5 m. Other parts of the breakwater and hydraulic boundary conditions remained the same, however the higher crown will limit overtopping reflecting waves will therefore have some influence on the magnitude of the loading. Figure 9.2 shows a totally different internal water movement compared to figure 9.1, pressure heights are significantly lower and a phase shift is present. The model with the higher crown element resulted in $H_{s,c} = 0.1 m$ and $\zeta = 0.96 m$. Modelled damping is even bigger than measured by van Hoven (2012), one can conclude the trapped air has a great influence on the movement of the internal water level.

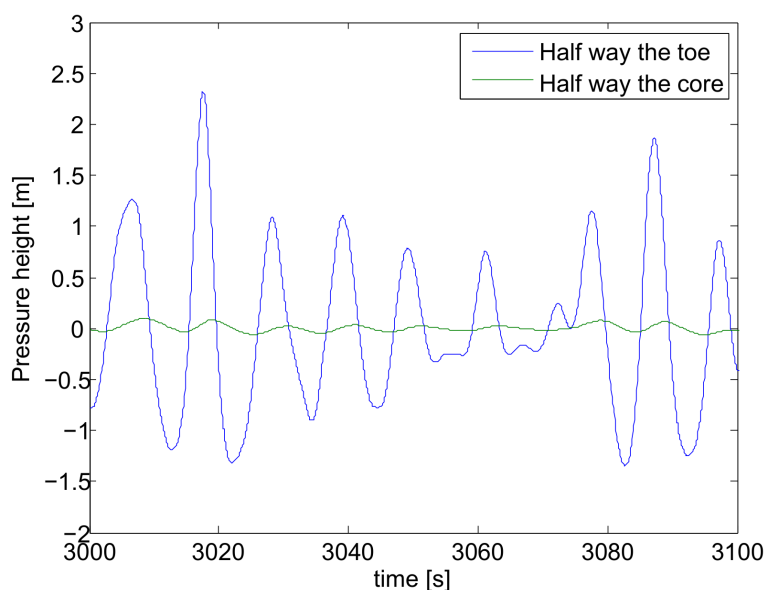


FIG. 9.2: Wave transmission in the northern head with a relative low water level.

Results southern breakwater

Unlike the northern breakwater the crown element of the southern breakwater is high enough to prevent water from filling up the breakwater, bottom of the crown is located at NAP+2.0 m. Therefore the internal water level is able to move and no pressure wave transmits through the breakwater core. Wave transmission in the southern breakwater looks like the transmission plotted in figure 9.2.

The calculated wave damping is smaller than the wave damping measured. Influence of trapped air is unlikely to have a major influence in the southern breakwater, the air escapes the core more easily, see figure 4.3 and the small amplitude of the internal water level make the influence of trapped air smaller. Therefore one can conclude a damping mechanism is present in the southern breakwater. The influence of the damping mechanisms described in chapter 6 will be determined in the next sections.

9.2 Siltation of toe structure

In general water flows more easily through porous media with bigger stone diameters, see table A.2, hence the presence of sand in the toe structure will result in a bigger flow resistance and damping of wave energy. To determine the influence of sand in the toe of the breakwater the entire toe is replaced by a sand body with the parameters described in table 9.1. It is unlikely the sand will only deposit in the toe structure, therefore part of the core material is also silted. Figure 9.3 shows the modelled cross section, the hatched area indicates the silted sand. The dashed line shows the original interface between the toe structure and the core material. All other parts of the breakwater and hydraulic conditions are similar to the baseline calculation.

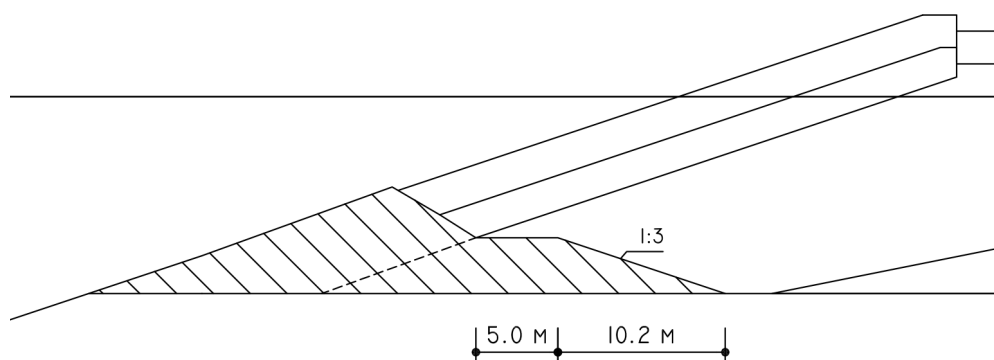


FIG. 9.3: *Cross section completely silted toe structure of the southern head.*

The modelled fluctuation of the pressures in the breakwater core is, in the order of 0.05 centimetres, the field measured resulted in a fluctuation in the order of 1 – 2 *cm*. Therefore one can conclude the toe is not fully silted. It is likely only a layer of sand deposited in the toe structure is causing the damping.

Partly silted toe structures

Instead of a completely silted toe structure layers of sand will be modelled with an increasing thickness until the measured damping is matched. The pressure gradient is likely to gradually decrease the further the wave travels into the breakwater, see figure 8.15. Transport of sediment is related to pressure gradients, see appendix B, a lower gradient will result in less sediment transport. Due to this gradually decreasing pressure gradient sand is expected to settle over a wide area. Therefore the siltation area is modelled relatively wide. A lot of turbulence is expected in the first part of the toe, therefore it is believed to be unlikely for sand to settle in the first two meters of the toe structure. Four cases with increasing sand layers are modelled. The figure below shows the cross section of the model with the biggest sand layers. All modelled sand layers have a flat top of 25 *m* and 1 : 3 slopes.

The total damping in case of a totally silted toe structure gives the impression that flow through sand is negligible due to the high flow resistance. This is checked by modelling the top meter of the supporting sand bed as a permeable porous medium, with the same flow parameters as the silted toe. The maximum positive and negative flow velocities half way the toe structure are

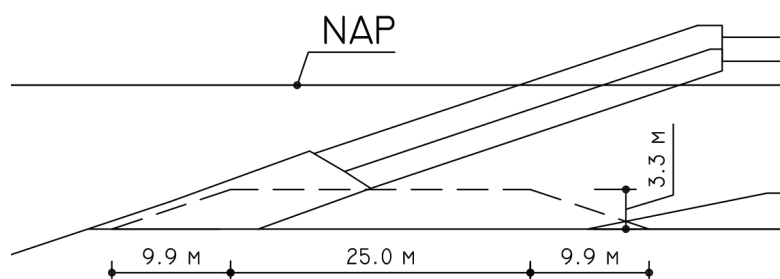


FIG. 9.4: Cross section southern head including a 3.3 m thick sand layer.

shown in figure 9.5, the dashed lines indicate the interfaces between the different media. The assumption is correct, the high flow resistance of sand make the flow velocities in the sand bed negligible. To reduce calculation time the sand layers will therefore be modelled as impermeable obstacles.

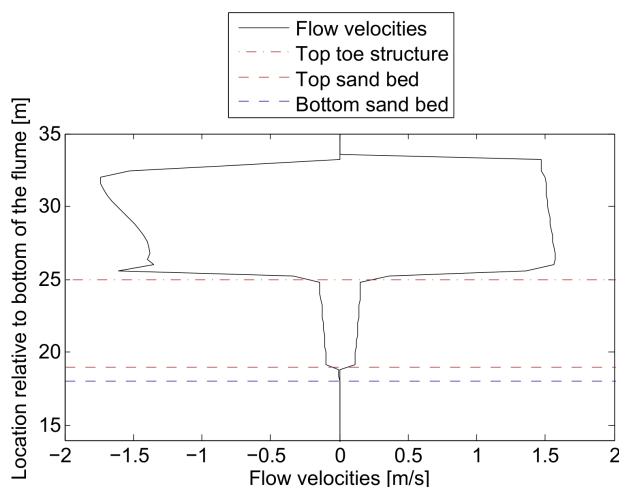


FIG. 9.5: Flow velocities inside sand layer.

Table 9.3 shows the modelled wave damping for all four cases compared to the measured damping and baseline calculation. The presence of a sand layer clearly influences the amount of wave damping. Further increasing the height of the sand layer would result in a closed breakwater toe, the gap between the impermeable asphalt slab and the impermeable modelled sand layer is only 0.1 m. Note to these number is the lack of oblique incident waves like described in section 9.1.1, taking this into account would increase the amount of damping.

TAB. 9.3: Modelled wave damping for a partly silted toe structure in the southern head.

	Height sand layer [m]	$H_{s,c}$ [m]	ζ [-]
Measured	-	0.01-0.02	0.99
Baseline	-	0.18	0.94
Sand 1	1	0.16	0.95
Sand 2	2	0.12	0.96
Sand 3	3	0.06	0.98
Sand 3.3	3.3	0.06	0.98

9.3 Deeper asphalt layer

In the original design of the southern breakwater head the height between the lowest point of the asphalt layer and the supporting sand bed is 3.4 m , see figure 3.3. Like described in section 6.3 multiple factors during construction and since construction finished could have resulted in a lower asphalt layer. A lower asphalt slab would reduce the area for the water to flow through increasing flow resistance and therefore increasing wave damping. Depth of the asphalt layer could vary significantly along the breakwater, damping could therefore have different magnitudes along the breakwater.

The asphalt slab could have changed in two directions, straight downward or the entire slab could slide downward pushing away toe material. To investigate whether a deeper asphalt slab could cause the measured damping several cross sections with different asphalt slabs are modelled. The height of the lowest point of the asphalt slab is assumed to dictate the amount of damping. Therefore all alterations to the original design focus on the lowest part of the asphalt slab, changes in this area will have the greatest influence on wave damping. In total four different cross sections are modelled, the lowest point of the asphalt slab being lowered with 1 , 2 , 3 and 3.2 m straight down. The lowest point of the top of the asphalt slab is lowered with the same vertical distance along the slope of the asphalt slab. Top of the asphalt slab and the connection to the crown element is not changed. The dashed line in figure 9.6 shows the changed cross section, in this case the asphalt slab is lowered with 3.2 m .

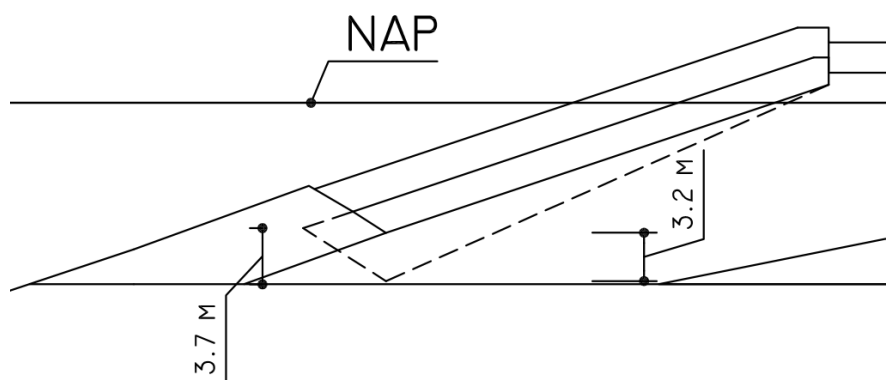


FIG. 9.6: Cross section southern head with 3.3 m lowered asphalt slab.

Table 9.4 shows the modelled wave damping for all four cases compared to the measured damping and modelled baseline calculation. Note to these number is the lack of oblique incident waves like described in section 9.1.1, taking this into account would increase the amount of damping.

TAB. 9.4: Modelled wave damping for lowered asphalt slabs in the southern head.

	Lowered [m]	$H_{s,c}$ [m]	ζ
Measured	-	0.01-0.02	0.99
Baseline	-	0.18	0.94
Asphalt 1	1	0.14	0.95
Asphalt 2	2	0.12	0.96
Asphalt 3	3	0.07	0.98
Asphalt 3.2	3.2	0.06	0.98

9.4 Selection damping mechanism

From the previous two sections one can conclude both damping mechanisms have a significant impact on the wave damping and could cause the measured damping. Flow in longitudinal direction through the core would reduce the effect of a changed cross section if only present over a small length of the breakwater. Therefore the changed cross section should be present over a considerable length.

Damping as a result of a changed cross section requires large changes to the geometry of the asphalt slab. The lowest point of the asphalt slab needs to be around 3.2 m lower than intended to match the measured damping. This could be the result of a straight downward lowering or sliding of the entire asphalt slab. In case of sliding, the slab should have moved about 10 m , due to the slope of the asphalt.

A layer of sand deposited in the toe and part of the core with a thickness of around 3.3 m found to be able to cause the measured damping. The nett longshore sediment transport is directed northwards along the Dutch coast, sand rich water is therefore passing the entire southern breakwater. This could explain sedimentation of only the southern breakwater and thereby explain the difference in damping in the northern and southern breakwater. Sedimentation is likely to occur along the entire southern breakwater.

Magnitude of the changes of a cross section needed for both mechanisms to cause the damping and the required length for the damping mechanism to be effective, make it more likely the damping is caused by sedimentation.

9.5 Damping during design storm

Until this point only the mild storm conditions present during measurements have been applied. This section will describe the behaviour of the southern breakwater during design storm conditions. Not only the amount of damping is of great interest but pressure gradients over the toe structure will provide information about the stability of the sand layer during storm conditions.

Storm conditions described in appendix C.2 are applied to the model of the southern head with a 3.3 m sand layer. The table below shows the conditions and resulting wave pressure and damping during the measurements and design storm conditions. Like expected the internal wave pressure increases during storm conditions. Increase is however larger than the increase of the loading, the smaller amount of damping is caused by the breakwater filling up with water. The impact of the breakwater filling up with water is described in the section in this chapter covering the baseline calculations.

TAB. 9.5: *Wave damping in the southern head during design storm conditions.*

	$H + \text{NAP} [m]$	$H_{s,i} [m]$	$H_{s,c} [m]$	ζ
Mild storm	1.45	2.9	0.01-0.02	0.99
Design storm	3.17	5.66	0.74	0.87

9.6 Stability of the sand layer

Siltation and erosion of sand is highly depending on hydraulic conditions. It is possible the sand is deposited in the toe during relatively mild conditions and eroded during storm conditions, similar to the winter and summer profiles of beaches. Washing out of sand will result in a lower damping of wave energy and could have great influence on the loading of the breakwater, especially in case of numerous major storms in a short time span.

In order for sand to erode water needs to flow over the sand layer. In case the core of the breakwater is filled with water, flow of water is restricted. Therefore a relative low water level combined with large waves normative to determine the stability of the sand layer. A water level equal to NAP is selected and a wave height equal to the normative wave height for lifting. The wind necessary to generate waves with these amplitudes will result in a set-up of water, therefore these conditions might not be possible to occur. However these conditions give a good insight in the stability and provide an upper limit of the forcing of erosion. A full storm of 1000 waves is modelled. Figure 9.7 shows both the inward and outward directed 2% highest pressure gradients.

Appendix B treats sediment stability transport formula for open filters. The toe structure of the breakwater can be considered to be a large open filter. An overall conclusion of the researches described in the appendix is the existence of a critical filter velocity $u_{f,c}$ and critical pressure gradient i_c , in case pressure gradients and filter velocities exceed these values erosion will occur. Research into erosion under wave loading by Wolters and Van Gent (2012) found that significant erosion occurs in case of a ratio of 3.7 or bigger between the 2% highest pressure gradients and the critical pressure gradient. In the same appendix these critical values are determined for the material properties of the toe and sand present in the IJmuiden breakwater; $u_{f,c} \approx 0.04 \text{ m/s}$ and $i_c \approx 0.03$. Top of the sand layer has a length of 25 m, see figure 9.4. At intervals of 1 m pressure gradients are determined, with a frequency of 5 Hz.

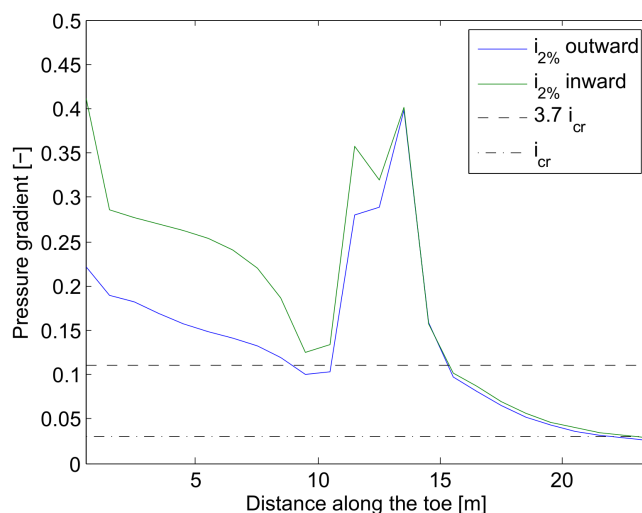


FIG. 9.7: Pressure gradient over the southern breakwater toe during desing storm, sand layer of 3.3 m.

From the figure above one can conclude both inward and outward directed pressure gradients exceed the critical value, and even 3.7 times the critical value. Therefore erosion of sand can be expected. However both pressure gradients are in the same order of magnitude and counteracting

each other making it hard to predict the nett sediment transport. Peaks in both pressure gradients are caused by the asphalt slab. Lowest point of the asphalt limits the area for the water to flow through, erosion will be most severe in this area. The next section will determine the amount of transport in order to determine whether the erosion will influence the damping mechanism.

9.6.1 Transport rates

During major storm events erosion of the sand layer is expected, especially in the area near the lowest point of the asphalt slab and the part of the sand bed nearest to sea. Erosion will lead to a lower damping of waves, therefore it is important to be able to estimate the amount of sand transported during a storm event. Like described in appendix B a formula for sediment transport rates through open filters was introduced by Klein Breteler et al. (1992):

$$T = \rho_s p_1 (i/i_c - 1)^{1.25} \quad (9.2)$$

Where T is the sediment transport rate in $kg/m/s$, ρ_s is the density of the transported sediment, p_1 is the transport intensity in $m^3/m/s$. The value for p_1 , was determined to be between $p_1 = 0.6 \cdot 10^{-6} - 9 \cdot 10^{-6} m^3/m/s$ a best fit was found for $p_1 = 1.5 \cdot 10^{-6} m^3/m/s$.

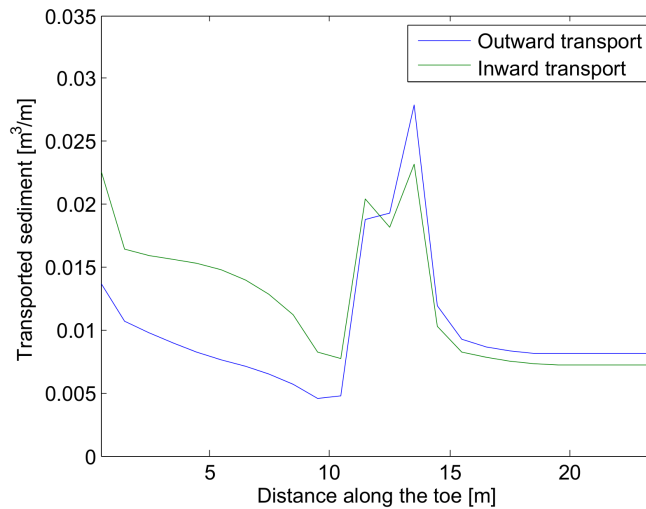


FIG. 9.8: Sediment transport in southern head during an entire design storm, with a sand layer of 3.3 m thick.

Sediment transport rates were calculated for all pressure gradients exceeding i_{cr} using equation 9.2 without the density term and $p_1 = 1.5 \cdot 10^{-6} m^3/m/s$. Adding all transports times the time occurring results in the amount of sediment transport during the modelled storm. Figure 9.8 shows the transport volumes in both inward and outward direction over a storm of 1000 waves.

To determine the magnitude of the lowering of the sand layer the transported volumes should be divided by the porosity of the toe structure, $n = 0.38$. From the figure one can conclude transport

rates are relatively small and inward and outward directed sediment transport counteract each other. It is likely erosion of the sand layer will be in the order of centimetres. Table 9.3 shows damping is nearly identical for a 3.0 *m* thick sand layer, therefore it is believed the damping mechanism is not influenced significantly during a storm. Important note to this conclusion is the lack of three-dimensional effects, currents directed along the breakwater might influence the stability of the sand layer, this should be further investigated. Another note is the applied sediment transport formula is not calibrated for stones with the diameter of the breakwater toe, additional research into the calibration of these formula for big stones would be valuable.

9.7 Conclusions

From the sections above one can conclude both a lower asphalt slab and siltation of the toe structure are able to cause the measured damping in the southern breakwater head. Taking into account a damping mechanism needs to be present over a significant length of breakwater in order to be effective makes damping as a result of a lower asphalt slab less likely. Sedimentation is due to the orientation of the southern breakwater relative to the net longshore sediment transport expected to be present over the entire breakwater. Therefore a sand layer in the toe of the southern breakwater with a thickness of about 3.3 *m* is believed to cause the measured damping in the southern breakwater head.

Stability of the sand layer is checked using open filter sediment transport formula. Erosion during major storms is expected however magnitude of the erosion is likely to be in the order of centimetres, such a small reduction of the sand layer will not have a significant influence on the amount of damping. Therefore the damping mechanism is believed to be stable during storm events. Since the damping mechanism and its behaviour during storm events is known loading and thereby the stability of the asphalt slab can be determined during design storm events. The next chapter covers the stability of the asphalt slab.

Chapter 10

Stability of the asphalt slab

Focus of this thesis is on wave damping and loading of the asphalt slab. This chapter will briefly get into the stability of the asphalt slab as a result of this loading. Aim of this chapter is to get insight in the probability of failure of the asphalt slab. Only a couple of fundamental calculations are performed. If failure can not be ruled out more thorough stability calculations should be performed including three-dimensional effects and fatigue, this is outside the scope of this thesis.

To determine the stability of the asphalt slab only the mechanism of lifting is treated, since this is believed to be the governing failure mechanism. Stability of the asphalt slab is depending on the magnitude of the forcing and strength of the asphalt slab. If the resulting upward force is larger than the resisting forces lifting of the impermeable slab occurs, this is considered failure due to the fact the core material is exposed to waves and might erode. The force equilibrium over a small section of the asphalt is shown in figure 10.1.

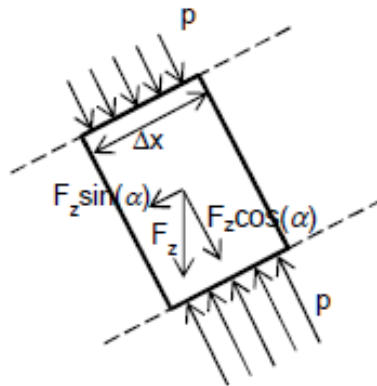


FIG. 10.1: Force equilibrium lifting asphalt slab, van Hoven (2013).

Lifting will occur if:

$$\Delta x(P_{top} - P_{bottom}) > F_z \cos(\alpha) \quad (10.1)$$

Where F is the resisting force of the asphalt slab, which is a combination of dead weight and bending strength, α is the angle of the asphalt slope, P are the pressures exerted by the water in and on the asphalt slab. Lifting of the asphalt can occur over the entire slab or locally.

10.1 Nett upward pressure

Forcing of the asphalt slab is a result of pressure differences between the bottom and the top of the asphalt slab. The amount of wave damping influences the upward pressure, a bigger damping will result in lower upward pressures, however it is not necessarily resulting in a lower forcing since pressure difference dictates forcing. Magnitude of the upward and downward pressures in time is therefore of great importance.

The upward pressure is determined at ten points regularly distributed over the asphalt slab, perpendicular to each point the downward force as a result of water on the outside slope is calculated. Subtracting the downward pressure from the upward pressure at each time step, $5 Hz$, results in the nett upward pressure at each point at each time step. These upward pressures do not take dead weight of the asphalt slab and armour units into account. Therefore in case of no wave action the submerged part of the breakwater will still experience an upward pressure equal to a water head with the height of the asphalt slab. Figure 10.2 shows the location of the calculated upward and downward pressures, in this example the cross section of the northern trunk is presented.

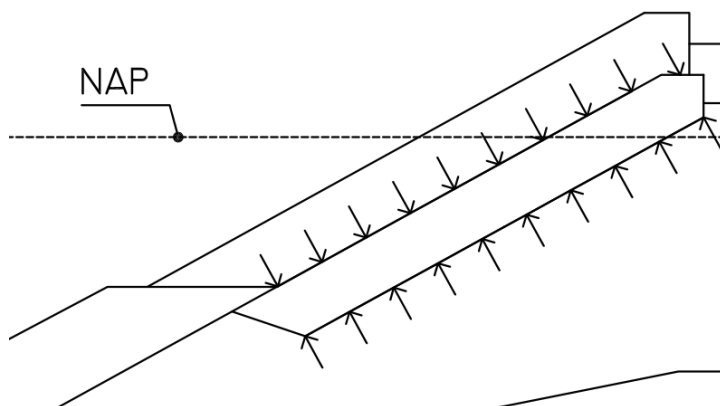


FIG. 10.2: Locations nett upward pressures are determined.

During calculation of the nett upward pressures deformations of the asphalt slab and other parts of the breakwater are not taken into account. All parts of the cross section are stationary, independent of the loading. In real life the asphalt slab, toe structure and armour layer might deform if loading exceeds a critical value, this deformation will lead to a changed flow pattern resulting in a different loading. These second order effects are not taken into account.

10.1.1 Influence of the water level

Like described in section 9.1.1 the water level with respect to the height of the crown element highly influences the way wave energy travels through the breakwater. In case the crown element is lower than the still water level wave energy will travel in a pressure wave through the breakwater, high pressures will occur instantly over the entire breakwater. In case the crown element is high enough to not influence the internal water level wave energy will flow through the porous media and damping will result in a phase shift. Due to this phase shift it might be possible that lower water levels will result in a higher forcing of the asphalt slab, due to the timing of upward and downward pressures.

To determine the influence of the water level on the magnitude of the nett upward pressures the model of the northern trunk is run at two water levels applying the same design wave height, a relatively high water level of NAP+3.17 m and a relatively low water level equal to NAP. Bottom of the crown element is located at NAP+1.2 m. From figure 10.3 one can conclude a relatively high water level will result in a higher total and local loading.

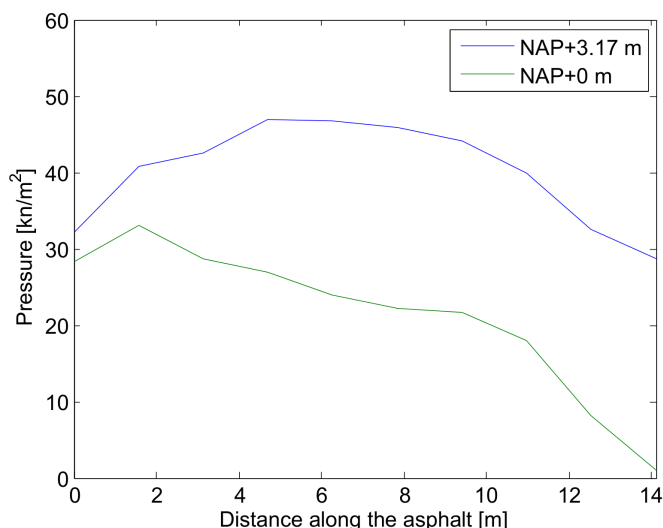


FIG. 10.3: Influence of a relatively low or high water level on the nett upward pressures.

10.1.2 Influence of a gap

The previous section describes the influence of the water level on the way wave energy travels through the breakwater core. In a similar way a gap in the asphalt layer will influence the pressure build up in the core. If there is a gap in the impermeable asphalt layer or crown element the water body will not be trapped and the internal water level can oscillate. Pressure build up will be lower, however the higher damping will result in a phase shift, therefore high upward pressures and low downward pressures might coincide and result in a higher nett upward pressure. In case the gap results in a lower loading of the asphalt slab it might be an interesting option to make the crown or asphalt layer partly permeable. In case of a strong increase of the forcing of the asphalt slab with a partly permeable crown this could be dangerous. A small damage of the asphalt layer could in this case lead to a higher forcing of the asphalt slab.

In order to get insight in the influence of such a gap, the same model is run with the standard impermeable crown element and with a crown element with a 2 m wide gap in the middle. Due to the geometrical differences the influence of such a gap could be different for the trunk and head sections of the breakwater. Therefore this test is performed twice, once on the head section and once on the trunk section of the northern breakwater. The normative hydraulic conditions are applied. Figures 10.4 and 10.5 show the influence of a gap in the crown element on the 2% highest upward pressures.

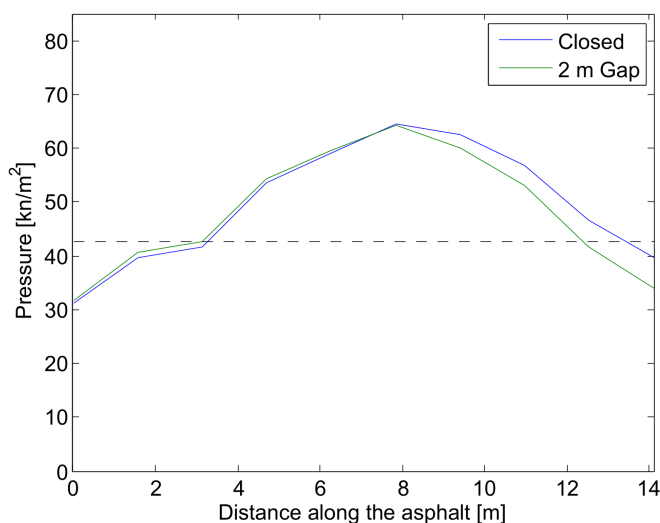


FIG. 10.4: Influence of a gap in the northern trunk on the nett upward pressures.

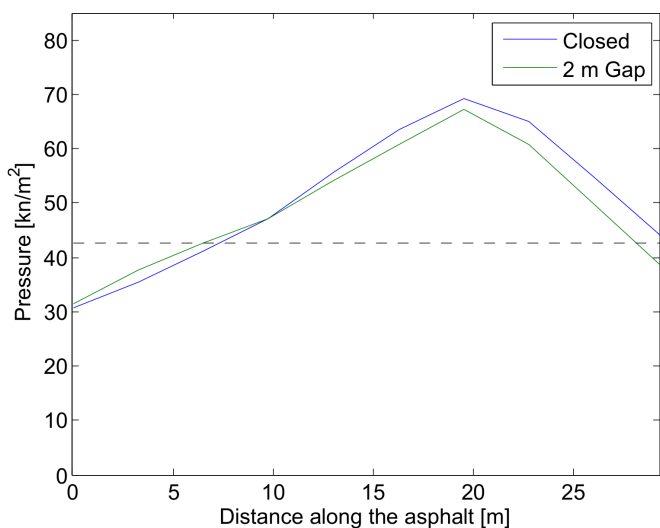


FIG. 10.5: Influence of a gap in the northern head on the nett upward pressures.

In both situations the creation of a gap in the crown element will have a positive influence on the forcing of the asphalt layer, nett upward pressures are lower. However besides the costs creating the gaps, they will have a negative influence on the strength of the crown element. A cost benefit analyses should be performed to investigate whether creating these gaps is beneficial, this is outside the scope of this thesis.

10.1.3 Influence of the armour layer

Armour units placed on the asphalt slab will influence the movement of water both outside and inside the breakwater. Biggest influence is expected on the outside slope, armour units will reduce flow of water therefore run-up and run-down are lower compared to a situation with a smooth slope (run-up and run-down are treated in section 2.3). Due to the lower run-down forcing of the asphalt slab, apart from the dead weight of the armour layer, is expected to be lower, more water will be present pushing down on the slope, reducing the nett upward pressure. The lower part of the armour units directly located above the toe will also influence the amount of water entering the breakwater and therefore contribute to wave damping. This assumption is checked running the model representing the trunk of the northern breakwater with and without armour units. In both cases the normative wave height and water level are applied.

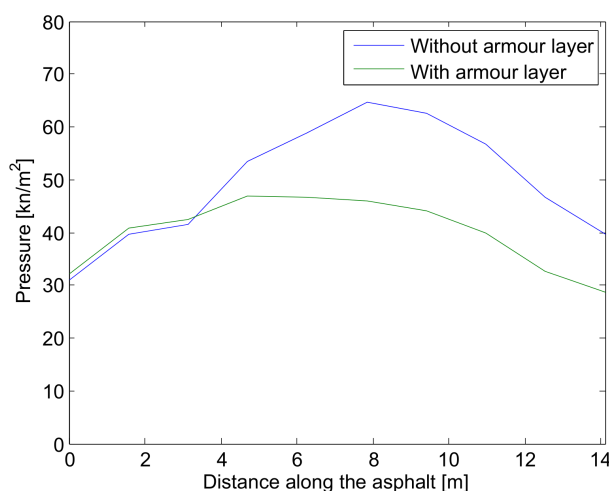


FIG. 10.6: Influence of an armour layer on the nett upward pressure.

Clearly the presence of an armour layer lowers the nett upward pressure on the asphalt slab. A remark should be placed, the run down of water through the armour layer. Due to the fact the armour layer is modelled as a porous medium, only providing cube diameter, porosity and flow resistances the run down could be underestimated in the model. The pores in the armour layer are not orientated randomly like modelled, actually most pores are forming some sort of gutters. Still the armour layer will limit run up and run down and therefore influence the downward pressures, however it might be less than presented above.

From this section one can conclude a relatively high water level and the removal of the armour layer will result in the highest nett upward pressures. Creating a gap in the crown element will reduce the upward pressures, however an analysis should be performed whether the benefits of a lower pressure are higher than the cost involved creating the gaps and the loss of strength of the crown element.

The following sections will therefore calculate the stability of the asphalt slab with a impermeable crown element, removed armour layer and relative high water levels. Inside the toe and part of the core of both cross sections of the southern breakwater a sand layer of 3.3 m thick is modelled, since this is assumed to be the damping mechanism responsible for the measured damping, see chapter 9.

10.2 Lifting of entire asphalt slab

In case the upward forces over the entire asphalt slab are higher than the resisting forces the entire slab will be lifted. This section will not take bending into account, the slab will be treated as if it is infinitely stiff, stability of the entire slab is determined. Bending strength and stresses are discussed in the section describing local lifting.

10.2.1 Forcing

To determine the total upward pressure the slab is divided into ten segments surrounding the points shown in figure 10.2. The pressures are assumed to be constant over the width of each segment, resulting in a total upward force described by:

$$F_{up} = \sum P_i \cdot L_i \quad (10.2)$$

Where F_{up} is the nett upward force, P is the nett upward pressure and L is the length over which the pressure is acting. Pressures in the middle of the slab act over a length $1/9L_{slab}$, pressures on both edges act over half this length. High pressures might not be present over the entire slab at the same time, therefore the 2% highest total upward force might be lower than the sum of the 2% highest local pressures. The upward force is determined for each time step, from this time series the 2% highest total upward forces are determined per running metre of breakwater, see table 10.1.

TAB. 10.1: 2% largest nett total upward forces on asphalt slab.

	F_{up} [kn/m]
Northern head	1,300
Northern trunk	674
Southern head	983
Southern trunk	817

10.2.2 Resistance

The upward force determined in the section above might be present over a certain cross section, however it is unlikely this upward force simultaneously occurs over the entire length of the breakwater. Resulting in lifting of a section of the asphalt slab with a certain width, adjacent parts of the asphalt slab will not be lifted. Therefore next to the dead weight of the asphalt slab a certain shear strength should be exceeded before failure occurs. This shear stress is highly depending on the quality and cohesiveness of the asphalt slab. These properties are unknown and hard to predict without further investigation into the asphalt layer, section 3.3. Therefore first the resistance against lifting of the entire asphalt slab will be determined purely as a result of the dead weight of the asphalt layer. In case this resistance is exceeded by the forcing the additionally needed shear strength will be estimated.

Each cross section has different geometric properties, slope and length of the asphalt slab vary. The resisting force perpendicular to the asphalt slab should be at least as big as the upward force to prevent lifting as a result of dead weight. Rewriting equation 10.1 results in the following stability criteria for the entire slab:

$$F_{up} < \rho_{as}DL\cos(\alpha) + V \quad (10.3)$$

Where F_{up} is the upward force over the entire slab, D , L and α are the thickness, length and angle of the asphalt slab, V is the shear force and $\rho_{as} = 2,300 \text{ kg/m}^3$ is the density of the asphalt, Davidse (2012). The table below shows the resulting minimal required thickness of the asphalt slab, taking no shear force into account.

TAB. 10.2: *Required asphalt thickness to prevent lifting of the entire slab, without armour layer.*

	Slope	α [°]	L [m]	F_{up} [kN/m]	D [m]
Northern head	1:3	19.5	29.3	1,300	2.1
Northern trunk	1:1.75	34.8	14.1	674	2.5
Southern head	1:3	19.5	29.3	1,207	1.9
Southern trunk	1:1.75	34.8	16.5	817	2.6

The designed thickness of the asphalt slab is between 2 – 2.25 m, therefore one can conclude the dead weight of the asphalt slab near the southern head is sufficient against lifting of the entire asphalt slab in case the designed amount of asphalt is still present. Both trunks and the northern breakwater head need additional weight or shear stress to prevent lifting of the entire asphalt slab.

The new maintenance approach of RWS states armour units below a level of NAP–2 m will be moved back or replaced in case of damage or removal, de Baar and Schravendeel (2013). The submerged weight of the an armour layer with a density of $\rho_{armour} = 2,800 \text{ kg/m}^3$ and a scube size of $d = 2.0 \text{ m}$ is therefore added to the resistance. The length of the armour layer varies between the different cross sections and is dictated by the geometry of the underwater part of the asphalt layer. The influence of the armour layer on the forcing is believed to be insignificant due to the high water levels modelled (NAP+3.17 – 3.37 m). The table below shows the needed asphalt thickness including the weight of the armour units.

TAB. 10.3: *Required asphalt thickness to prevent lifting of the entire slab, including armour layer below NAP-2 m.*

	L_{armour} [m]	F_{up}^* [kN/m]	D [m]
Northern head	17.9	588	1.2
Northern trunk	7.6	217	1.9
Southern head	14.7	483	1.2
Southern trunk	9.6	274	1.9

* Upward force minus the submerged weight of the armour.

Influence of the armour units is significant on the required asphalt thickness. In case the designed asphalt thickness is present over the entire breakwater lifting of the entire asphalt slab should not occur, even without taking the shear strength of the breakwater into account.

10.3 Local lifting

Like described in the previous section lifting of the entire asphalt slab is unlikely to occur, the resisting force as a result of the dead weight of the asphalt slab and armour layer are sufficient. Locally the nett upward force might exceed the resisting force as a result of dead weight, in this case a certain bending strength is needed to prevent failure.

The asphalt slab will be modelled as a beam on two supports. The connection to the crown element and the bottom of the asphalt slab are believed to be unable to prevent any rotation, hinged supports are therefore modelled. Due to the support by the core a downward directed bending moment is believed to be impossible. Dead weight of both the asphalt layer and the (partial) armour layer are modelled as distributed load, taking the slope angle α into account.

10.3.1 Forcing

For lifting of the entire slab treated in the previous section only the magnitude of the total lifting was dictating stability. In case of local lifting the distribution of the pressure along the cross section is also influencing stability. The 2% highest local nett upward pressures are plotted in figures 10.7 and 10.8. The dashed lines indicate the perpendicular component of the weight of a asphalt slab with a thickness of 2 m. Clearly in every cross section the upward force exceeds the resisting force locally, resulting in an upward bending moment.

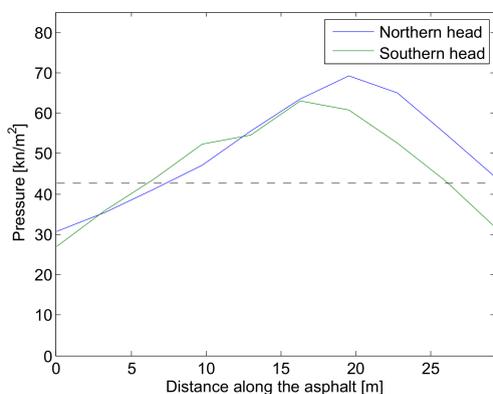


FIG. 10.7: 2% highest nett upward pressures breakwater heads.

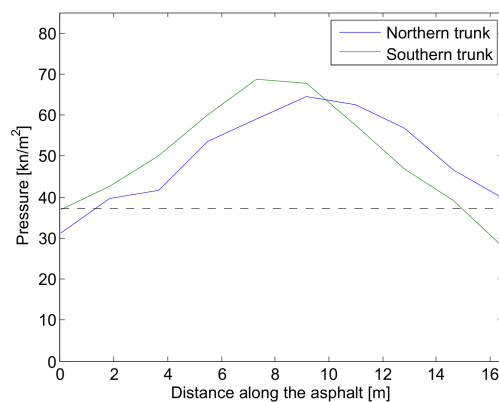


FIG. 10.8: 2% highest nett upward pressures breakwater trunks.

The bending moments in all cross sections are determined assuming an asphalt layer of 2 m thick present over the entire cross section. To determine the necessity and influence of the armour layer calculations are performed without an armour layer, with an armour layer below NAP−2 m and a complete armour layer. Only the weight of the armour layer is taken into account, the influence on the water movement both inside and outside the breakwater is not included. Like the upward force in the previous section this bending moment is calculated for each time step, the 2% highest bending moments are presented in the table below.

TAB. 10.4: 2% highest bending moments for different armour layers.

	Without armour M [kNm]	Partial armour M [kNm]	Complete armour M [kNm]
Northern head	1,255	900	0
Northern trunk	422	206	0
Southern head	1,047	817	0
Southern trunk	669	272	0

10.3.2 Resistance

Like described in section 3.3 the quality and cohesiveness of the asphalt layer is varying over the length of the breakwater. The amount and size of weak spots is unknown. The asphalt is divided into two qualities, a low quality asphalt with no tensile strength and a high quality asphalt with a maximal allowable tensile strength of $\sigma = 3.77 \text{ n/mm}^2$, Davidse (2012). An upward directed bending moment results in tensile stresses in the upper part of the asphalt layer. In case the entire slab consist of high quality asphalt the tensile stresses will be described by:

$$\sigma = \frac{M}{W} = \frac{M}{1/6 \cdot b \cdot D^2} \quad (10.4)$$

Where σ is the tensile stress, M is the bending moment and W is the section modulus. If the calculated tensile stress is lower than $\sigma = 3.77 \text{ n/mm}^2$ the bending strength of a cross section consisting of high quality asphalt has a sufficiently large bending strength. Table 10.5 show the tensile stresses in case of a 2 m thick asphalt layer with high quality.

TAB. 10.5: Tensile stresses due to bending for different armour layers.

	Without armour σ [n/mm ²]	Partial armour σ [n/mm ²]
Northern head	1.9	1.35
Northern trunk	0.63	0.31
Southern head	1.57	1.22
Southern trunk	1.0	0.40

Clearly a 2 m thick high quality asphalt layer will be able to withstand the bending moments, even if the entire armour layer is removed. A reduction of the thickness of the asphalt layer will have a double effect on its resistance against upward pressures. The reduced weight will result in a higher upward bending moment, and the smaller height will reduce the section modulus. Reduction of the section modulus is quadratic with height.

The cross section of the northern breakwater head seems to be governing, therefore this cross section is selected to calculate the minimal required asphalt thickness. In case of a completely removed armour layer a thickness of 1.7 m and in case of a partial armour layer a thickness of 1.6 m will be sufficient to provide bending strength against local lifting assuming high quality asphalt. One should take into consideration this height reduction if present over the entire slab might cause lifting of the entire asphalt slab, see the previous section.

A cross section consisting entirely of low quality asphalt will not be able to withstand any bending moments since it has no tensile strength. Therefore there should at least be a top layer of high quality asphalt to provide bending strength. In case of a cross section composed of both low and high quality asphalt stresses can not be described by equation 10.4, this equation is only applicable for symmetric, square and homogeneous cross sections.

In case of a non homogeneous cross section the distribution of stresses will be different. The figure below shows this distribution for a cross section where only a small top layer has a tensile strength.

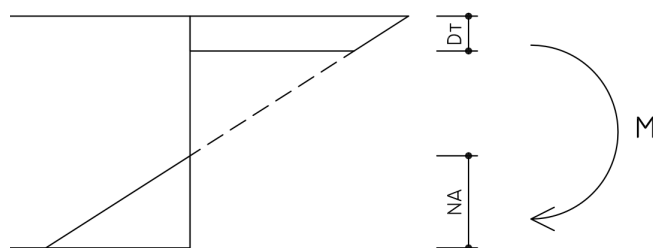


FIG. 10.9: *Distribution of stresses over a cross section composed of low and high quality asphalt.*

In the figure above D_t indicates the thickness of the high quality asphalt and NA indicates the neutral axis, which is depending on the magnitude of D_t . Part of the cross section just above the neutral axis is the low quality asphalt layer without tensile strength. Due to the presence of stones in the stone asphalt the low quality asphalt is believed to be strong enough to withstand pressures. Using this stress distribution the bending strength of the beam as a function of the thickness of the high quality asphalt cover can be determined, this relation is presented in the figure below. The bending stress is calculated assuming a total asphalt thickness of 2 m.

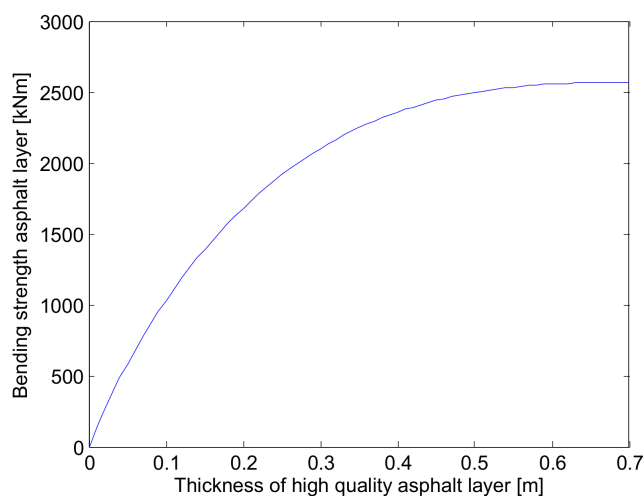


FIG. 10.10: *Bending strength of the asphalt slab for different layers of high quality asphalt.*

Using this relation the minimal required thickness of a high quality asphalt layer is determined and presented in the table below. These values are assuming a total asphalt thickness of 2 m, similar to the forcing of a good asphalt layer described earlier in this section a reduction of the

total asphalt height will effect both nett bending loading and bending strength. Important note to these values is the required bounding between low and high quality asphalt.

TAB. 10.6: *Required high quality covering asphalt layer.*

	Without armour D_t [m]	Partial armour D_t [m]
Northern head	0.14	0.10
Northern trunk	0.05	0.03
Southern head	0.12	0.09
Southern trunk	0.07	0.04

10.4 Conclusions

Without any additional information about the local quality of the stone asphalt lifting of the asphalt slab can not be ruled out if the armour units are removed above a level of NAP-2 m. Dead weight of an asphalt layer with the designed thickness of 2 – 2.25 m and partial armour layer are not big enough to prevent lifting. Therefore either the weight should be increased, an armour layer up until the crown would be sufficient, or the asphalt slab needs to have a certain bending strength.

An asphalt layer consisting of low quality asphalt will not have any bending strength, since the low quality asphalt is believed to have no tensile strength. Therefore the asphalt slab only has a bending strength if the upper part exists of high quality asphalt. The required amount of high quality asphalt depends on the location of the investigated cross section and the height of the entire asphalt layer. In case the amount of high quality asphalt is insufficient an additional layer could be applied, a good bond with the existing asphalt layer is essential.

Chapter 11

Final conclusions and recommendations

The main conclusions of this thesis are listed below followed by the main recommendations.

11.1 Conclusions

The main research question of this thesis is answered via answering the sub questions stated in the introduction of this thesis.

What mechanisms can cause the measured difference in damping of wind waves?

Three important mechanisms influence wave transmission in the core of the breakwaters; trapped air, siltation of the toe and a lower located asphalt layer.

The influence of trapped air is hard to predict and is highly depending on the shape and airtightness of the cross section and hydraulic conditions. Depending on the water level relative to the crown element trapped air can both increase or decrease the amount of damping. During relative high water levels trapped air prevents the generation of pressure waves, thereby trapped air increases damping. In case of relative low water levels trapped air might cause resonance, thereby decreasing the amount of damping. Despite the influence of trapped air on wave transmission it is not able to cause the difference in damping measured between both breakwaters.

Due to the impermeable asphalt slab and the fact flow through the supporting sand bed proved to be negligible all exchange of water takes place through the toe structure. The flow resistance of the toe therefore dictates the magnitude of the damping. Two damping mechanisms increasing the flow resistance of the toe structure proved to be able to cause the measured damping; a lower asphalt slab and siltation of the toe of the southern breakwater.

Which mechanism is most likely to cause the measured difference in damping of wind waves?

The difference in damping can either be caused by a lower asphalt slab or a silted toe. A lowered asphalt slab in the order of 3.2 *m* or a sand layer with a thickness in the order of 3.3 *m* would be sufficient.

In order to be effective a damping mechanism needs to be present over a significant length of the breakwater. In case a damping mechanism is present over a short distance water will flow through the permeable core in longitudinal direction reducing the effect of the damping mechanism. Depending on the location the asphalt slab was designed to have a thickness between 2 – 2.25 *m*. A lowering of the asphalt slab by 3.2 *m* meters is therefore relative large and unlikely to be present over a significant length of the breakwater.

Due to the northward directed net longshore sediment transport along the Dutch coast, sediment passes the entire southern breakwater. Siltation of the toe is therefore likely to be present along the entire southern breakwater. Siltation of the northern breakwater is less likely due to the direction of the sediment transport, explaining the measured difference in wave damping between both breakwaters. The additional damping of wind waves in the southern breakwater is therefore most likely caused by siltation of the toe of the southern breakwater.

Is the damping mechanism influenced by storm events?

The stability of the sand layer causing the damping can be expressed by a critical pressure gradient using open filter sediment transport formula. During major storm events the pressure gradients just above the sand layer exceed the critical gradient, hence erosion is expected. Magnitude of the erosion during a storm event is likely to be in the order of centimetres. The influence of an erosion with such small magnitude is insignificant on the amount of damping.

Can lifting of the asphalt slab during storm events be ruled out?

In order to get insight in the quality and strength of the asphalt slab two cores were drilled in 2004. One showed high quality cohesive asphalt the other low quality with little cohesion. Based on only these two cores it is impossible to predict the bending strength of the asphalt slab. In case locally the asphalt slab consist of low quality asphalt the cross section has little to no bending strength. In this case lifting can only be ruled out if the dead weight of the asphalt and a possible armour layer are sufficient to prevent upward bending moments.

The dead weight of only an asphalt slab with the designed thickness of 2 – 2.25 *m* is not sufficient to prevent lifting. Applying an armour layer above a level of NAP – 2 *m*, in line with the new maintenance program of RWS, is still not sufficient. Ruling out lifting purely based on dead weight is possible applying an armour layer up until the crown element.

The asphalt slab has a bending strength in case it consist out of high quality asphalt. High quality asphalt located in the upper part of the slab results in the biggest bending strength. Due to the large thickness of the slab a layer in the order of 0.10 *m* would be sufficient to prevent lifting, assuming the asphalt slab has a thickness of 2 *m* and the armour layer is maintained below a level of NAP – 2 *m*.

Main research question

Answering of all the sub questions leads to answering the main research question of this thesis:

”What causes the larger damping of wind waves in the southern breakwater of IJmuiden, and is the asphalt slab stable during storm conditions?”

The additional damping of wind waves measured in the southern breakwater is likely to be caused by siltation of the toe structure. A sand layer with a thickness in the order of 3.3 m is sufficient. The asphalt slab is only stable during storm conditions in case the armour layer is maintained up until the crown element or in case of high quality asphalt.

11.2 Recommendations

Recommendations are divided into two categories. First category discusses recommendations to further research wave damping. Subsequently recommendations concerning the asphalt slab are stated.

Further research into wave damping

Wave damping determined during this research is based on a couple of simplifications and assumptions. Additional research on the following topics would be valuable.

Trapped air

The presence of trapped air in the northern breakwater should be investigated. The presence is measured near the head during relatively mild storm conditions, however it is unknown whether the asphalt slab and crown element are airtight enough to ensure the presence of trapped air during major storm events and whether the air is trapped along the entire northern breakwater. Pressure measurements right underneath the crown element and deeper in the core at multiple locations should provide this information.

Another topic for further research is the influence of trapped air on the motion of water inside the breakwater and forcing of the asphalt slab. Trapped air prevents pressure waves from generating during storm conditions, which is favourable. However during low water trapped air might cause resonance, which is unfavourable. The possibility and consequences of resonance should be determined. A numerical model able to include air pressures could be of great value for such a research.

Stability of the sand layer

Erosion of the sand layer in the toe and core of the southern breakwater will result in a reduced damping of wind waves and thereby an increased loading of the asphalt slab. Erosion as a result of wave loading is determined using open filter sediment equations. These formula are never validated for rock this large under wave loading. Further research into these formula is required to ensure the stability of the sand bed and thereby the damping mechanism.

Another uncertainty are long term processes and three-dimensional effects involved in sediment transport. During the stability calculation of the sand bed only waves perpendicular to the breakwater were taken into account. Currents and waves oblique or in the longitudinal direction might influence the stability of the sand layer. Especially near the heads of the breakwater these effects might have a significant influence on sedimentation and erosion in the toe of the breakwater. These processes should be further investigated, pressure measurements could be valuable to evaluate the long term development of the damping of wind waves.

Three-dimensional effects

During this thesis wave damping was determined using two-dimensional cross sections. Especially near the heads of the breakwater three-dimensional effects might have a big influence on damping. A three-dimensional numerical model could provide information about damping in these areas.

Additional pressure measurements

The input regarding damping for this thesis is based on two measurement locations, one in each breakwater head. Additional measurements along both breakwater would highly enlarge insight in damping mechanisms and could be of great value to determine time and location dependency of the damping.

Stability of the asphalt slab

Basic stability calculations performed in this thesis showed the necessity of either a complete armour layer of a certain amount of high quality asphalt to prevent lifting. A more elaborate stability calculation needs to be performed. This calculation should include three-dimensional effects and fatigue.

In order to be able to determine the strength of the asphalt slab more information about the asphalt slab should be collected. Most essential are the density, tensile strength and thickness of the asphalt layer. It is impossible to determine the strength of the asphalt based on two drilled cores with totally different asphalt quality. Therefore it is recommended to drill cores at the locations where the armour layer is most likely to be removed by waves. Analysing quality and quantity of the asphalt should provide information about the stability of the asphalt slab. If the bending strength of the asphalt slab proves to be insufficient applying an additional layer of material with a high tensile strength might be a feasible solution. The height of the asphalt layer results in a large lever between this material and the neutral axis, resulting in additional bending strength. The bond between the new cast material and the existing asphalt needs to be assured.

References

- Blauwendraad, J. *System dynamics (in Dutch)*. Lecture notes CT2022, 2008.
- Bregman, M. Porosity of placed rock layers (in Dutch). Master's thesis, Delft University of Technology, 1998.
- Burcharth, H.F. and Andersen, O.H. On the one-dimensional steady and unsteady porous flow equations. *Coastal engineering*, 24 233-257, 1995.
- CIRIA, . *Rock Manual: the use of rock in hydraulic engineering*, 2007.
- CUR, report 233. Interface stability of granular filter structures. Technical report, Stichting CURNET, 2010.
- Davidse, M.P. Strength and durability stone asphalt breakwaters IJmuiden (in Dutch). Technical report, KOAC-NPC, 2012.
- de Baar, A. and Schravendeel, R. New maintenance strategy breakwaters IJmuiden (in Dutch). *Waterhuishouding en Waterbouw*, September 2013.
- De Graauw, A.; Van der Meulen, T., and Van der Does de Bye, M. Design criteria for granular filters. Technical report, WL Delft Hydraulics, 1983.
- Den Adel, H. Transport model for filters (in Dutch). Technical report, WL Delft Hydraulics, 1992.
- Dudgeon, C.R. An experimental study of the flow of water through coarse granular media. *La Houille Blanche*, No 7, pp 785-801, 1966.
- Ergun, S. Fluid flow through packed columns. *Chemical engineering Progress*, 48, 1952.
- Fand, R.M.; Kim, B.Y.K.; Lam, A.C.C., and Phan, R.T. Resistance to the flow of fluids through simple and complex porous media whose matrices are composed of randomly packed spheres. *Journal of Fluids Engineering*, Vol 109, pp 268-274, 1987.
- GeoWeb, Rijksoverheid, May 2014. URL <http://www.rwsgeoweb.nl/geoweb41/?Viewer=Havenhoofden%20IJmuiden>.
- Hannoura, A.A. and Mc Corquodale, J.A. Virtual mass of coarse granular media. *Journal of the Waterway, Port, Coastal and Ocean Div.*, Vol 104, pp 191-200, 1978.
- Hirt, C.W. and Nichols, B.D. Methods for calculating multi-dimensional, transient free surface flows past bodies. In *Proceedings First international Conference Numerical Ship Hydrodynamics*, 1975.

- Holthuijsen, L.H. *Waves in Oceanic and Coastal Waters*. Cambridge University Press, 2007.
- IH-Cantabria, . *IH-2VOF course manual*, 2012.
- Jensen, B.; Jacobsen, N.G., and Christensen, E.D. Investigations on the porous media equations and resistance coefficients for coastal structures. *Coastal Engineering 84 56-72*, 2014.
- Kieftenburg, A.T.M.M. Swan calculations for the Dutch coast (in Dutch). Technical report, Rijkswaterstaat, 2006.
- Klein Breteler, M. Sand transport in granular filters, horizontal steady current (in Dutch). Technical report, WL Delft Hydraulics, 1989.
- Klein Breteler, M.; Den Adel, H., and Koenders, M.A. Slope protection of set stone, design rules for filter layer (in Dutch). Technical report, WL Delft Hydraulics, 1992.
- Koene, R.J.; Jansen, H., and Schravendeel, R. Proven strength breakwaters IJmuiden (in Dutch). Technical report, Rijkswaterstaat, 2013.
- Kuiper, C. and van Gent, M.R.A. Breakwaters of IJmuiden, 2d scale model test into failure mechanisms (in Dutch). Technical report, WL Delft hydraulic, 2006.
- Luijendijk, A.; de Vroeg, H.; Swinkels, C., and Walstra, D.J. Coastal response on multiple scales: a pilot study on the IJmuiden port. In *Proc. of the Coastal Sediment 2011*, 2011.
- Maps, Bing. IJmuiden satellite images, jan 2014. URL <http://www.bing.com/maps/>.
- Northsea-atlas, Rijksoverheid. Grain size sand, May 2014. URL <http://www.noordzeeatlas.nl/Kaart/korrelgrootte.htm>.
- O'Prinsen, N.M. Construction of Dutch breakwaters (in Dutch). Master's thesis, Delft University of Technology, 1993.
- Oumeraci, H. and Partenscky, H.W. Wave-induced pore pressure in rubble mound breakwater. In *Proc. of the 22nd International Conference on Coastal Engineering*, 1991.
- Prashanth, J.; Subba, R.; Shirlal Kiran, G.; K., Balakrishna Rao, and Vishwanath, . Wave run-up, run-down studies on reshaped berm breakwater with artificial armour units. *International Journal of Earth Sciences and Engineering*, August 2012.
- Schiereck, G.J. *Introduction to bed, bank and shoreline protection*. Delft University Press, 2001.
- Shih, R.W.K. Permeability characteristics of rubble material - new formulae. In *22nd International Conference on Coastal Engineering*, pp 1499-1512, 1990.
- Sleath, . Measurements of bed load in oscillatory flow. *ASCE Journal of the Waterway Port coastal and Ocean Division*, 104, 1978.
- Smale, A.J. and Groeneweg, J. Additional research into hydraulic boundary conditions IJmuiden (in Dutch). Technical report, Deltares, 2012.
- Smith, G. Comparison of stationary and oscillatory flow through porous media. Master's thesis, Queen's University, Canada, 1991.

- Troch, P. *Experimental study and numerical modelling of pore pressure attenuation inside a rubble mound breakwater*. PhD thesis, Dept. of Civil Engineering, Ghent University Belgium, 2000.
- van der Veer, F. Noorderpier IJmuiden, August 2014. URL <http://www.oud.vanderveerfotografie.nl/>.
- van Gent, M.R.A. Formulae to describe porous flow. Technical report, Delft University of Technology, 1992.
- van Gent, M.R.A. Stationary and oscillatory flow through coarse porous media. Technical report, Delft University of Technology, 1993.
- van Hoven, A. Pore pressure measurements breakwaters of IJmuiden (in Dutch). Technical report, Deltares, 2012.
- van Hoven, A. Further failure probability consideration breakwaters of IJmuiden (in Dutch). Technical report, Deltares, 2013.
- van Hoven, A. Pore pressure measurements breakwaters IJmuiden interim, rapport storm season 2013-2014 (in Dutch). Technical report, Deltares, 2014.
- Vanneste, D.F.A. and Troch, P. Experimental research on pore pressure attenuation in rubble-mound breakwaters. In *Proc. of the 32 nd International Conference on Coastal Engineering*, 2010.
- Williams, A.F. Permeability of rubble mound material. Technical report, Mast G6-S, Project I, Hydraulic Research, 1992.
- Wolters, G. and Van Gent, M.R.A. Granular open filters on a horizontal bed under wave and current loading. *Coastal Engineering Proceedings*, 1(33), 2012.

List of Figures

1.1	Location of IJmuiden.	1
1.2	Layout of the outer harbour of IJmuiden.	2
1.3	Designed cross section of the breakwater.	2
1.4	Damaged asphalt slab after summer storm of 1970.	3
1.5	Configuration of pressure sensors.	4
2.1	Scheme of the influence of hydraulic and structural parameters on stability.	8
2.2	Clarification breakwater elements.	9
2.3	Definition of a wave.	10
2.4	Breaker types.	11
2.5	Schematic representation of wave run-up and run-down.	12
2.6	Sketch of pore pressure damping in a core.	13
2.7	Lifting forces due to a water level difference and a passing wave.	13
3.1	Breakwater layout.	14
3.2	Cross section northern breakwater head.	15
3.3	Cross section southern breakwater head.	16
3.4	Cross section northern breakwater trunk.	16
3.5	Cross section southern breakwater trunk.	17
3.6	Pictures of the construction of the IJmuiden breakwaters.	19
4.1	Configuration of the pressure sensors installed near both breakwater heads.	20
4.2	Measured tidal wave in and on the northern breakwater.	21
4.3	Measured tidal wave in and on the southern breakwater.	22
4.4	Measured wind waves in and on the northern breakwater during a mild storm.	22
4.5	Measured wind waves in and on the southern breakwater during a mild storm.	23
4.6	Measured wind waves in the northern breakwater during a severe storm.	24
4.7	Measured wind waves in the southern breakwater during a severe storm.	24
5.1	Storage inertia resistance model representing the northern breakwater head.	26
5.2	Reaction to a harmonic excitation in case of resonance.	29
6.1	Development of the bathymetry in the vicinity of the IJmuiden breakwaters.	34
6.2	Asphalt cast to stabilize core during construction.	35
6.3	Armour units settling into the asphalt slab.	36
6.4	Slope instability of the asphalt slab.	37
7.1	Averaging area for porous flow.	41
7.2	False breaking phenomena.	42
8.1	Range of applicability of different wave theories.	45
8.2	Comparison between modelled flow velocity profile and linear wave theory.	45
8.3	Cross section scale model test.	46
8.4	Measured pore pressure damping.	47

8.5	Comparison between modelled and measured damping for regular wave series.	49
8.6	Transmitted regular waves.	49
8.7	Comparison between energy density spectra numerical model and scale model.	50
8.8	Numerical determined δ values.	50
8.9	Transmitted irregular waves numerical model and scale model.	50
8.10	Cross section scale model IJmuiden breakwater.	52
8.11	Measured 2 % highest seaward pressure gradients.	53
8.12	Schematic representation of the calculation of upward forces.	53
8.13	Cross section of the numerical model.	55
8.14	Probability of exceedance of the modelled waves at NAP-20 m	56
8.15	Comparison numerical determined and measured pressure gradients.	57
9.1	Wave transmission in the northern head with a relative high water level.	61
9.2	Wave transmission in the northern head with a relative low water level.	62
9.3	Cross section completely silted toe structure of the southern head.	63
9.4	Cross section southern head including a 3.3 m thick sand layer.	64
9.5	Flow velocities inside sand layer.	64
9.6	Cross section southern head with 3.3 m lowered asphalt slab.	65
9.7	Pressure gradient over the southern breakwater toe during desing storm, sand layer of 3.3 m.	67
9.8	Sediment transport in southern head during an entire design storm, with a sand layer of 3.3 m thick.	68
10.1	Force equilibrium lifting asphalt slab.	70
10.2	Locations nett upward pressures are determind.	71
10.3	Influence of a relatively low or high water level on the nett upward pressures.	72
10.4	Influence of a gap in the northern trunk on the nett upward pressures.	73
10.5	Influence of a gap in the northern head on the nett upward pressures.	73
10.6	Influence of an armour layer on the nett upward pressure.	74
10.7	2% highest nett upward pressures breakwater heads.	77
10.8	2% highest nett upward pressures breakwater trunks.	77
10.9	Distribution of stresses over a cross section composed of low and high quality asphalt.	79
10.10	Bending strength of the aspalt slab for different layers of high quality asphalt.	79
A.1	Classification flow regimes.	93
A.2	Resistance regions.	95
A.3	Representation of the turbulent flow equation.	97
B.1	Forces acting on a grain.	99
B.2	Shields diagram.	100
B.3	Flow velocities open filter.	101
B.4	Test set-up sediment rates through open filter.	103
B.5	Critical shear stress under wave loading.	104
C.1	Numerical wave field representing conditions February 2012.	107
C.2	Locations hydraulic boundary conditions are determined.	108
C.3	Numerical modelled normative wave field northern head.	108
C.4	Numerical modelled normative wave field northern trunk.	109
C.5	Numerical modelled normative wave field southern head.	109
C.6	Numerical modelled normative wave field southern trunk.	109

List of Tables

2.1	Ranges of grading.	9
3.1	Grading, stone diameter and porosity of construction materials.	17
3.2	Hydraulic boundary conditions for the normative cross sections.	19
8.1	Determined δ values applying different Forchheimer shape factors.	48
8.2	Scaling breakwater materials.	52
8.3	Waves generated during scale model tests.	52
8.4	Measured upward pressures with 2 % exceedance probability.	54
8.5	Modelled wave properties, at NAP-20 m.	56
8.6	Numerical determined pressures with 2% exceedance probability.	57
9.1	Structural parameters applied for baseline calculation.	60
9.2	Comparison between results of the baseline calculation and field measurements.	61
9.3	Modelled wave damping for a partly silted toe structure in the southern head.	64
9.4	Modelled wave damping for lowered asphalt slabs in the southern head.	65
9.5	Wave damping in the southern head during design storm conditions.	66
10.1	2% largest nett total upward forces on asphalt slab.	75
10.2	Required asphalt thickness to prevent lifting of the entire slab, without armour layer.	76
10.3	Required asphalt thickness to prevent lifting of the entire slab, including armour layer below NAP-2 m.	76
10.4	2% highest bending moments for different armour layers.	78
10.5	Tensile stresses due to bending for different armour layers.	78
10.6	Required high quality covering asphalt layer.	80
A.1	Reynolds number for different flow regimes.	93
A.2	Stone diameter, filter velocity, Reynolds number and flow regime for different porous media.	93
A.3	Listing of Forchheimer coefficients.	98
B.1	Sediment transport coefficients.	102
C.1	Normative hydraulic boundary conditions.	107
C.2	Modelled normative hydraulic boundary conditions.	108

Appendices

Appendix A

Flow through porous media

In order to get insight in the pressure build up inside the breakwater core and the pressure gradients over the toe structure it is necessary to be able to describe the motion of water through the porous parts of the breakwater. This appendix covers the most suitable models to describe flow of water through porous media.

Interest level in this report is on a macroscopic scale. Shape, size, location and connection between individual pores is not described, but properties are averaged over a certain area. This approach is selected because resulting forces are the area of interest, not the exact flow through individual grains. This approach introduces the material properties porosity, grading and (nominal) stone diameter, for a description see section 2.1. These properties combined with the hydraulic conditions determine the flow resistance of the different porous media.

A.1 Flow regimes

Interaction between porous media and moving fluids can result in different types of flow, called flow regimes. The occurring regime depends on the filter velocity u , grain diameter d and the fluid viscosity ν and is expressed by the Reynolds number:

$$Re = \frac{ud}{\nu} \tag{A.1}$$

Three flow regimes can be distinguished: Darcy or laminar flow, Forchheimer flow and fully turbulent flow, figure A.1 and table A.1 show the flow regimes and the corresponding Reynolds numbers. Different flow regimes are described using different flow resistance models, transition areas are present between regimes.

Where Re_p is a slightly different definition of the Reynolds number, the flow velocity inside the pore and the pore diameter are used, instead of the filter velocity and grain diameter. Resulting in a smaller Reynolds number, $Re \approx 1.5 \cdot Re_p$.

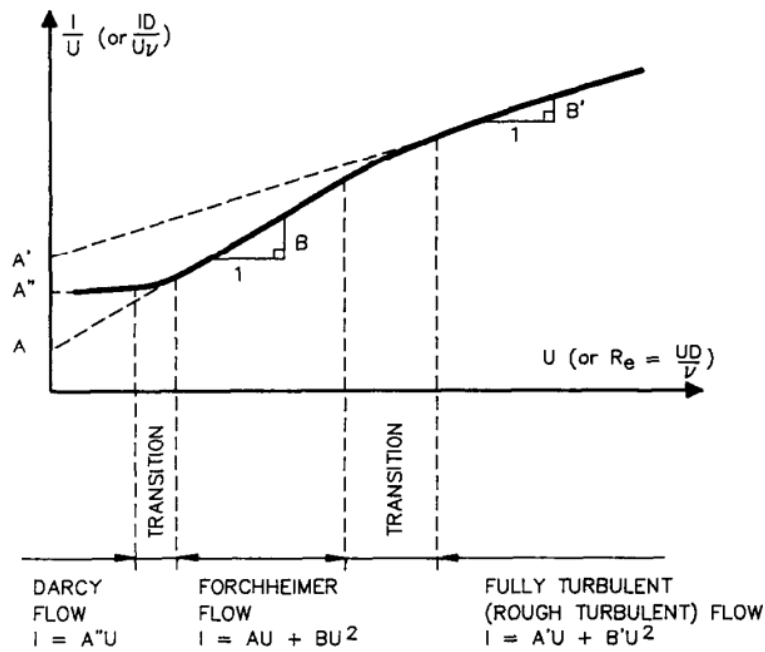


FIG. A.1: Classification flow regimes, Burcharth (1991).

TAB. A.1: Reynolds number for different flow regimes, Burcharth and Andersen (1995).

Flow regime	Re_p
Darcy flow regime	$Re_p < 1$
Forchheimer regime	$10 < Re_p < 150$
fully turbulent flow	$300 < Re_p$

An indication of the diameter d , filter velocity u and Reynolds number Re for different materials used in breakwaters is provided by table A.2. Hydraulic conditions are not implemented in the table, therefore the table should only be used as a first indication of the expected flow regime.

TAB. A.2: Stone diameter, filter velocity, Reynolds number and flow regime for different porous media, Troch (2000).

Material	d [m]	u [m/s]	Re [-]	Flow regime
Sand	$< O(10^{-3})$	$< O(10^{-3})$	$< O(1)$	Darcy
Small pebbles	0,01	$O(10^{-2})$	$O(10^2)$	Forchheimer
Rubble 2-300 kg	0,1-0,3	$O(10^{-1})$	$O(10^4)$	Fully turbulent
Riprap 1-6 tonne	0,7-1,2	$O(1)$	$O(10^6)$	Fully turbulent
Armour layer	$> 1,2$	$> O(1)$	$> O(10^6)$	Fully turbulent

A.2 Darcy flow

The Darcy flow is named after Henry Darcy, in 1856 he performed researched into stationary flow through sand beds, he empirically derived the Darcy law:

$$i = a''u \quad (\text{A.2})$$

Where i is the pressure gradient, u is the filter velocity and a'' is the hydraulic conductivity a material depending constant. This equation only holds a linear term for friction, and is only applicable for low and constant flow velocities. For the flow through coarse material the Darcy model is not applicable because of the large velocities and accelerations, the Forchheimer model is more suitable in those cases.

A.3 Forchheimer model

In 1991 Forchheimer added a non-linear resistance term to the flow model of Darcy. Making it applicable to stationary flow through coarser materials, where turbulent resistance is no longer negligible. The resulting empirical equation is called the Forchheimer equation:

$$i = au + bu^2 \quad (\text{A.3})$$

Where i is the hydraulic gradient, u is the filter velocity and a is the linear resistance term and b the quadratic resistance term. Magnitude of these coefficients depend on material and fluid properties. The linear term describes contribution of laminar flow, the quadratic term represents the contribution of turbulent flow. van Gent (1992) provided theoretical background for this empirical equation using the Navier-Stokes equations.

Ergun (1952) formulated an expression for the coefficients a and b for stationary flow.

$$a = \alpha \frac{(1-n)^2}{n^3} \frac{\nu}{gd^2} \quad \text{and} \quad b = \beta \frac{1-n}{n^3} \frac{1}{gd} \quad (\text{A.4})$$

Where α and β are shape factor depending on grading, shape and roughness of used material. There is not yet a equation derived to determine the shape factors analytically, see section A.5 for a listing of empirically determined shape factors.

Forchheimer for non-stationary flow

The Forchheimer equation, (equation A.3), is only valid for stationary flow. Polubarinova Kochina added a time-dependent term in 1962. The formula is known as the extended Forchheimer equation.

$$I = au + bu^2 + c \frac{du}{dt} \quad (\text{A.5})$$

Where c is a dimensional inertia coefficient, theoretical derivation by van Gent (1992) using Navier-Stokes equations let to the following expression:

$$c = \frac{1 + \gamma \frac{1-n}{n}}{ng} \quad (\text{A.6})$$

γ is the dimensionless coefficient for the 'added mass', there is an extra momentum needed to accelerate the same volume of water in a porous medium. This mechanism is called added mass because the increased required momentum suggests a larger mass.

In order to get a first estimate of the relative importance of the three resistance terms two parameters are used. The before mentioned Reynolds number and the Keulegan-Carpenter number (KC). $KC = (u_m \cdot T)/d_{n50}$ where T is the wave period, and u_m is the maximal velocity. The KC number expresses the length of a wave motion compared grain diameter. The magnitude of the turbulent resistance relative to the laminar resistance is linear to Re. The importance of the turbulent resistance term relative to the inertial resistance term is linear with the KC. The magnitude of the inertial resistance relative to the laminar resistance is linear with Re/KC. The relative importance of these terms is presented in figure A.2, where T indicates turbulence, I inertia and L laminar.

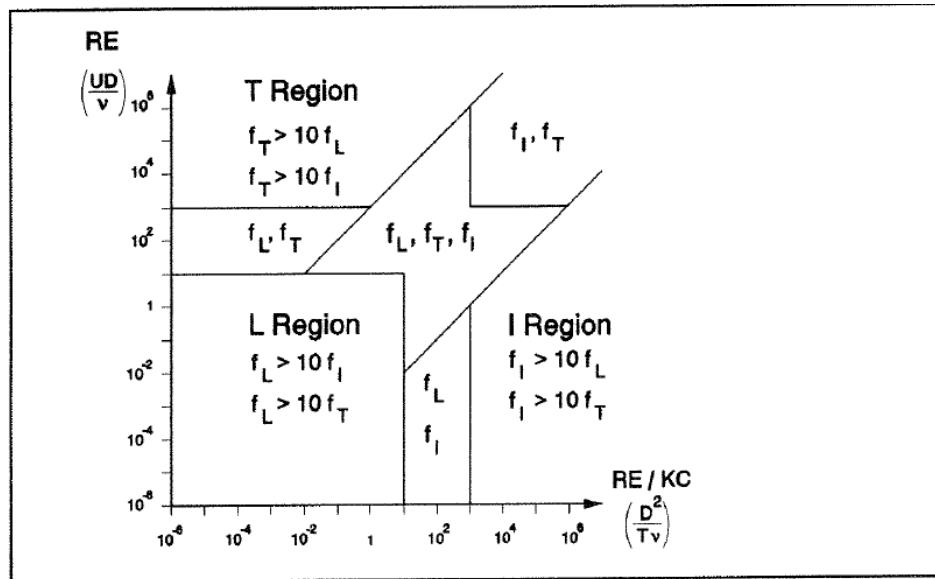


FIG. A.2: Resistance regions, van Gent (1993).

van Gent (1993) researched the β and γ values for oscillating flow and compared the results with the values for stationary flow. Van Gent concluded the values are deviating and developed a new expression for β stating a stationary part β_c and an extra contribution caused by non-stationary flow β' , resulting in $\beta = \beta_c + \beta'$. Explanation for this approach is during a change of flow direction boundary layers and small eddies will be destroyed, this requires an additional amount of momentum. The amount of momentum needed will be larger if the inertia term is larger. The

inertia term is inversely proportional to KC , like stated above. Resulting in $\beta' = 7.5\beta_c/KC$. The new expression for b states:

$$b = \beta_c \left(1 + \frac{7.5}{KC}\right) \frac{1-n}{n^3} \frac{1}{gd_{n50}} \quad (\text{A.7})$$

In this case $KC = \tilde{u} \cdot T / n d_{n50}$. Reason for this slightly altered KC is the time it takes for boundary layers to develop. As a result of this delayed formation of the boundary layer the friction at a certain point of time is not dependent on the velocity at that point of time. Therefore the use of a characteristic velocity \tilde{u} is more useful than the momentary velocity. β_c can be found from stationary flow test, if such parametric research is not available a value of 1.1 is proposed by van Gent (1993).

During the same research van Gent derived a different expression for the c -coefficient used in equation A.5. The new expression is depending on the acceleration number $Ac = \tilde{u} / n T g$.

$$c = \frac{1 + \frac{1-n}{n} \left(0.85 - \frac{0.015}{Ac}\right)}{n \cdot g} \quad \text{for } Ac > \frac{0.015}{\frac{n}{1-n} + 0.8} \quad (\text{A.8})$$

A.4 Fully turbulent flow

In case the Reynolds number exceeds a certain critical value flow becomes fully turbulent, for coarse granular material this value is 300, see table A.1. The linear friction term in the Forchheimer equation (equation A.5) becomes insignificant, resulting in only the quadratic term.

Burcharth and Andersen (1995) suggested a different approach for fully turbulent flow. The critical Reynolds number Re_c , 300 for coarse granular material see table A.1, indicates the lower boundary of the turbulent flow, see figure A.3.

Burcharth and Andersen (1995) proposed the following formula for turbulent flow:

$$i = i_c + b(u - u_c)^2 \quad (\text{A.9})$$

Where the filter velocity corresponding to the critical Reynolds number is given by $u_c = Re_c \nu / d$, i_c is the critical gradient and can be obtained by inserting u_c into equation A.3. Resulting in the following flow equation:

$$i_c = Re_c \alpha \frac{(1-n)^2}{n^3} \frac{u_c^2}{gd^3} + Re_c^2 \beta \frac{(1-n)}{n^3} \frac{u_c^2}{gd^3} \quad (\text{A.10})$$

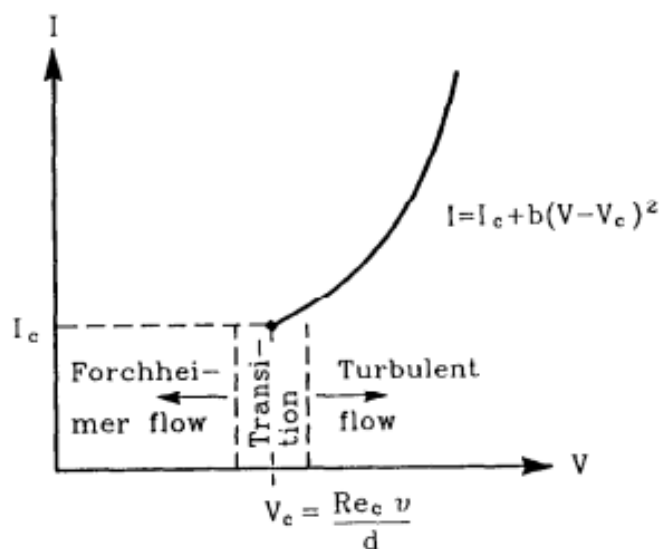


FIG. A.3: Representation of the turbulent flow equation, Burcharth and Andersen (1995).

A.5 Shape factors

Previous sections outlined models to describe the flow of water through porous media. All models contain friction coefficients (a'' , a and b), which are expressed using shape coefficients (α and β). Magnitude of these coefficients is essential to be able to correctly describe flow of water through porous media, table A.3 on the next page gives an overview values found in literature.

TAB. A.3: *Listing of Forchheimer coefficients, Burcharth and Andersen (1995) adapted by author.*

Material	Packing	d_{85}/d_{15}	α	β	Reynoldsnumber(Re)	Source
Spheres	Cubic	1	900-6000	1.0-1.3	630-14000	Sm
		1	640-900	0.47-1.1	630-14000	Sm
	Random	1	41-1700	1.1-1.5	180-9000	D
		1.8	3100	1.6	3700-7700	D
		1	220	1.5	120-410	F
		2	240	1.6	120-410	F
	1	2070	0.69		G	
Semi round rock	Random	1.9	≈ 3000	2.7	800-2100	B
		1.3	unknown	2.4	7850-7500	W
		1.3	0	0.88	unknown	G
		1.4-1.9	3000	2.45	unknown	T
Round Rock	Random	1.4	≈ 10000	2.2	<2100-8050	B
		1.7	1400-15000	2.2-2.9	500-3600	D
		unknown	160-9800	1.7-2.2	unknown	H
		1.3	unknown	1.9	750-7500	W
Very round rock	Random	1.3	1066	0.29	unknown	G
		1.4	10070	2.15	unknown	T
Irragular rock	Random	1.4-1.8	1400-13000	2.4-3.0	600-10300	B
		1.6	270-1400	4.1-11	400-8200	D
		unknown	90-540	3.0-2.7	unknown	H
		1.3-1.4	980-2100	2.5-2.9	300-5700	Sh
		1.3	unknown	3.7	750-7500	W
		1.0-1.7	1000	1.1	unknown	G
	1.4-1.8	1400-13000	2.45-3.45	unknown	T	
Equant rock	Random	1.2	?	3.6	750-7500	W
Tabular rock	random	1.4	3000	1.5	1500-18000	Sm
		1.2	unknown	3.7	750-7500	W

Legend: B: Burcharth and Andersen (1995), D: Dudgeon (1966), F: Fand et al. (1987), G: van Gent (1993), H: Hannoura and Mc Corquodale (1978), Sh: Shih (1990), Sm: Smith (1991), T: Troch (2000) and W: Williams (1992)

Appendix B

Sediment transport

Siltation of the toe structure is believed to be one of the possible mechanisms causing the measured damping. In order to be able to make a decision about the probability of siltation of the breakwater to occur it is important to have a basic understanding of sediment transport in a global way, but especially transport through filters. This appendix will treat general sediment transport principles, the later sections focus on sediment transport through granular material. Aim is to get insight in critical flow velocities and pressure gradients causing sediment transport in granular materials and the transport rates.

B.1 Sediment transport of a sand bed

If one looks at a sand bed at the level of grain diameters one sees a sand bed is never perfectly flat, grains will extrude out of the surface. This roughness of the sand bed results in forces on grains when water is flowing over it, figure B.1 shows these forces and the resisting force due to own weight and possible locking by surrounding particles.

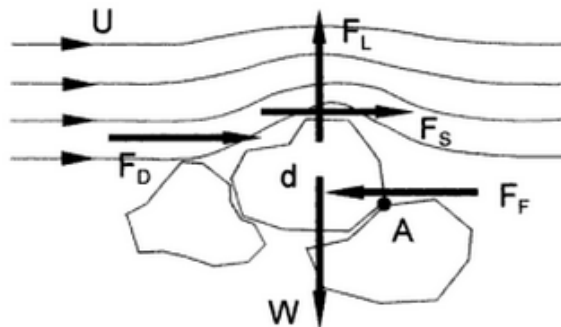


FIG. B.1: *Forces acting on a grain, Schiereck (2001).*

In case the loading forces are bigger than the resisting forces sedimentation will occur. Transport of these loose particles can be divided into two transport modes; bed load and suspended load. The bed load is a transport of sediment by rolling over the bed. By suspended load the sand is lifted and kept in suspension for a longer time and distance.

Magnitudes of the forcing of a grain are functions of the density of water ρ_w , flow velocity u , grain diameter d , roughness, shape and positioning of the grain. Due to this complexity there are hardly any analytical formula describing the forces on individual grains. Sediment transport can be investigated at two scales the microscopic and macroscopic scale. Microscopic focuses on movement of individual grains, macroscopic describes the movement of sediment averaged over a certain area. Research into sediment transport is typically on a macroscopic scale and formula are empirical.

Shields

One of the best known theories describing sediment transport is that of Shields. In 1936 Shields performed research into sediment transport, he did not investigate movement of a single grain but he formulated an approach to determine the critical shear velocity u_{*c} over a entire bed. He introduced the Shields parameter, depending on the application the Shields parameter can both be a stability or mobility parameter. Shields gives a relation between the Reynolds particle number and the dimensionless shear stress.

$$\psi_c = \frac{\tau_c}{\rho_s - \rho_w g d} = \frac{u_{*c}^2}{\Delta g d} = f(Re_p) \quad (\text{B.1})$$

Where ψ_c is the critical Shields parameter, τ_c is the critical shear stress, $u_{*c}^2 = \tau_c / \rho_w$ is the critical shear velocity, $Re_p = u_{*c} d / \nu$ is the particle Reynolds-number, ν is the kinematic viscosity. The figure below shows the relation between the Shields number and Reynolds particle number.

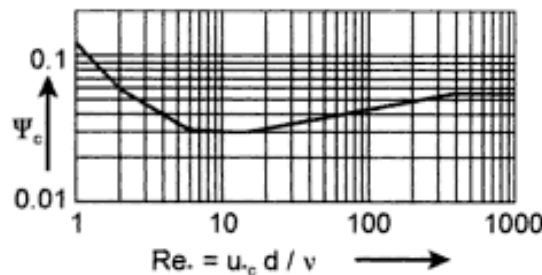


FIG. B.2: *Shields diagram, Schiereck (2001).*

Note to this approach is the definition of motion, the threshold (shear) velocity approach proposed by Shields makes it necessary to define when movement of sediment can be qualified as sediment transport. Due to the irregularities in nature like positioning and shape of individual grains the critical velocity will be different for each grain. For this purpose movement of sediment is separated in 7 groups:

1. no movement at all
2. occasional movement at some locations
3. frequent movement at some locations
4. frequent movement at many locations
5. frequent movement at all locations
6. continuous movement at all locations

7. general transport of grains

Transport rates when the critical velocity defined by Shields is reached are in group 6. Whenever a critical flow velocity is presented in literature it is important to have an idea what kind of movement was taken into account formulating this velocity.

The Shields parameter is not only used to determine the critical flow velocities, it is also used to quantify sediment transport. In 1971 Paintal formulated the following transport formula:

$$\begin{aligned} T_s^* &= 6.56 \cdot 10^{18} \cdot \psi^{16} & \text{for } \psi < 0.05 \\ T_s^* &= 13\psi & \text{for } \psi > 0.05 \end{aligned} \quad (\text{B.2})$$

$$T_s^* = \frac{T_s}{\sqrt{\Delta g d^3}}$$

Where T_s is the transport rate, in this definition $m^3/m/s$ and ψ is the Shields number, Δ the relative density of the grain, d the grain diameter and g the gravitational acceleration.

B.2 Sediment transport in filters

To prevent washing out of sand from underneath hydraulic structures often filters are applied. Two types of filters exist; geometrical closed and geometrical open filters. Geometrical closed filters are constructed in such a way sand particles are too big to penetrate through the covering layer. This can either be realised using geotextiles or placement of rock layers with an increasing diameter. If constructed correctly there will be no sediment transport from base material through geometrical closed filters.

Geometrical open filters lower the flow velocities near the bed by placing a rock layer, figure B.3 provides a sketch of the flow velocities as a result of the filter. There are two types of geometrical open filters, hydraulic closed filters (no sediment transport, flow velocities near the bed are lower than a critical velocity) and transport filters (transport of base material occurs).

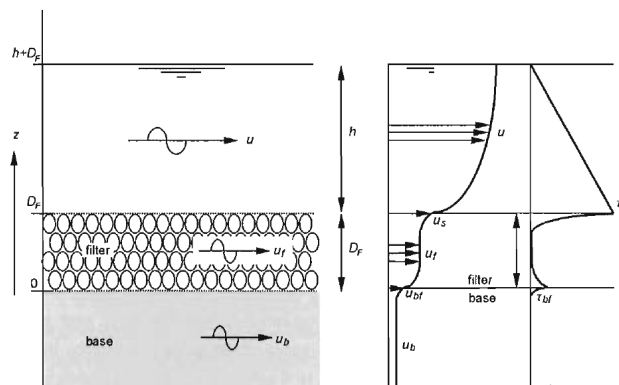


FIG. B.3: *Flow velocities open filter, CUR (2010).*

Uniform flow

Klein Breteler (1989) and Den Adel (1992) researched critical flow velocities in transport filters. Granular filters were placed on a sand bed in a flume and a steady uniform flow was applied. Measuring sediment transport and flow velocities of the water resulted in the following formulas for the critical filter velocity $u_{f,c}$ in case of a horizontal filter bed:

$$\begin{aligned} u_{f,c} &= \left(\frac{n_f}{c} \left(\frac{d_{15,f}}{\nu} \right)^m \sqrt{\psi g \Delta_b d_{50,b}} \right)^{1/(1-m)} & \text{for } 0.1 \text{ mm} < d_{50,b} < 1 \text{ mm} \\ u_{f,c} &= \frac{n_f}{0.22} \sqrt{\psi g \Delta_b d_{50,b}} & \text{for } d_{50,b} > 0.7 \text{ mm} \end{aligned} \quad (\text{B.3})$$

Where indices f and b indicate properties concerning the filter or base materials, n is the porosity, ψ the Shields parameter, d_x is the diameter exceeded by $x\%$ of the stones, g is the gravitational acceleration, Δ is the relative submerged density, ν is the kinematic viscosity of water and c and m are constants depending on $d_{50,b}$. Values for these constants determined by Klein Breteler et al. (1992) are presented in table B.1.

TAB. B.1: *Sediment transport coefficients by Klein Breteler et al. (1992).*

$d_{50,b}$ [m]	c [-]	m [-]
0.1	1.18	0.25
0.15	0.78	0.2
0.2	0.71	0.18
0.3	0.56	0.15
0.4	0.45	0.11
0.5	0.35	0.07
0.6	0.29	0.04
0.7	0.22	0
0.8	0.22	0
1	0.22	0

De Graauw et al. (1983) measured critical gradients in filter beds for uniform flow. Measurements showed in case the ratio between the characteristic diameter of the filter and base material is constant, the critical gradient decreases with an increasing characteristic diameter of the base material. The following formula was proposed for the critical gradient i_c :

$$i_c = \left(\frac{0.06}{n_f^3 d_{15,f}^{4/3}} + \frac{n_f^{5/3} d_{15,f}^{1/3}}{1000 d_{50,b}^{5/3}} \right) u_{*c}^2 \quad (\text{B.4})$$

Where u_{*c} is the critical shear velocity of the base material, which can be determined using the Shields diagram, figure B.2.

Transport rates

In case the critical flow velocity or gradient is exceeded it is important to be able to determine the amount of transport through a filter. Klein Breteler et al. (1992) combined a theoretical microscopic approach with an empirical macroscopic approach to formulate formulas describing the transport rates through a filter in case the critical velocity or gradient is exceeded. He investigated a homogeneous sand bed under uniform flow. Set-up of his test is shown in figure B.4, clearly only sediment transport through the filter is measured, unlike other researches there is no suspended sediment transport possible.

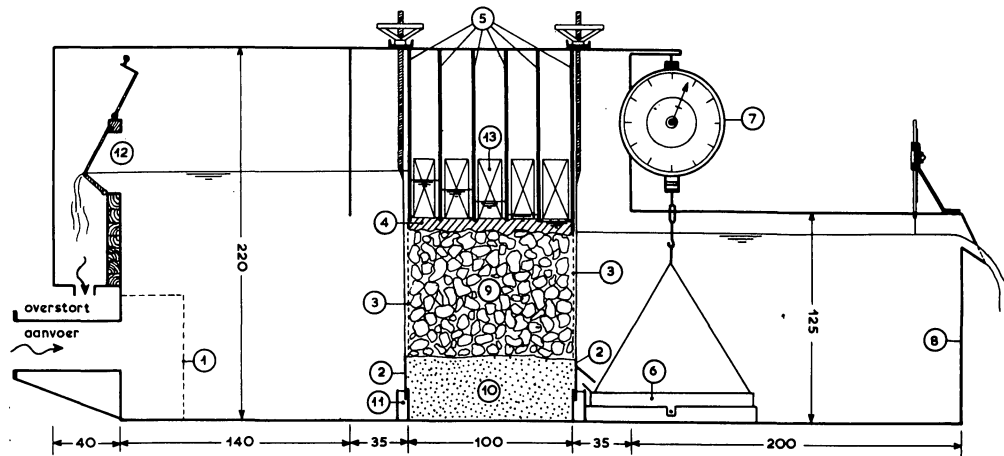


FIG. B.4: Test set-up sediment rates through open filter, Klein Breteler et al. (1992).

Measurement in the picture are in millimetres and the number represent the following parts of the set-up:

- | | |
|-----------------------|--|
| 1 Sieve | 2 Slide to compensate eroded base material |
| 3 Wire mesh | 4 Impermeable plastic layer |
| 5 Parallel boards | 6 Container catching transported sediment |
| 7 Scale | 8 Weir |
| 9 Filter material | 10 Base material |
| 11 Sealing clay layer | 12 Water height regulator |
| 13 Ballast | |

Two different formula describing sediment transport rates were found during this research:

$$T = \rho_s p_1 (i/i_c - 1)^{1.25} \quad (\text{B.5})$$

$$T = \rho_s p_2 ((u_f/u_{f,c})^2 - 1)^{1.5} \quad (\text{B.6})$$

Where T is the sediment transport rate in $kg/m/s$, ρ_s is the density of the transported sediment, p_i are transport intensities in $m^3/m/s$. The value for p_i , was found to be independent of the diameter, and in the range of $0.6 \cdot 10^{-6} - 9.0 \cdot 10^{-6} m^3/m/s$, with a best fit for $p_i = 1.5 \cdot 10^{-6} m^3/m/s$.

B.3 Sediment transport under wave loading

The equations presented above are all based on steady flow. The basic principles are in case of wave loading similar, however some correction should be applied. The Shields diagram presented in figure B.2 is slightly different for cyclic loading, relatively small diameter stones have a smaller Shields number and therefore a lower critical shear velocity. Figure B.5 shows the Shields diagram adopted for the dimensionless stone diameter and wave loading by Sleath (1978).

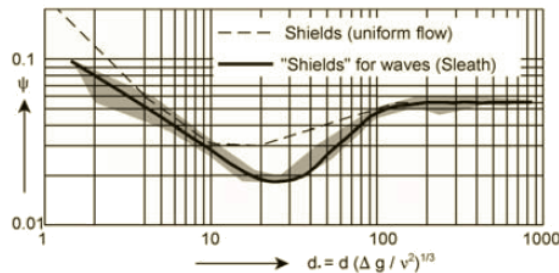


FIG. B.5: Critical shear stress under wave loading, Schiereck (2001).

Klein Breteler et al. (1992) assumed cyclic flow can be interpreted as quasi-stationary in case the orbital motion of the water inside the porous media is large compared to the $d_{f,15}$. This reasoning is based on the fact the velocity profile in porous media is strongly depending on local geometry compared to the influence of the duration of flow. As a result of this reasoning the critical velocities and gradients as a result of wave loading should be comparable to steady flow conditions.

Wolters and Van Gent (2012) performed research into sediment transport in filter layers as a result of wave loading. Main focus of this research was getting more insight in the transport of base material through transport filters, in order to be able to design more efficient open filters. Scale model research was performed measuring transport under current, wave and combined current wave loading in an open wave flume.

Main conclusions of the research are; bed material transport in a granular filter can be described as a function of the hydraulic gradient ($i_{2\%}/i_c$), independent of the loading conditions. Sediment transport is overestimated by a factor 30 to 920 if determined with equation B.5, on the other hand the increase in transport with increasing i/i_{cr} is higher $(i/i_{cr})^{(5.8)}$ instead of $(i/i_{cr})^{(1.25)}$. Difference in the magnitude of the sediment transport rates is mainly caused by the set-up of the experiments. Using an open wave flume instead of a filter box like Klein Breteler et al. (1992) results in a different flow distribution through the open filter, and also suspended load will be taken into account using a wave flume. Important note was a strong increase of sediment transport is measured for $i_{2\%}/i_c > 3.7$, significant erosion in prototype scale is expected.

B.4 Stability parameters silted sand IJmuiden breakwater

From the sections above one can conclude the stability of sand is both depending on the dimensions of the sand particles and the dimensions of the filter, or in case of IJmuiden the toe structure. This section will focus on the stability parameters of the sand bed deposited in the toe of the southern breakwater of IJmuiden. Loading parameters will be discussed in section 9.6. Aim is to provide a critical pressure gradient and filter velocity for which erosion of the silted sand starts. These stability number will be used to evaluate the stability of the silted sand and give an estimate of the amount of sand possible to erode during one storm.

The following values are used and can be found in section 3.3 and used as input to determine the stability parameters: $n_f = 0.38$, $d_{15,f} = 0.80 \text{ m}$, $d_{50,b} = 0.22 \cdot 10^{-3} \text{ m}$, $\rho_w = 1025 \text{ kg/m}^3$, $\rho_s = 2650 \text{ kg/m}^3$ and $\nu = 1.33 \cdot 10^{-6} \text{ m}^2/\text{s}$.

The dimensionless diameter d_* used in figure B.5 is given by:

$$d_* = d(\Delta g/\nu^2)^{1/3} \quad (\text{B.7})$$

Where Δ is the relative density of the submerged sand particle, $\Delta = (\rho_s - \rho_w)/\rho_w$. Resulting in $d_* = 4.54$ and from the diagram $\psi = 0.045$. Using equation B.1 one can determine the corresponding critical shear velocity $u_{*c} = 0.012 \text{ m/s}$. Filling in these number in equation B.3 and B.4 results in: $u_{f,c} \approx 0.04 \text{ m/s}$ and $i_c \approx 0.03$.

Appendix C

Hydraulic boundary conditions

This appendix provides an more elaborate description of the hydraulic boundary conditions applied during the numerical modelling performed during this thesis. First an overview of the measured or determined hydraulic conditions is provided, after which the wave field created by the numerical model representing these conditions.

C.1 Field measurements

This section treats the hydraulic boundary conditions present during field measurements by van Hoven (2012) described in chapter 4 of this thesis. Measurement concerning this research took place during the winter of 2011 and 2012 starting on the 5th of February. Measurements took place at three locations, one at each breakwater near the head, see chapter 4, and at the permanent measurement installation of RWS just of shore of the southern breakwater. At each breakwater head 4 pressure sensors were installed, two on the outer slope of the breakwater and two inside the core material. The data of the different measurement equipment resulted in a measured sea level of NAP+1.45 m and waves characterized by $H_s = 2.9$ m and $T_m = 9$ s during the peak of this mild storm.

Numerical wave field

In order to be able to calculate the amount of wave damping using a numerical model similar hydraulic boundary conditions need to be applied. A wave field containing a 1000 waves described by a JONSWAP wave spectrum is created. The modelled wave characteristics approximate the measured characteristics closely, $H_s = 2.88$ m and $T_m = 9.11$ s, distribution of wave height and period and the wave spectrum is shown in figure C.1.

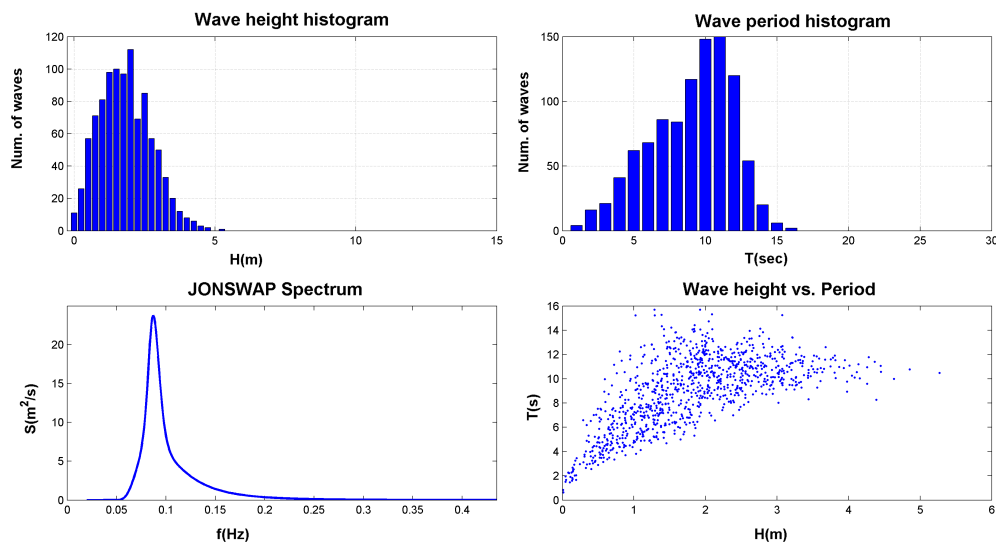


FIG. C.1: Numerical modelled wave field representing conditions measurements February 2012.

C.2 Normative hydraulic boundary conditions

At request of RWS Smale and Groeneweg (2012) researched the hydraulic boundary conditions for the breakwaters of IJmuiden. Aim of this research was to get insight in the decisive hydraulic boundary conditions and the probability these conditions simultaneously occur on multiple locations along the breakwater. During this research the probabilistic programme Hydra-K of RWS and a SWAN model to translate the waves to near shore conditions was used. The decisive loading of the breakwaters was taken to be only related to the wave height, influence of the wave period and water level was not taken into account. Later the wave period and water levels complying with these wave heights were determined.

The hydraulic boundary conditions were calculated at a total of 24 location, both inside and outside of the breakwaters. Figure C.2 shows the locations and the corresponding numbers.

Like described in chapter 3 points 9 and 13 for the northern and 1 and 2 for the southern breakwater are believed to represent the normative cross sections. For these locations the following hydraulic conditions were found by Smale and Groeneweg (2012) with an exceedance probability of once in 50 years.

TAB. C.1: Normative hydraulic boundary conditions, Smale and Groeneweg (2012).

	Location	H_s [m]	T_p [s]	h [m]
	North head	10	5.46	+3.37
	North trunk	13	4.75	+3.37
	South head	1	5.55	+3.17
	South trunk	2	5.83	+3.17

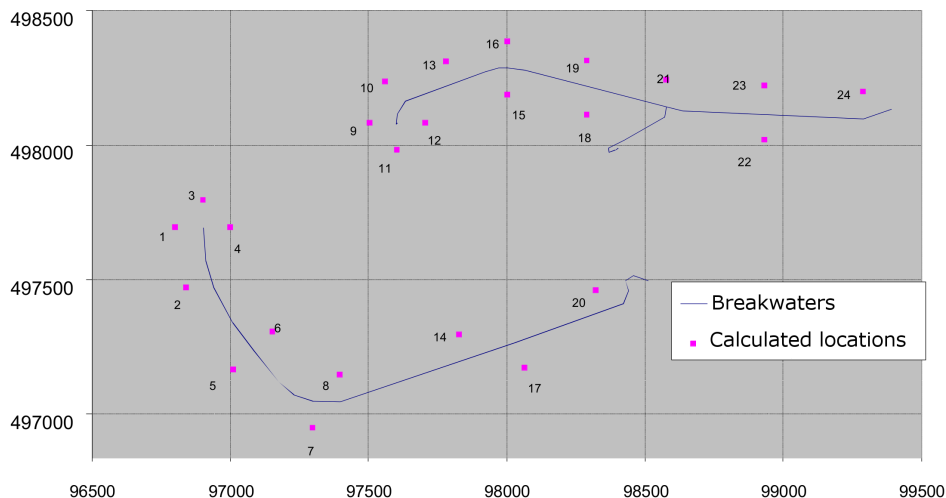


FIG. C.2: Locations hydraulic boundary conditions are determined, Smale and Groeneweg (2012).

Numerical wave fields

The normative hydraulic conditions found by Smale and Groeneweg (2012) are transformed into numerical wave fields. Table C.2 shows the modelled wave are similar only a bit larger than measured. Figure C.3 till C.6 show the distribution of wave height and period and the wave spectrum in a separate figure for each wave field.

TAB. C.2: Modelled normative hydraulic boundary conditions.

	Measured		Modelled	
	H_s [m]	T_p [s]	H_s [m]	T_p [s]
North head	5.46	9.1	5.57	9.09
North trunk	4.75	8.98	4.89	8.95
South head	5.55	8.61	5.66	8.70
South trunk	5.83	8.76	5.97	8.60

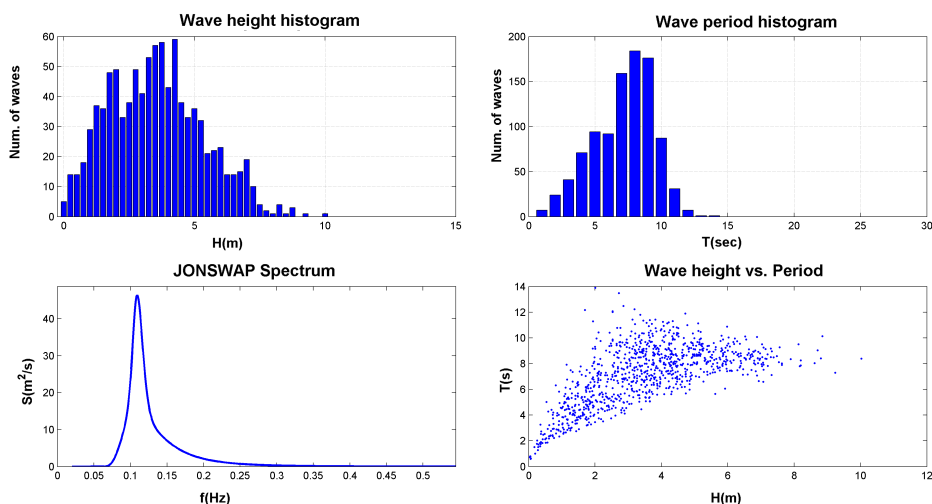


FIG. C.3: Numerical modelled normative wave field northern head.

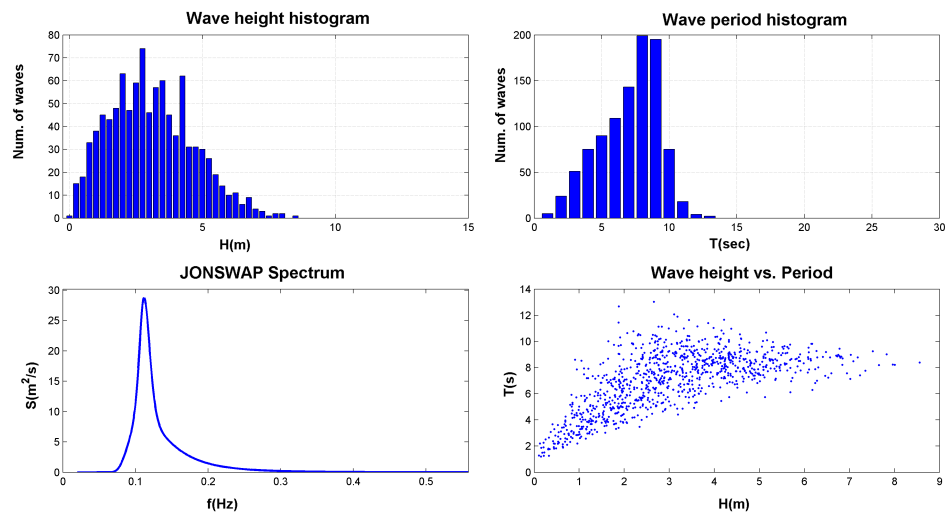


FIG. C.4: Numerical modelled normative wave field northern trunk.

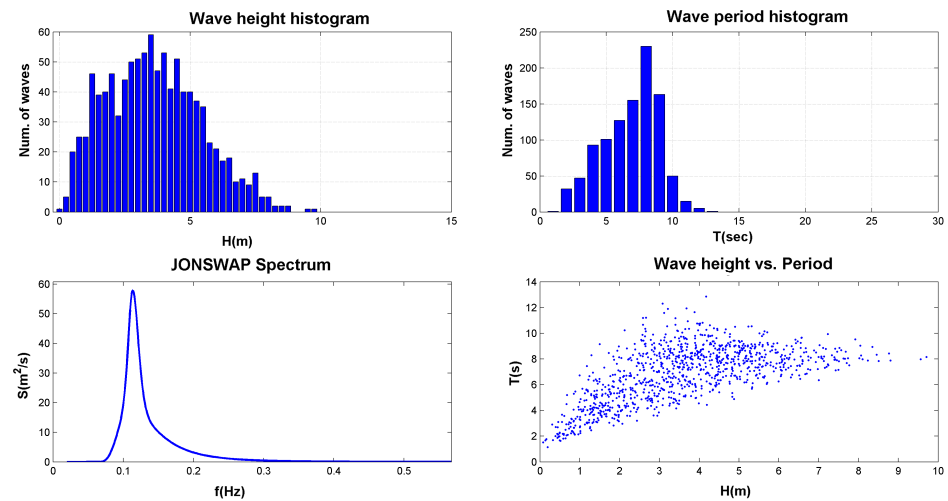


FIG. C.5: Numerical modelled normative wave field southern head.

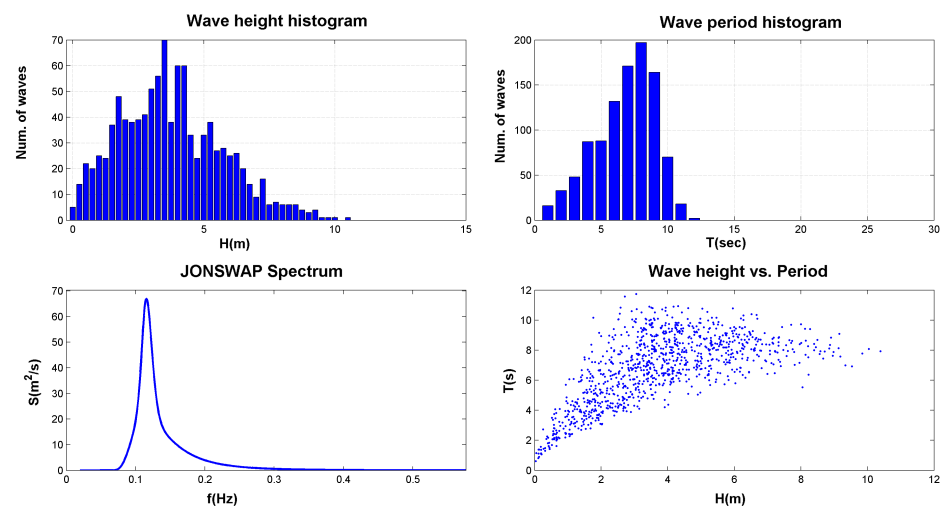


FIG. C.6: Numerical modelled normative wave field southern trunk.